

THESIS FOR THE DEGREE OF DOCTOR OF PHILOSOPHY

# **Studies on the Recovery of Secondary Antimony Compounds from Waste**

Toni Yvonne Karlsson



Department of Chemistry and Chemical Engineering  
CHALMERS UNIVERSITY OF TECHNOLOGY  
Gothenburg, Sweden 2017

Studies on the Recovery of Secondary Antimony Compounds from Waste  
TONI YVONNE KARLSSON  
ISBN: 978-91-7597-663-1

© TONI Y. KARLSSON, 2017.

Doktorsavhandlingar vid Chalmers tekniska högshola  
Serie nr 4344  
ISSN 0346-718X

Nuclear Chemistry and Industrial Materials Recycling  
Department of Chemistry and Chemical Engineering  
Chalmers University of Technology  
SE-412 96, Gothenburg  
Sweden  
Telephone: +46 (0) 31-772 1000

Cover: SEM micrographs of cubic (left) and orthorhombic (right)  $\text{Sb}_2\text{O}_3$ .

Chalmers Reproservice  
Gothenburg, Sweden, 2017

# Studies on the Recovery of Secondary Antimony Compounds from Waste

TONI KARLSSON

Nuclear Chemistry and Industrial Materials Recycling  
Department of Chemistry and Chemical Engineering  
Chalmers University of Technology

## Abstract

The global supply of antimony is dominated by one country which has led the European Union to classify antimony as a critical raw material. Other than the rare-earth elements antimony has the highest supply risk. Therefore, a feasibility study on the recycling of antimony and antimony compounds is of great importance. This research focuses on two types of antimony containing wastes: (1) metal oxide varistors (MOVs) and (2) municipal solid waste incineration (MSWI) fly ash to determine if it is possible to recover secondary antimony. Recovery of antimony is highlighted because it is a critical element and the known natural resources are rapidly becoming depleted.

The MOVs contain a significant amount of antimony but have minimal waste volumes. Characterization of the MOV determined the microstructure of the MOV contained the three major phases (1) the zinc rich phase dominated by ZnO grains, (2) the antimony rich phase containing  $Zn_{2.33}Sb_{0.67}O_4$ ,  $Zn_7Sb_2O_{12}$ , and  $Zn_2Bi_3Sb_3O_{14}$  compounds, and (3) the bismuth rich phase made up of  $Bi_2O_3$ . To increase the antimony concentration, the MOV was pulverized and leached in a pre-treatment step. The pretreatment step removed the bulk ZnO grains from the MOV resulting in a zinc-sulfate leachate and antimony rich insoluble residue having a fivefold increase in antimony concentration. Removal of the minor metals such as cobalt, manganese, and nickel from the zinc sulfate leachate was done by activated cementation using Cu/Sb as activators and zinc dust as the reducing agent. It was determined for the MOV leachate system that the optimized cementations conditions for copper concentration, antimony concentration, zinc dust addition, temperature and pH were found to be  $0.8 \text{ g}\cdot\text{L}^{-1}$  Sb,  $0.4 \text{ g}\cdot\text{L}^{-1}$  Cu,  $T = 40 \text{ }^\circ\text{C}$ ,  $0.2 \text{ g}\cdot\text{L}^{-1}$  Zn addition in a solution of pH 5.0. A two-step batch cementation process resulted in 98 % removal of cobalt and 100 % removal of nickel making the purified zinc sulfate leachate suitable for zinc electrowinning. The antimony rich leach residue was subjected to heat treatment as well as carbothermal reduction in nitrogen atmosphere. Findings suggest that thermolysis of the MOV leaching residue and separation of antimony was not possible below  $1000 \text{ }^\circ\text{C}$ . However, carbothermal reduction of the MOV leaching residue showed it was possible to separate antimony at temperatures between  $700 - 825 \text{ }^\circ\text{C}$  by the decomposition of  $Zn_7Sb_2O_{12}$ . In this process antimony oxide,  $Sb_4O_6(\text{g})$ , was separated from the MOV residue leaving zinc oxide and other metals including bismuth, cobalt, manganese, and nickel. The volatilized  $Sb_4O_6$  can be recovered through condensation from the gaseous state.

Two MSWI fly ash samples were used (1) untreated and (2) HALOSEP-treated fly ash to determine the amount of antimony which could be extracted from MSWI fly ash as a function of pH. The HALOgen SEPARation (HALOSEP) process is used to remove water soluble salts such as NaCl, KCl,  $CaCl_2$ , and  $MgCl_2$  and to alter the leaching properties of the fly ash with respect to metals such as antimony, lead, and zinc. Results showed that the maximum amount of antimony that could be extracted from the ashes was approximately 20 % using a pH 1 HCl solution with L/S of 20. Increasing the pH gave lower antimony yields. It was determined that very little of the antimony could be recovered or removed from the fly ash, which makes commercialization of such a process difficult. However, leaching did cause the concentration of antimony in the dry residue to increase due to dissolution of bulk minerals, which suggests a two-step leaching process could be preferable for antimony recovery.

Keywords: Antimony, Cementation, Fly Ash, Leaching, Metal Oxide Varistor, Morphology, Municipal Solid Waste, Recycling, Thermolysis, Zinc

## LIST OF PUBLICATIONS

This thesis is based mainly on the work reported in the following papers:

### **Paper I:**

T. Gutknecht, A. M. K. Gustafsson, C. Forsgren, C. Ekberg and B.-M. Steenari (2015). "Investigations into Recycling Zinc from Used Metal Oxide Varistors via pH Selective Leaching: Characterization, Leaching, and Residue Analysis." The Scientific World Journal. vol. 2015. Article ID 653219. 11 pages

### **Paper II:**

T. Gutknecht, Y. Colombus and B.-M. Steenari (2017). "Recycling Zinc from Metal Oxide Varistors through Leaching and Cementation of Cobalt and Nickel." Journal of Sustainable Metallurgy **3**(2): 239-250.

### **Paper III:**

T. Karlsson, Y. Colombus and B.-M. Steenari. "Investigation of the Kinetics and the Morphology of Cementation Products Formed During Purification of Zinc Sulfate Electrolyte." Manuscript.

### **Paper IV:**

T. Gutknecht, C. Forsgren and B.-M. Steenari (2017). "Investigations into high temperature separation of antimony from metal oxide varistors." Journal of Cleaner Production **162**: 474-483.

### **Paper V:**

T. Gutknecht, C. Forsgren and B.-M. Steenari. "Recovery of Antimony: A laboratory study on the thermal decomposition and carbothermal reduction of Sb(III), Bi(III), Zn(II) oxides and antimony compounds from metal oxide varistors." Accepted to Journal of Sustainable Metallurgy 11/2017.

### **Paper VI:**

T. Karlsson, H. Jilvero, Y. Colombus, L. Nordhag, E. Rasmussen, C. Forsgren, and B.-M. Steenari. "pH-Dependent Leaching of Sb, Pb, and Zn from MSWI Fly Ash Before and After an Acid Treatment." Submitted to Waste Management 09/2017.

## STATEMENT OF CONTRIBUTION

Toni Karlsson (formerly Toni Gutknecht) is responsible for the authoring and most of the laboratory work in all papers with the support of the supervisors and co-authors. However, in paper III experiments were performed by Yuda Columbus for his Master's thesis research. Yuda Columbus also assisted in experimentation on papers II and VI.

# Table of Contents

<b>1. INTRODUCTION</b>	1
<b>2. BACKGROUND</b>	3
2.1. ANTIMONY	3
2.2. CHEMISTRY OF ANTIMONY	5
2.2.1. Primary Production	5
2.2.2. Antimony (III) Oxide	6
2.2.3. Other Antimony Compounds	7
2.3. ANTIMONY RECYCLING	8
2.4. WASTE CONTAINING ANTIMONY	9
2.4.1. Metal Oxide Varistor (MOV)	9
2.4.2. Municipal Solid Waste Incineration (MSWI) Fly Ash	11
<b>3. THEORY</b>	15
3.1. LEACHING	15
3.2. CEMENTATION	15
3.3. THERMAL TREATMENT	18
<b>4. MATERIALS &amp; METHODS</b>	20
4.1. MOV	20
4.1.1. Pretreatment	21
4.1.2. Leachate Purification Using Cementation	22
4.1.3. Cementation Product Morphology	22
4.1.4. Antimony Separation from the MOV Residue	23
4.2. FLY ASH	24
<b>5. RESULTS &amp; DISCUSSION</b>	26
5.1. ANTIMONY RECOVERY FROM THE MOV	27
5.1.1. MOV Pretreatment - Concentrating the Antimony	28
5.1.2. Leachate Purification Using Activated Cementation	31
5.1.3. Cementation Product Morphology	34
5.1.4. Antimony Separation from the MOV Residue	42
5.1.5. MOV Residue Morphology During Thermolysis and Carbothermal Reduction	45
5.2. ANTIMONY RECOVERY FROM MSWI FLY ASH	51
<b>6. SUMMARY &amp; CONCLUSIONS</b>	56
<b>7. FUTURE WORK</b>	60
<b>8. ACKNOWLEDGMENTS</b>	61
<b>9. REFERENCES</b>	62



## 1. INTRODUCTION

The United Nations sustainable development goal 12 is to ensure sustainable consumption and production patterns [1]. This goal states that two measures, i.e. the material footprint and the domestic consumption, provide an accounting of global material extraction and use, as well as flows or consumption of materials in countries. The material footprint reflects the amount of primary materials required to meet a country's needs. In developing countries the material footprint is significantly higher than in undeveloped countries. One way to decrease this measure is to increase the availability and use of secondary metals in production of goods. The general objectives for waste policy in the European Union and the US are thus to reduce the amount of the waste generated, maximize the recycling and re-use of matter, limit incineration to be applied only for non-recyclable materials, phase out landfilling to be used for non-recyclable and non-recoverable waste, and to ensure full implementation of the common waste policy targets in all member state policies [2].

In a sustainable system for use of materials, not only the production of goods needs to be sustainable, but also the management of residues and wastes. Brundtland [3] defines sustainability as, "the kind of development that meets the needs of the present without compromising the ability of future generations to meet their own needs." In the United States and some European countries landfilling has been the most used means for waste disposal [4]. However, nowadays recycling of materials from production waste and used products is recognized as a more sustainable way of managing waste than landfilling, since reclaiming materials from a landfill is not easily accomplished.

Metals are of limited supply within the earth's crust but most can be recycled and reused without loss of their properties. This research focuses on the recovery of a specific metalloid, antimony, from two waste streams. The first is metal oxide varistors (MOVs) commonly used on the power grid for protection against excessive transient voltages while the second is municipal solid waste incineration (MSWI) fly ash. There are several studies on the refining of main metals from raw materials and recycling sources. According to the report on the environmental benefits of recycling [5], Al, Cu, Pb, Ni, Sn, and Zn, recycling processes require about a quarter of the energy of primary processing, and also minimize CO<sub>2</sub> emissions. Although no data could be produced about antimony refining from primary and secondary sources, we can infer from data concerning other metals that Sb recycling has a smaller carbon footprint and needs less energy compared to the production from primary sources.

The amount of known extractable antimony remaining is estimated to be approximately 1.8 million tons [6], while the amount extracted up to 2012 was nearly 7 million tons [7], meaning only 21 % of primary antimony remains for extraction. At current mining rates, known antimony reserves will be depleted by 2027 [8]. Since there are 5 million more tons of antimony available from recoverable sources such as waste than available for extraction, the feasibility of antimony recycling and technology development needed to be investigated [7].

Over 50 % of antimony is used as a flame retardant [9] in for instance plastics, curtains, furniture, and other textiles, with many of these items ending up as municipal solid waste (MSW). It is estimated that the average antimony concentration in MSW is around 10 – 60 mg·kg<sup>-1</sup> [10, 11]. After incineration, the concentration of antimony in fly ash varies depending on the starting material and incineration conditions, but it has been shown to be less than < 2000 mg Sb·kg<sup>-1</sup> dry ash [12-15]. Due to the low antimony concentration designing a recycling route from an MSW waste stream can be difficult and cost ineffective [16]. MOVs however contain between 30,000 – 50,000 mg Sb·kg<sup>-1</sup> which is one of the highest concentrations, except for lead acid batteries, in consumer goods.

In Sweden, there is an initiative to recycle MOVs as opposed to landfilling due to environmental concerns, rising costs of landfilling, awareness of the value of the material in the MOV, and the quantity of material available for recycling. In 2013, one company in Sweden produced 132 tons of MOV [17] and in the last 5 years, 523 tons of MOV have been produced. Considering this is only one company in a relatively small country the amount of MOV produced and eventually available for recycling is encouraging as a source of secondary antimony and zinc. The used MOVs are primarily not mixed with other types of waste materials, at least in Sweden, but kept in a separate flow. This makes them an ideal case for a dedicated recycling method.

The incineration of municipal solid waste has become an integral part of many modern waste management systems in Europe, especially in Sweden where less than 1 % of household waste is landfilled [18]. Most household waste fractions are recycled and when that is not possible, they are incinerated to produce heat and electricity. The amount of municipal solid waste going to energy recovery in Sweden was 2,250,000 tons in 2015 [19, 20]. In addition to Swedish MSW, 3,491,190 tons of other waste, mainly industrial, was incinerated in Sweden, while 1,328,500 tons of MSW was imported from other countries, mainly from Norway, UK and Ireland, for energy recovery in Swedish combustion plants [20]. In total, about 7 million tons of waste was incinerated in Sweden during 2015. With an ash content of approximately 20 %, this corresponds to nearly 1.4 million tons of ash, of which almost 300,000 tons ends up as fly ash [19, 20]. MSWI fly ash often leaches salts and metals in amounts that are too high to comply with limit values for hazardous waste landfilling [21]. The extraction of antimony from MSWI fly ash is motivated due to the extremely low antimony leaching limit for admissions of the ash in landfills and the large amount of fly ash generated each year.

This work aims to determine if antimony can be extracted and recycled from waste, specifically MOVs and MSWI fly ash. The first step was to identify antimony containing compounds as well as characterize each of the materials. Since there is a limited amount of antimony being recycled today, several techniques were investigated for antimony extraction including leaching and thermal treatment. In literature, data on the thermal behavior of  $\text{Sb}_2\text{O}_3$  shows significant ambiguity. This is unfortunate since  $\text{Sb}_2\text{O}_3$  is the most important antimony compound from an industrial perspective and is used as a starting material in MOVs. Therefore, thermal properties of  $\text{Sb}_2\text{O}_3$  were also investigated.

## 2. BACKGROUND

### 2.1. ANTIMONY

Antimony is listed as a critical metal for the European Union [22] as well as a strategic metal for the United States Department of Defense [23] due to its supply, availability and increased use in consumer goods. The European Union is entirely dependent on imports of antimony, though total EU consumption in 2007 (792 tons) only accounted for 0.5 % of global production [22]. It is predicted that, apart from antimony, a national security emergency in the US would entail a severe shortage of just three other metals [23]. In 2016 the US imported 22,000 metric tons of antimony ores and concentrates, oxides, and metal for consumption [24] predominantly from the People's Republic of China. The trend from 1991 to 2016 for the US import reliance of antimony can be seen in Figure 1a in addition to the cost per pound.

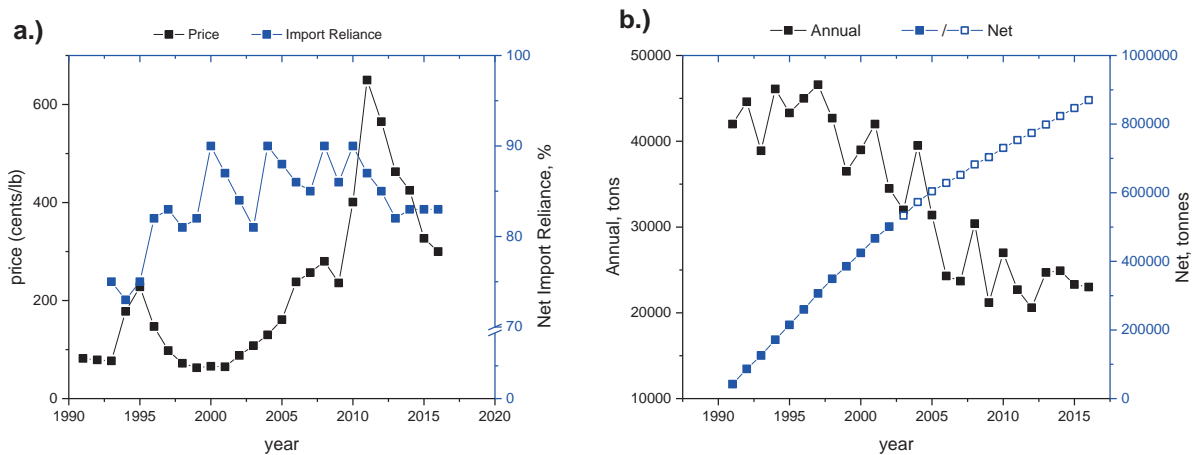


Figure 1: (a) cost per pound and US reliance on imports of antimony. (b) US annual consumption of antimony with accumulative consumption from 1991 to 2016. Adapted from [25].

In 2008 a total of 187,000 ton of antimony was produced, 91 % of which was produced in China. It is forecasted that there will be a large deficit of antimony by 2020 [26], and antimony will reach its peak production by 2018 [7]. The annual US consumption of antimony shown in Figure 1b, illustrates the general decline in consumption pattern in the US since the early 1990s. The net consumption starting from 1991 shows a line with two slopes. The first from 1991 – 2003 and the second from 2003 to 2016. The lower consumption rate seems to be correlated with the price of antimony.

There are over 100 minerals of antimony found naturally, however the most industrially important antimony compound is antimony oxide [27]. Commercial antimony compounds along with their main uses are listed in Table 1.

Table 1: A list of antimony compounds and their most common uses [10, 27, 28].

Antimony Compounds	Uses
Sb Metal	batteries, solder, electrical wire, pipe, ammunition catalyst for polyethylene terephthalate (PET) production
Antimony Oxide $Sb_2O_3$	halogen-compound flame retarding formulations paints, plastics, textiles and rubber white pigment in paints
Antimony Pentoxide $Sb_2O_5$	flame retardants
Sodium Antimonite, $NaSb(OH)_6$	flame retardants decolorizing glass refining agents for optical glass
Antimony Trisulfide, $Sb_2S_3$	pigment in black, vermilion, yellow, and orange camouflage paints because it reflects infrared radar liners of automobile brakes
Antimony Pentasulfide, $Sb_2S_5$	vulcanizing agent in the production of red rubber
Other antimony compounds	used in catalysts, pesticides, ammunition, and medicines

One of the most important industrial uses of antimony is as a flame retardant in clothes, toys, plastics, aircraft, automobile seat covers, etc. Antimony trioxide is used as a polycondensation catalyst in the manufacture of PET [29] and in cloths manufacturing as a catalyst for polyester production. Typical antimony concentrations in PET are 150-250 mg/kg [29]. Antimony metal has other uses such as hardeners in lead for batteries, bearing metal, and solder while nonmetal uses include antimony as an additive in glasses and ceramics, ammunition primers, fireworks, and in pigments. The distribution of antimony used in the US from 2001 to 2014 is shown in Figure 2 where the majority of antimony was used as a flame retardant [25].

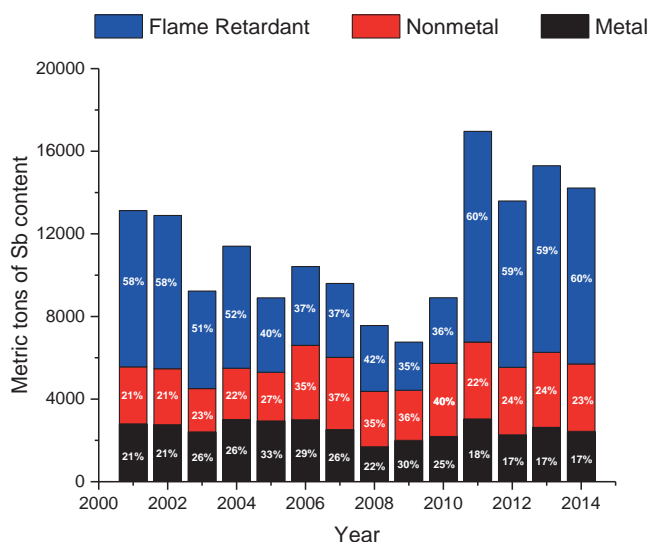


Figure 2: The amount and distribution of antimony used in the US from 2001 – 2014. Adapted from [25].

Future uses of antimony may be as a compound in semiconductors and as an antimony-tin-oxide alloy which has the same characteristics as indium-tin-oxide but is cheaper [22, 30]. Antimony can also be used in LCD displays, OLEDs or photovoltaic cells [22]. Antimony is being used industrially even though only relatively small amounts are needed. Because more products contain antimony the amount of antimony used annually is increasing, which, enhances the importance of recycling and recycling technologies.

## 2.2. CHEMISTRY OF ANTIMONY

Antimony is a silvery white metalloid located in group 5 row 11 of the periodic table and has an atomic mass of 121. It is found in the earth's crust at  $0.2 \text{ g}\cdot\text{ton}^{-1}$  [9] and is typically not found alone in nature because of its high affinity for other metals (i.e. copper, lead, silver) and sulfur [31]. Therefore antimony is typically produced as a byproduct from mining zinc, nickel, and other metals. Even though antimony is considered a metal, it is a poor conductor of electricity and heat, is brittle, and has a density of  $6.697 \text{ g}\cdot\text{cm}^{-3}$  at  $25 \text{ }^\circ\text{C}$  [24]. Antimony melts at  $630 \text{ }^\circ\text{C}$  and boils at  $1380 \text{ }^\circ\text{C}$ ; with a Mohr's hardness ranging from 3 to 3.5 it is too brittle to be used without alloying [32].

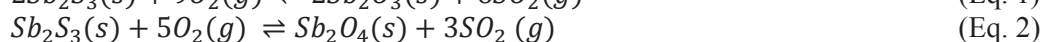
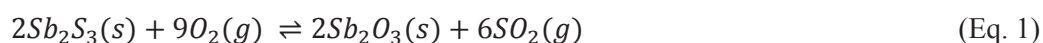
Antimony is found in the  $-III$ ,  $0$ ,  $+III$ , and  $+V$  oxidation states and is not known to serve any purpose in living organisms [33]. Most papers state that Sb ( $+III$ ) is more toxic than Sb ( $V$ ) however there is a lack of evidence and toxicity depends on many variables such as the organism or exposure route and time [33, 34]. In oxic media Sb ( $V$ ) and in anoxic Sb ( $+III$ ) are most stable. However, thermodynamic data is limited for both species with only a select few low molecular mass species reported for each. This lack of data is, in part, because both Sb ( $+III$ ) and Sb ( $V$ ) ions hydrolyze easily in aqueous solution, thus making it difficult to determine the concentrations of 'free' antimony ions in solution except in highly acidic or basic media or in very dilute solutions [35].

### 2.2.1. Primary Production

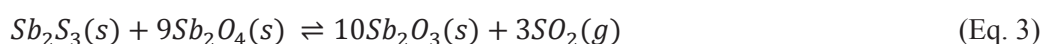
Antimony is commonly found in volcanic rock and sandstone at a concentration of approximately  $1 \text{ g}\cdot\text{ton}^{-1}$  [30]. There are two types of antimony ore deposits: simple and complex. Simple antimony deposits consist mainly of stibnite ( $\text{Sb}_2\text{S}_3$ ) while complex antimony deposits consist of stibnite along with pyrite ( $\text{FeS}_2$ ), arsenopyrite ( $\text{FeAsS}$ ), cinnabar ( $\text{HgS}$ ) or scheelite ( $\text{CaWO}_4$ ) [36]. Complex ore deposits are mined primarily for gold, lead, silver, tungsten, or zinc with antimony being recovered as a byproduct. Other sources of antimony besides ores are intermediates in processing lead and copper ores [22].

From mine to metal antimony goes through a typical purification/separation process starting with beneficiation which depends on the state of the antimony, the minerals associated with it in the ore and to a lesser extent how the ores are dispersed into the rock [36]. Typically, low grade and complex ores are beneficiated by floatation. Antimony ore is recovered primarily by pyrometallurgical techniques where Sb ( $III$ ) sulfide is converted into an oxide, which is then reduced producing Sb metal [36]. Removal of antimony as volatile  $\text{Sb}_2\text{O}_3$  from low grade ore is done only by pyrometallurgy [31]. Similarly, the ore can be partially roasted and allowed to react with sulfide to form the metal and sulfur dioxide [36]. Reverberatory furnaces are used mostly for the direct reduction of antimony rich oxide materials.

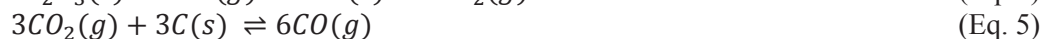
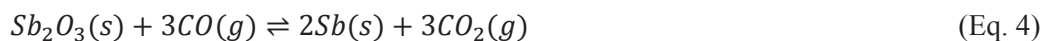
Volatilizing roasting of antimony sulfide has the advantage that volatile  $\text{Sb}_2\text{O}_3$  is produced selectively and is separated from the residue [36]. The oxide forms between  $290 \text{ }^\circ\text{C}$  and  $340 \text{ }^\circ\text{C}$  in an oxidizing atmosphere. The maximum reaction rate occurs near  $500 \text{ }^\circ\text{C}$  at which point a mixed valent Sb ( $III/V$ ) oxide begins to form if the oxygen concentration is in excess [31]. The reactions proceed as seen in Equation 1 – 2 where  $\text{Sb}_2\text{O}_4$  represents the mixed valent oxide.



Above  $560^\circ\text{C}$  the reaction rate drops considerably due to competing reactions. At this temperature the mixed valent oxide will react with Sb ( $III$ ) sulfide to form Sb ( $III$ ) oxide following Eq. 3.



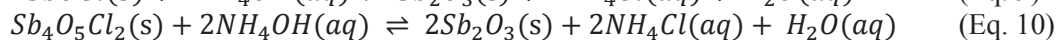
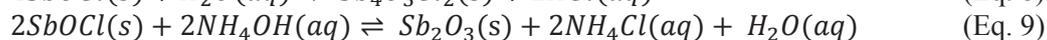
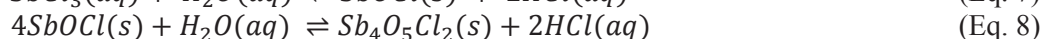
The reduction process must be tailored to occur rapidly, preferentially forming  $Sb_2O_3$ . During the condensation of Sb (III) oxide, the oxygen concentration in the gas phase must be kept low enough to prevent further oxidation to  $Sb_2O_4$ . Antimony oxides can be reduced with charcoal in a reverberatory furnace at temperatures near 1200 °C (carbothermal reduction). The reaction proceeds according to the following reactions in Equation 4 – 5 [31]. Apart from some work on the thermodynamics of the slag compositions used in Sb smelting, most of the publications concerning smelting technology date from around 1950.



Industrial hydrometallurgical antimony production practices consist of a two-step process of leaching followed by electrodeposition. Typically there are only two systems used for leaching, alkaline sulfide which is the dominating system and acidic chloride. The alkaline-sulfide system is most utilized because it is antimony selective and has minimal corrosion. However the chloride system is being applied with more success industrially [27]. When antimony is already oxidized it can be directly converted to the chloride with HCl according to Equation 6.



If the solution from the above reaction were placed into an electrochemical cell metallic antimony could be produced and collected on the cathode. The Sb-Cl system can also be treated by hydrolysis leading to precipitation of Sb from solution as solid Sb-oxychloride. Further treatment with ammonia produces antimony oxide as shown in Equation 7 - 10 [27]:



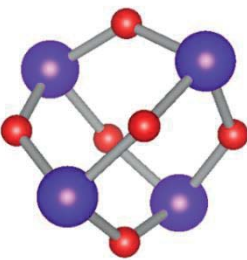
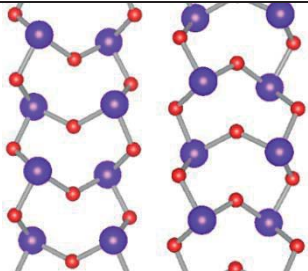
### 2.2.2. Antimony (III) Oxide

There are two known polymorphs of  $Sb_2O_3$ , cubic senarmontite and orthorhombic valentinite that have the properties listed in Table 2. The structure of antimony (III) oxide in the vapor phase has been shown to be discrete  $Sb_4O_6$  molecules which dissociate into  $SbO_3$  trigonal pyramidal units at high temperatures. Upon heating the cubic phase changes to a denser ( $5.20 - 5.79 \text{ g}\cdot\text{mL}^{-1}$ ) orthorhombic structure and a structural change to a polymeric form  $[Sb_2O_3]_n$ .  $Sb_2O_3$  is white in color, has a melting point of 655 °C and volatilizes thereafter.



Senarmontite directly sublimates at a temperature of 502 °C [37, 38] while valentinite is stable to 630 °C where sublimation and oxidation to  $Sb_2O_4$  are competing reactions. It is not known what the rate controlling step is in the oxidation of valentinite but it has been speculated by Centers [39] to be sublimation controlled when senarmontite sublimates to low-energy valentinite before oxidizing. The mixed valent oxide, Sb(III)Sb(V) $O_4$ , typically written as  $Sb_2O_4$  occurs in two crystal forms. The yellow mineral cervantite is orthorhombic  $\alpha$ - $Sb_2O_4$  and is converted into the monoclinic form by heating to 1100 °C [32].  $Sb_2O_4$  is very slightly soluble in KOH, HCl and HI [40] and can be synthesized by oxidation of  $Sb_2O_3$ .

Table 2: Properties of antimony (III) oxides.

Property	Senarmontite	Valentinite
<b>Chemical Formula</b>	$\alpha$ -Sb <sub>2</sub> O <sub>3</sub>	$\beta$ -Sb <sub>2</sub> O <sub>3</sub>
<b>Crystal Structure</b>	Cubic	Orthorhombic
<b>Structure [41, 42]</b>		
<b>Description</b>	Low temperature form consisting of molecular units of Sb <sub>4</sub> O <sub>6</sub> . Sb lies at the corners of a regular tetrahedron with 6 oxygen atoms lying on the edges.	Layered structure held together by weak Sb-O interactions. Each link contains three O <sup>2-</sup> ions and shares four Sb <sup>3+</sup> ions.
<b>Stability (both forms found naturally) [39]</b>	Low temperature, heating causes a solid-solid transition to $\beta$ -Sb <sub>2</sub> O <sub>3</sub> .	Metastable at ambient temperatures.
<b>Sublimation</b>	502 °C	mass loss starts at 450 °C
<b>Oxidation Temp Sb<sub>2</sub>O<sub>3</sub> to Sb<sub>2</sub>O<sub>4</sub> [43]</b>	> 510 °C	NA
<b>Density (g·cm<sup>-3</sup>) [40]</b>	5.2	5.67
<b>IR Peak (cm<sup>-1</sup>) [38]</b>	950, 740-720, and 385	690, 585, 540, 460, 352

Sb<sub>2</sub>O<sub>3</sub> is insoluble in water, dilute HNO<sub>3</sub> or dilute H<sub>2</sub>SO<sub>4</sub>, but soluble in concentrated HCl and organic acids [32, 40]. Dilution of a solution of Sb<sub>2</sub>O<sub>3</sub> in HCl results in increased pH causing precipitation of insoluble oxychlorides of various composition, for example SbOCl, Sb<sub>4</sub>O<sub>5</sub>Cl<sub>2</sub> and Sb<sub>8</sub>O<sub>11</sub>Cl<sub>2</sub> [32, 44]. Sb<sub>2</sub>O<sub>3</sub> is an amphoteric oxide due to its solubility in bases giving antimonates (III) [32]. Antimony (III) is a Lewis base due to its ability to donate a lone pair of electrons to a suitable Lewis acid. The ability of antimony (III) to act as a Lewis base is decreased depending on the electronegativity of the bonded atoms. Thus, antimony halides act as Lewis acids and can exhibit coordination chemistry with ligands such as phosphines and ethers [32]. Upon deprotonation carboxylic acids can form carboxylate ligands which can coordinate to antimony. The alpha-hydroxyl carboxylic acids such as glycolic, lactic and tartaric acid are able to form alpha-hydroxy carboxylates which are able to coordinate to antimony [45].

### 2.2.3. Other Antimony Compounds

Sb<sub>2</sub>O<sub>5</sub> is not a stable compound and is prepared by high temperature, high pressure oxidation of Sb<sub>2</sub>O<sub>3</sub> [46]. An impure Sb<sub>2</sub>O<sub>5</sub> can be prepared by carefully drying a hydrated, hydrolysis product of SbCl<sub>5</sub> [32]. Sb<sub>2</sub>O<sub>5</sub> is virtually insoluble in water but will dissolve in concentrated HCl. If the solution in concentrated HCl is diluted, hydrated antimony (V) oxide is precipitated. Sb<sub>2</sub>O<sub>5</sub> decomposes around 300 °C [32].

Chlorination can have a significant effect on the volatility of antimony. When antimony oxide becomes chlorinated during, for instance MSW incineration, antimony chlorides (SbCl<sub>3</sub>, SbCl<sub>5</sub>) are formed. These are highly volatile and the major fraction of Sb from these chlorinated compounds would be found in the gaseous phase. Pure SbCl<sub>3</sub> can be produced by distillation of the crude SbCl<sub>3</sub> or its solution in strong HCl in the presence of some Sb metal or Fe to reduce Sb (V) and iron (III) compounds [36]. SbCl<sub>3</sub> can also be recovered from complex antimony sulfide ores by reaction with CaCl<sub>2</sub>. The reaction takes place in an oxidizing (use FeCl<sub>3</sub> as reducing agent) atmosphere at ~500 °C where more than 90 % of the Sb is volatilized as SbCl<sub>3</sub> [36]. SbCl<sub>3</sub> has a melting temperature of 73 °C and a boiling point of 223 °C. It is hygroscopic and soluble in benzene, carbon disulfide, carbon tetrachloride, acetone, and ethanol.

F, Cl, Br, and I react violently with Sb to form a trihalide or a mixture of tri- and pentahalides [36]. The reaction between antimony and HCl yields  $\text{SbCl}_3$  or a mixture of  $\text{SbCl}_3$  and  $\text{SbCl}_5$ . Sb is resistant to concentrated HF, dilute HCl, and dilute nitric acids [36].

### 2.3. ANTIMONY RECYCLING

There are 5 million more tons of antimony available from recoverable sources such as waste than are available for extraction from ore [7]. It is therefore necessary to develop new methods to recover antimony from items which contain it. Antimony is typically present in industrial and commercial products in small amounts, which makes the recycling of antimony extremely difficult [47]. Conventional recycling routes are typically not applicable to metals such as antimony [16] if no pretreatment step(s) to create concentrates are taken. Pretreatment is performed in order to increase the antimony concentration or to allow for the proper separation of metals in further hydro- or pyrometallurgical recycling steps. From a recycling perspective, hardly any secondary antimony is recovered.

There are several waste streams from which antimony can be recovered; one success story is the recycling of antimony from lead acid batteries. In the lead acid battery, antimony is used in lead-antimony alloy plates as a hardener. The concentration of antimony in lead acid batteries has been declining due to advances in battery technology; however, the use of lead acid batteries continues to increase. In 2014 the US recycled 99 % (21.1 million tons) of lead acid batteries [48]. It is the most recycled product in the US due to the successful implementation of a policy restricting battery disposal in landfills and the availability of collection sites. Lead acid batteries are the main source of secondary antimony where the antimony concentration is around 5 – 11 wt% [49]. Antimony is recovered from the secondary lead smelter as an antimonial lead mixture and put back into the production of new batteries [8]. In 2016, the US recycled 4000 metric tons of antimony [24]. The estimated value of secondary antimony produced in the US (2016) was 26 million USD [8]. Figure 3 shows the amount of secondary antimony produced in the US from 1991 to 2016 [25].

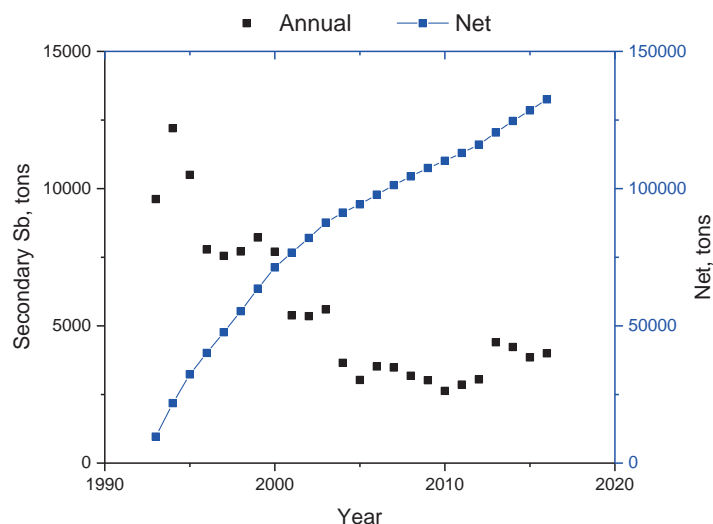


Figure 3: Annual secondary antimony production in the US from 1991 to 2016. As well as the net cumulative secondary antimony production since 1991. Adapted from [25].

In ammunition, lead is alloyed with antimony (2 - 5 wt%) [50]; therefore, the accumulation of ammunition fired at shooting ranges could be a potential source of secondary antimony. In a study by Johnson et al. 2005 [50], the antimony concentration in shooting range soil samples was shown to be 35 to 17,500  $\text{mg}\cdot\text{kg}^{-1}$ .

Antimony recovery from municipal solid waste (MSW) incineration ash is another possible source of secondary antimony. MSW contains items having antimony thinly dispersed within them. Incineration can be thought of as a type of pretreatment step. Household wastes such as textiles contain  $25.9 \text{ mg} \cdot \text{kg}^{-1}$  antimony while plastics and rubber contain  $12.9 \text{ mg} \cdot \text{kg}^{-1}$  and  $8.4 \text{ mg} \cdot \text{kg}^{-1}$  respectively [51]. Items such as curtains contain larger concentrations of antimony than for example wood waste. It is estimated that the average antimony concentration in MSW is around  $10 - 60 \text{ mg} \cdot \text{kg}^{-1}$  [10, 11]. After incineration, the concentration of antimony in fly ash varies depending on the starting material and incineration conditions, but it has been shown to be less than  $< 2000 \text{ mg Sb} \cdot \text{kg}^{-1}$  dry ash [12-14].

In some cases, antimony is added to ceramics as a pigment and it can also be used to enhance specific characteristics. Antimony oxide is used in a type of ceramic known as the metal oxide varistor, which is a zinc oxide based ceramic semiconducting device with a high degree of non-linear current-voltage characteristics. The main application of zinc oxide varistors is in circuits for overvoltage protection. An example of its use is in surge arrestors or lightening protectors on power lines [52]. Zinc oxide varistors are commonly referred to as metal oxide varistors (MOVs) due to the presence of zinc and other metals such as antimony and bismuth. It is not known how much antimony is available from varistors worldwide. However, used varistors could be a good source of recovered antimony since their Sb concentration is relatively high ranging between 3 - 5 wt%. In Sweden, it has been estimated that from 2009 to 2013 just over 520 tons of varistors were produced [17]. If secondary antimony oxide were to be recovered from those at their end of life, 23 tons of antimony would be available for reuse. In 2015 Sweden imported nearly 100 tons of antimony (III) oxide [53].

## 2.4. WASTE CONTAINING ANTIMONY

### 2.4.1. Metal Oxide Varistor (MOV)

The desired property of a MOV is that it be a perfect insulator up to the breakdown voltage above which point it should become highly conductive. Surge arrestors are important parts of power and rail systems because they offer protection from over voltages due to lightning or transients in the power grid. The need to replace or build power lines is increasing with demand from developing countries. Thus, many surge arrestors need to be replaced to accommodate larger voltage requirements. The end of life surge arrestors can be disassembled giving rise to a material rich in antimony and zinc oxides amongst other metals. Figure 4 shows the different areas where surge arrestors are used. The surge arrestor contains many parts such as: porcelain insulator, venting duct, spring, desiccant bag, copper sheet, sealing cover, sealing ring, indication plates, ZnO blocks, and flange cover [54]. This work will focus solely on the metal oxide varistor, i.e. zinc oxide varistor. The MOVs are housed inside the surge arrestor where they are stacked in series and separated by a thin layer of aluminum [55].



Figure 4: Surge arrestor at a) power station in Borås Sweden, b) connected to railway line, c) power lines outside housing developments, and d) portable electronics.

MOVs are made by combining powdered metal oxides of zinc, antimony, bismuth, manganese, nickel and cobalt. Typically MOVs contains greater than 90 mol% ZnO, around 3 mol% of both Bi<sub>2</sub>O<sub>3</sub> and Sb<sub>2</sub>O<sub>3</sub> with the other metal oxides accounting for the remaining 4 mol% [4, 56]. The purpose of Sb<sub>2</sub>O<sub>3</sub> in the MOV is to decrease the average size of the ZnO grains [57-59]. The current-voltage behavior of the MOV is attributed mainly to the presence of Bi<sub>2</sub>O<sub>3</sub> [58] which also strongly alters the sintering behavior by producing a liquid phase with ZnO enabling liquid phase sintering [56, 60, 61]. It has been reported in literature that metal oxides such as MnO<sub>2</sub>, NiO and Co<sub>2</sub>O<sub>3</sub> and other minor metal oxides may be present in the MOV added to enhance the characteristics of the MOV [55-57, 59-61]. The homogenized metal oxide powder is sintered in a process during which three main microstructural phases form [55, 59, 62]:

1. ZnO grains,
2. the antimony-rich phase, and
3. the bismuth-rich intergranular phase.

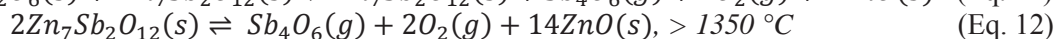
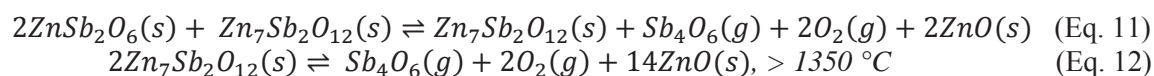
The ZnO grain phase is by far the most dominant region due to the MOV being composed mostly of zinc oxide [63]. The antimony-rich phase resulting from sintering and reactions between the metal oxides have been known to include a pyrochlore [57, 58, 64] as well as a spinel-like phase each with different stoichiometry [58, 65]. Pyrochlore is a zinc-bismuth-antimony-oxide (Zn<sub>2</sub>Bi<sub>3</sub>Sb<sub>3</sub>O<sub>12</sub>) [66] while the spinel phase has been shown to exist in both the cubic (Zn<sub>2.33</sub>Sb<sub>0.67</sub>O<sub>4</sub>) and orthorhombic (Zn<sub>7</sub>Sb<sub>2</sub>O<sub>12</sub>) configurations [67].

Zinc oxide is soluble in both acidic and basic media. The most common way to produce zinc is by roast-leach-electrowinning (RLE) where ZnS is converted (at high temperatures) into ZnO [68], zinc along with other low level impurities are co-leached using sulfuric acid, H<sub>2</sub>SO<sub>4</sub>. Impurities act as catalysts for hydrogen evolution, co-deposit with zinc, and causing large drops in current efficiency reduction [69, 70]. It has been shown that even low concentrations of impurities such as antimony and cobalt in the electrolyte can reduce the current efficiency of zinc electrowinning by nearly 80 % [70].

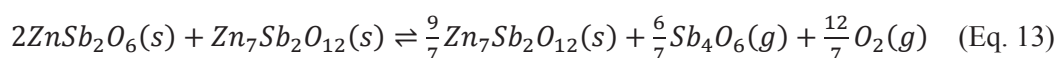
To purify the zinc rich leachate, cementation is used. Since H<sub>2</sub>SO<sub>4</sub> is used commercially in zinc production it is natural to select H<sub>2</sub>SO<sub>4</sub> as an ideal leachate for extraction of zinc from the MOV material. Ideally an acid adjusted to a selected free H<sup>+</sup> concentration which only leached zinc would be preferred, but it is known from literature that leaching of cobalt and nickel will likely accompany the zinc during acid leaching of the MOV material [70-72].

In addition to cementation there are many methods which can be used to purify a liquid stream such as an impure zinc sulfate leachate including: activated charcoal adsorption, ion exchange, solvent extraction, and precipitation. Cementation is suitable when there is a small amount of impurities to remove and was chosen here because of the low concentration of cobalt and nickel impurities. The addition of zinc dust increases the zinc ion concentration and its proven ability to remove noble (higher reduction potential) metals from solution. Cementation can also be used in conjunction with solvent extraction [73].

Selectively removing the zinc oxide phase would leave the Bi<sub>2</sub>O<sub>3</sub> intergranular phase and the antimony rich phase [59]. Work done by Filipek et al. [74] showed that change in mass occurred due to the decomposition of ZnSb<sub>2</sub>O<sub>6</sub> and Zn<sub>7</sub>Sb<sub>2</sub>O<sub>12</sub> at 1500 °C when heating in air. Their work also showed that in air β-Zn<sub>7</sub>Sb<sub>2</sub>O<sub>12</sub> remained in equilibrium with ZnO up to 1225 °C, whereas β-Zn<sub>7</sub>Sb<sub>2</sub>O<sub>12</sub> transitioned to α-Zn<sub>7</sub>Sb<sub>2</sub>O<sub>12</sub>. At temperatures greater than 1350 °C α-Zn<sub>7</sub>Sb<sub>2</sub>O<sub>12</sub> decomposes to ZnO releasing Sb<sub>4</sub>O<sub>6</sub>(g) and O<sub>2</sub>(g) [75]. The reactions are given by Equations 11 – 12 [74]:



In argon, samples with ZnO and  $\beta$ -Zn<sub>7</sub>Sb<sub>2</sub>O<sub>12</sub> remain in the solid state until approximately 1115 °C when Zn<sub>7</sub>Sb<sub>2</sub>O<sub>12</sub> starts to decompose according to the reaction given in Equation 13. Above this temperature it may be possible to recover antimony as Sb<sub>4</sub>O<sub>6(g)</sub>.



Using carbothermal reduction may make it possible to recover the antimony by volatilization and then condensation of Sb metal or Sb<sub>4</sub>O<sub>6(g)</sub> from reduction of the spinel/pyrochlore (Zn<sub>7</sub>Sb<sub>2</sub>O<sub>12</sub>, Zn<sub>2.33</sub>Sb<sub>0.67</sub>O<sub>4</sub>, and Zn<sub>2</sub>Bi<sub>3</sub>Sb<sub>3</sub>O<sub>14</sub>) compounds. From an industrial perspective, the addition of carbon to both zinc and antimony oxides has been shown to lower the reduction temperature [31, 76].

#### 2.4.2. Municipal Solid Waste Incineration (MSWI) Fly Ash

Antimony is present in MSW mainly as Sb<sub>2</sub>O<sub>3</sub> and Sb<sub>2</sub>O<sub>5</sub> since it is a flame retardant and also used as a catalyst in polymerization of plastics. Over 60 % of antimony is used as a flame retardant and of that 35 % comes as a flame retardant in consumer electrical and electronic equipment. Due to the increased use of electronics and an ever expanding consumer and product base there seems to be no decline in the concentration of antimony in municipal waste incinerator feedstock. This makes the ash a candidate for a secondary source of antimony. There is an increased incentive to recycle antimony from incineration residues due to its toxicological and hazardous properties [11]. The concentration of antimony in fly ash is normally around 100 – 1300 mg·kg<sup>-1</sup> [77]. However, the partitioning of antimony between the bottom ash, fly ash and APC residues is highly sensitive on the incineration conditions [77, 78].

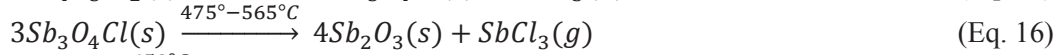
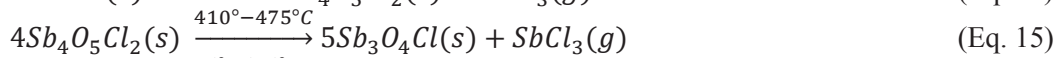
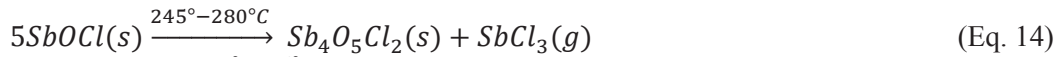
The feedstock for municipal solid waste incineration (MSWI) is complex and can contain many hazardous elements. The demands placed on air pollution control (APC) systems are very rigid. A series of processes, such as filters, scrubbers, and catalytic reactors are used to prevent potentially hazardous gases and particles from reaching the atmosphere and the soil. From these processes, APC residues are formed. One of the most troublesome APC residues is the fly ash collected in the filters. Fly ash particles are not homogeneous and the composition depends on the incineration environment, the APC control system and the composition of the incinerator feed material [79]. Particle size is generally small and the fly ash contains high levels of potentially toxic substances, which are susceptible to leaching into soil, water supplies, and being taken up by organisms. The most notable of the problematic substances are As, Sb, Cd, Cu, Cr, Pb, Hg, Zn [77, 80, 81]. Typically, an increased incineration temperature will increase the volatilization of metals such as Pb, Sb, and Zn. Thus, these metals will partition more to the fly ash than to the bottom ash (slag) [77].

Antimony within consumer goods occurs mainly in the Sb (III) redox state, which is more volatile than the oxidized Sb (V). Therefore, Sb (III) should preferentially go to the APC residues and fly ash while the less volatile Sb (V) partitions between the bottom and fly ash [82]. In the presence of CaO, Sb (III) will be oxidized to Sb (V) by formation of less volatile calcium antimonates found in the bottom ash [83] but possibly also in fly ash.

Belevi and Moench [78] determined that the majority of antimony partitioned to the fly ash and APC residues with the majority, up to 88 %, going to APC residues. Others have reported around 50 % of the antimony ending up in the fly ash and APC residues [84]. A study done by Dorge et al. [85] specifically on the thermal treatment of Sb-rich halogenated waste concluded that at 850 °C, 64 % of Sb was volatilized having a +III oxidation state, but increasing the temperature to 1000 °C resulted in the same amount of Sb volatilization but with a higher amount of the oxidized Sb (V) species. Similarly, work by Klein et al. [85], determined the transformation of Sb<sub>2</sub>O<sub>3</sub> to Sb<sub>2</sub>O<sub>5</sub>, would require a temperature of 1100 °C. This indicates that higher incineration temperatures result in more Sb (V) in the fly ash and APC residues which is known to be the less toxic form.

In a study done by Takaoka et al. [12] three different fly ash samples from a continuous stoker type MSW combustor were studied. Using the antimony K-edge x-ray absorption near edge structure (XANES) spectra it was concluded that Sb was penta-valent in all fly ash wastes, most likely present as  $Sb_2O_5$  [12]. In a speciation study done by van der Hoek et al. [86] determined that Sb (V) is the predominate species found in fly ash leachates, with only a minor amount of Sb (III) detected, independent of the alkalinity of the fly ash used. Their findings also suggested that the oxidation state and possibly the chemical state of antimony was the same in all ash samples independent of furnace types, waste feed, and particles carried over from the furnace, dust collector type and the method used for acid gas removal [12].

$Sb_2O_3$  is the most industrially used Sb containing compound where it is used as a flame retardant along with halogens (Cl or Br). When  $Sb_2O_3$  is joined with a halogenated organic compound they have a synergistic effect resulting in an effective flame retardation agent [87]. During the incineration of MSW which contain plastics,  $SbCl_3$  may be released according to Equations 14 - 17.



Chlorination can have a significant effect on the volatility of antimony. Calculations made by Paoletti et al. [88] determined that antimony oxides formed in the combustion chamber are easily converted to antimony chlorides or oxychlorides if enough oxygen and chlorine are available. Antimony chlorides are more volatile than the oxides [85, 88]. Since MSW commonly has a high chlorine content, the formation of antimony chloride is possible. If the overall conditions in the incinerator are oxidizing formation of  $Sb_2O_3$ ,  $Sb_2O_4$  and  $Sb_2O_5$  is more likely [85].

As with MOVs, the recovery of secondary antimony from MSWI fly ashes will require a pretreatment step(s). Unlike MOVs the fly ash contains many elements from which it may prove difficult to produce a pure antimony stream. Leachability of metal species in the ash can be affected by the porosity and surface area of the ash particles, element speciation, and the concentration gradient of the leached element. The adsorption of dissolved ions on ash bulk mineral surfaces can also be considered as a secondary reaction [89]. Antimony species reported in literature, believed to be present in APC and fly ash, include  $Sb_2O_3$ ,  $SbO_2$ ,  $Sb_2O_4$ ,  $Sb_2O_5$ ,  $SbCl_3$ ,  $SbCl_5$ ,  $SnSbS_4$ ,  $Pb_3Sb_2O_7$ , Sb-oxychlorides, and calcium antimonates [10, 12, 84, 90].

Both the cubic and orthorhombic crystal forms of  $Sb_2O_3$  are soluble in KOH, HCl, tartaric acid and acetic acid [40]. Cubic  $Sb_2O_3$  is more thermodynamically stable and has a lower solubility than orthorhombic  $Sb_2O_3$  [91]. It has been shown that cubic  $Sb_2O_3$  is not stable in chloride bearing solutions [44]. This means the Sb concentrations in solution decrease over time. In neutral to weakly-acid solutions, the solubility is independent of pH, which indicates the formation of the predominate neutral  $Sb(OH)_3(aq)$  complex according to [92]:



$Sb_2O_5$  is virtually insoluble in water but will dissolve in concentrated HCl, although the dissolved species have not been identified. If the solution in concentrated HCl is diluted, hydrated antimony (V) oxide is precipitated [32]. The mixed valent oxide,  $Sb_2O_4$  of antimony  $Sb(III)Sb(V)O_4$  occurs in two crystal forms. The yellow mineral cervantite is orthorhombic  $Sb_2O_4$  and is converted into the monoclinic form by heating to 1100 °C.  $Sb_2O_4$  is very slightly soluble in KOH, HCl and HI [40] and can be synthesized by oxidation of  $Sb_2O_3$ . Antimony chlorides have a high solubility in HCl,  $CHCl_3$ , as well as organic acids such as tartaric acid [40, 93].

Numerous authors [21, 81, 90, 94] have investigated the extraction of zinc from MSW fly ashes. Their results suggest that HCl, HNO<sub>3</sub>, H<sub>2</sub>SO<sub>4</sub> and EDTA are the most efficient in leaching zinc from fly ashes. However, important parameters such as pH, L/S, temperature and time need to be considered and optimized. A study by Fedje et al. [21] showed that less than 1 % of zinc could be leaching when using organic acids such as acetic, formic, lactic and oxalic acid at an L/S of 5 [21]. Since it has been reported that leaching Sb and Zn using HCl is feasible, and because HCl is available as a byproduct at the incineration facility, it seems to be a logical choice for an investigation.

MSWI fly ash often leaches salts and metals in amounts that are too high to comply with limit values for hazardous waste landfilling [21]. In addition, there are restrictions for how much leachable chloride and sulfate that ash may contain and still be allowed at a landfill [95]. This has led to the situation where most Swedish MSWI fly ashes are exported to Norway for landfilling in an old limestone quarry on the island of Langøya, operated by NOAH AS. At this facility, waste acids from other industries are used to stabilize the alkaline fly ash [96]. There are emerging technologies which can offer solutions allowing fly ash to be treated and landfilled locally to avoid the export of hazardous waste. The HALOgen SEPARation (HALOSEP) [97] process is, as the name indicates, a process in which mainly water soluble salts (chlorides and sulfates), but also metal compounds, are removed from the MSWI fly ash. The process has been brought to market by Stena Metall AB, Sweden. In the process, two waste streams are co-treated to produce more stable and less hazardous products.

The fly ash is captured at the combustion plant as solid particles in a bag filter or electrostatic precipitator. It includes common ash minerals, volatile heavy metals, unburnt carbon, salts and also residues from the air pollution control system (lime or activated carbon). Many MSWI units also include an acid scrubber where water is used to capture water soluble acid gases in the flue gases, mainly hydrochloric acid formed by the combustion of waste which contains chlorides, e.g. PVC plastics or food waste. Figure 5 shows a simplified schematic of the HALOSEP process. The alkaline fly ash is leached and neutralized with acidic scrubber liquid (dilute HCl) available at the combustion plant.

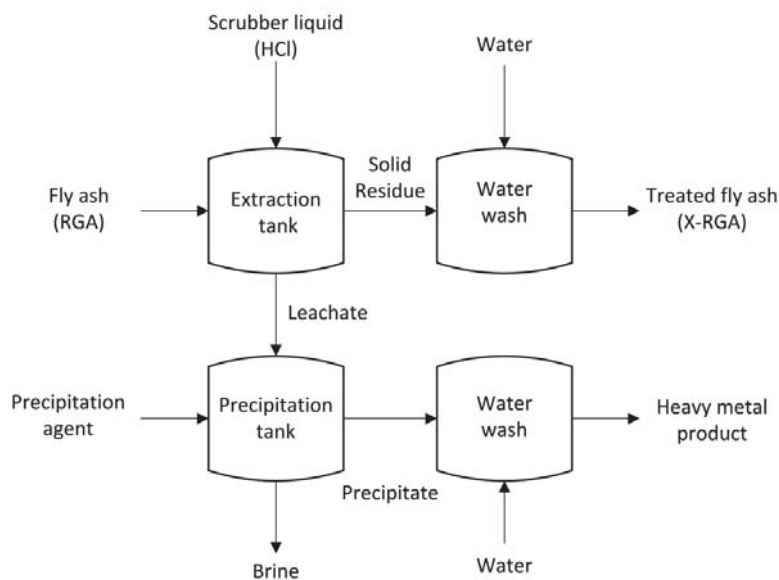


Figure 5: A simplified process schematic of the HALOSEP process.

In the extraction tank, the scrubber liquid is mixed with the fly ash coming from an ash silo. The mixture will have a minimum pH of around 4, after mixture with the pH 1 scrubber liquid, and is kept at that level during leaching. In these conditions, most of the water soluble salts are dissolved and also some of the metal compounds. The solid residue is separated and washed before being transported for further use as a construction material or disposed of in a landfill. The leachate goes to a precipitation tank where the metals are precipitated. The metal precipitate is washed and can be sold to a smelter for metal recycling. The residual brine will mainly consist of salts such as NaCl, KCl or CaCl<sub>2</sub>.

The HALOSEP process has been shown to result in the reduction of fly ash weight by approximately 50-55 %, and most often the treated ash is stable enough to pass leaching tests [98]. However, one issue with the HALOSEP process which has been identified is that although the leaching of most of the metals is significantly decreased, the mobility of antimony is in some cases too high to comply with non-hazardous waste landfill acceptance criteria. Antimony is subjected to strict regulations in the EU landfill directive. Thus, there is a need to evaluate the leachability of antimony from MSWI fly ash both before and after the HALOSEP treatment, as well as the pH range in which antimony is most mobile.

### 3. THEORY

#### 3.1. LEACHING

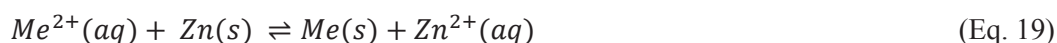
Leaching is the dissolution and transport of a soluble compound from a solid phase into a solvent. It has been shown that the speciation of elements is one of the most important factors affecting their leachability [99]. When designing a recycling process the selection of leaching agent is vitally important because of its influence on the sequential recycling steps. Other parameters to take into consideration when choosing a suitable leaching process include leachate concentration, time, temperature, surface area/particle size, liquid to solid (L/S) ratio, and the properties of the metal to be extracted.

#### 3.2. CEMENTATION

Cementation is an old technology used to recover metal ions from solution. It is carried out by the addition of a less noble metal usually cheap and nontoxic causing reduction and precipitation of the more noble metal from solution. The more noble metal is deposited on the less noble metal surface. An example of a commonly used active metal is zinc which is typically used for two reasons: (1) it is needed as a reducing agent and (2) it increases the zinc concentration in solution. Cementation reactions can be very complex and involve multiple chemical and mass transfer steps including [100]:

- Transport of the electroactive species from the bulk solution to the surface,
- Electron transfer from the dissolving metal species to the electroactive species,
- Incorporation of the deposited metal into the crystal lattice,
- Desorption of the metal ion, and
- Transportation of the dissolved metal ion from the surface to the bulk solution.

The overall cementation reaction using zinc as the reducing metal can be written as shown in Equation 19, where Me is a metal with a more positive reduction potential than zinc. Common metals which are removed by cementation include antimony, arsenic, cadmium, cobalt, copper, iron, nickel, thallium, etc. Like leaching, cementation is a heterogeneous reaction where the system involves more than one phase.



The standard reduction potential ( $E^\circ$ ) can be used to thermodynamically estimate if a metal in solution can be cemented from a zinc-sulfate leachate upon addition of zinc dust. Because of their presence in the MOV antimony, bismuth, cobalt, manganese and nickel were considered and their standard reduction potential are given in Table 3 versus the standard hydrogen electrode (SHE). Metals with a reduction potential higher than zinc ( $E^\circ > -0.762 \text{ V}$ ) are thermodynamically predicted to be reduced upon addition of zinc dust. For cobalt cementation the reaction should proceed according to Equations 20 - 22.

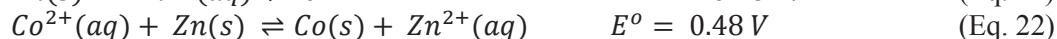


Table 3: Selected standard reduction potentials in aqueous solutions at 25 °C vs. SHE [32, 101].

Reduction half-reaction	Potential, $E^\circ$ (V) vs SHE
$Mn^{3+} + e^- \rightarrow Mn^{2+}$	+1.56
$Cu^{2+} + 2e^- \rightarrow Cu$	+0.339
$SbO^+ + e^- \rightarrow Sb$	+0.204
$Bi^{3+} + 3e^- \rightarrow Bi$	+0.20
$2H^+ + 2e^- \rightarrow H_2$	0.00
$Ni^{2+} + 2e^- \rightarrow Ni$	-0.236
$Co^{2+} + 2e^- \rightarrow Co$	-0.282
$Zn^{2+} + 2e^- \rightarrow Zn$	-0.762
$Mn^{2+} + 2e^- \rightarrow Mn$	-1.182

The reduction of cobalt together with the oxidation of the zinc yields a reaction with a cell potential difference of 0.48 V. The potential difference can be related to the standard Gibb's free energy,  $\Delta G^\circ$ , by Equation 24.

$$\Delta G^\circ = -nFE^\circ \quad (\text{Eq. 23})$$

$$\ln k = -\frac{\Delta G^\circ}{RT} \quad (\text{Eq. 24})$$

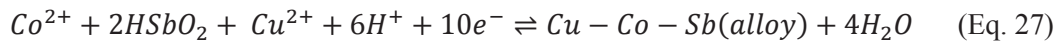
Where, n is the number of electrons transferred in the oxidation-reduction reaction, F is Faraday's constant and  $E^\circ$  is the standard potential of the chemical reaction given in Equation 22 yielding a standard Gibb's free energy of  $\Delta G^\circ = -92.7 \text{ kJ}$  as calculated using Equation 23. From the standard potential, the equilibrium constant,  $K_{eq}$ , is calculated using Equation 24 to be  $1.7 \times 10^{16}$  [70]. The equilibrium constant suggests the cobalt cementation reaction given in Equation 22 should proceed and not back react. However, this is not seen experimentally due to slow reaction kinetics of cobalt [102].

Activators are used to accelerate the cementation of cobalt. Typical activators include Cu/As or Cu/Sb [72, 103]. Since antimony may be present in the MOV leachate in small amounts it is the natural choice for an activator. The mechanisms describing the behavior of the activators in the cementation process are not well understood [70] and most research focuses on process optimization.

When used as activators, copper and antimony are thought to form an alloy with cobalt [70]. Fontana and Winand [70, 104] were able to identify CoSb and CoSb<sub>2</sub> in the cementation product using XRD. No diffraction peaks indicating the presence of metallic Sb or Co were observed. Makimoto [105] developed an antimony and lead containing zinc dust for purification and proposed that on the antimony of the Zn-Sb<sub>(9.1-1.0%)-Pb(0.5-5%)</sub> alloy cobalt is being reduced according to Eq. 25, and on the zinc of the Zn-Sb<sub>(9.1-1.0%)-Pb(0.5-5%)</sub> alloy zinc is being oxidized as shown by Eq. 26.



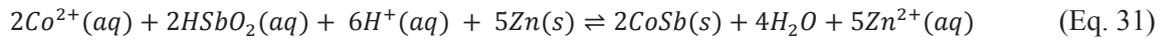
Blanders and Winland [106] proposed that cobalt forms an alloy with copper and antimony according to Equation 27. For cementation Eq. 27 is coupled with Eq. 28.



Kroleva [107] suggested the formation of a Cu<sub>2</sub>Sb alloy which enhances cobalt formation shown in Eq. 29 and Eq. 30.

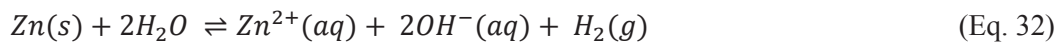


Using potential-pH diagrams Tozawa et al. [105] suggested that cementation of cobalt with antimony and copper between pH 3-5 proceeds according to Equation 31. However, their investigation of the cementation product using SEM-EDX showed that copper and antimony co-existed but not with cobalt. The cobalt was found around the copper-antimony deposit.



Although, there are many theories on the role of activators during cementation the mechanism by which it proceeds is not well understood [103]. In addition to activators, parameters that are known to affect cementation reactions are pH, temperature, activator concentration, and zinc dust quantity [70-72, 102, 103, 105, 108-113].

The solution pH during cementation may be one of the most important parameters. The addition of zinc dust causes the pH of the solution to rise according to Equation 32. The pH of the leachate must be kept low enough as to not precipitate basic zinc sulfate salts such as:  $Zn(OH)_2ZnSO_4 \cdot 4H_2O$  [103, 111]. It has been suggested by Børve et al. [103] that on an industrial scale, it is more important to avoid hydrogen production than the formation of basic zinc sulfate precipitation although both can be detrimental. Thus, the pH needs to be kept low enough during cementation experiments to ensure that no zinc salts are formed. However, locally this can be unavoidable due the charge imbalance in the double layer.



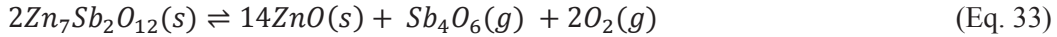
Lew [114] reported that the mass transfer coefficient for zinc is much smaller than for hydrogen which results in a higher zinc concentration in the double layer surrounding the zinc dust particle. The zinc cations will create a charge imbalance that will be equilibrated by anions, possibly hydroxyl and sulfate ions [100]. Reaction of the zinc dust with the leachate causes the localized pH to rise and precipitation of basic salts:  $ZnSO_4$ ,  $ZnO$ , or  $Zn(OH)_2$ . Zinc salts are fatal in cementation because it coats the zinc dust, eliminating the surface chemistry needed for cementation of other metals.

Elevated temperatures result in a faster rate of cobalt cemented from the solution due to increased reaction kinetics [100, 115]. Literature suggests that the optimal temperature for cobalt cementation is between 75 and 90 °C [71, 111, 113]. From an industrial perspective, temperatures higher than 70 °C are used for cobalt cementation but it has been seen by Van der Pas et al. [102] that once above 85 °C hydrogen evolution retards the cobalt cementation.

Van der Pas et al. [102] concluded that the optimal conditions for cementation in a solution containing 30  $mg \cdot L^{-1}$  cobalt were 30  $mg \cdot L^{-1}$  copper and 1.5  $mg \cdot L^{-1}$  antimony (both as activators) as well as the addition of 4  $g \cdot L^{-1}$  zinc at a solution temperature of 70 °C. Børve [103] suggested that optimal conditions for cobalt (15  $mg \cdot L^{-1}$ ) cementation arise when the solution contains 50-100  $mg \cdot L^{-1}$  copper and 3-4  $mg \cdot L^{-1}$  antimony (both as activators) with a solution temperature less than 80 °C. Work by Boyanov et al. [109] determined that maximum cobalt removal occurs at a temperature of 80-85 °C, copper concentration of 200-300  $mg \cdot L^{-1}$  and 18 times the stoichiometric amount of zinc dust. According to their work [109], maximum removal of cobalt and nickel occurs when the Sb:Co ratio is between 0.5:1 and 2:1.

### 3.3. THERMAL TREATMENT

Many different technologies are used in the production of metals and metal products. Technologies which operate at high temperatures and involve the interaction between molten material and gases is known as pyrometallurgy. Thermolysis simply uses energy in the form of heat to bring about the decomposition of a compound. Antimony oxide is produced by volatilizing antimony metal in an oxidizing atmosphere [27]. Therefore, high temperature decomposition achieved by thermolysis was considered as a suitable process for recovering antimony by condensing volatilized  $Sb_4O_6$ . Work by Filipek and Dąbrowska [74] suggests that the breakdown of the  $Zn_7Sb_2O_{12}$  spinel phase occurs at temperatures above 1350 °C in argon which would then be the temperature at which it may be possible to recover antimony as  $Sb_4O_6(g)$  following Equation 33.



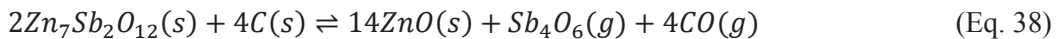
A generic reaction for thermolysis is given in Equation 34. The decomposition of a metal oxide to yield a metal is a reduction reaction. Carbothermal reduction, a type of smelting reaction, occurs when charcoal is added to the metal oxide as the reducing agent is shown in Equation 35. There are two reactions taking place simultaneously during carbothermal reduction with the second being the Boudouard reaction (Eq. 36).



Antimony is typically classified as a volatile heavy metal and low grade ores are commonly produced by pyrometallurgical methods [31]. The volatile nature of antimony oxide can be utilized in designing a high temperature method for separating gaseous antimony or antimony oxide from the matrix of the MOV leaching residue. Industrially, reduction of antimony oxide to metallic antimony is achieved by heating and the addition of carbon in a reverberatory furnace. Similarly, for high temperature zinc production, carbon is added to zinc oxide causing carbothermal reduction of zinc according to the reaction given in Equation 37 [116, 117]. Carbothermal reduction reactions are responsible for nearly half of the world's production of zinc and occurs when zinc oxide and carbon are heated to temperatures near 1100 °C [116].



Carbothermal reduction of the  $Zn_7Sb_2O_{12}$  spinel phase can be expressed as in Equation 38 for temperatures less than 900 °C. Above 900 °C, the reduction of zinc occurs according to Eq. 37. In industrial processes volatilization of antimony is reduced by the addition of an alkaline flux [31]. However, volatilized antimony oxide could be recovered in flues, condensing pipes, bag houses, precipitators or a combination of these [118].



Thermodynamic models based on the calculation of the variation of Gibbs free energy ( $\Delta G$ ) can point out which reactions are more likely to take place under the conditions in a thermal decomposition or carbothermal reduction. Thermodynamic calculations do not exactly model the real processes, since significant simplifications have to be made (ideal thermodynamic conditions, homogeneous distribution of the elements, chemical equilibrium, etc.), which can be far from reality in some systems. Nevertheless, thermodynamic models can be powerful tools for understanding chemical behavior during thermal and reducing conditions. The thermodynamics of the high temperature reactions and equilibrium amounts of compounds were investigated using HSC 9.2.2 software and the thermodynamic constants it contained [119].

Thermodynamic evaluation was done over a temperature range between 100 and 1000 °C on a closed system using pure phases. The possible reactions occurring during thermal treatment of  $\text{Sb}_2\text{O}_3$ ,  $\text{Bi}_2\text{O}_3$  and  $\text{ZnO}$  are shown as a function of equilibrium composition in Figure 6a.  $\text{Sb}_2\text{O}_3(\text{s})$  starts to equilibrate with  $\text{Sb}_2\text{O}_3(\text{l})$  near 630 °C, the predicted melting temperature of  $\text{Sb}_2\text{O}_3$ . It is also seen that  $\text{Sb}_4\text{O}_6(\text{g})$  forms around the same temperature.  $\text{Bi}_2\text{O}_3(\text{s})$  is stable through the entire temperature range. Melting of  $\text{Bi}_2\text{O}_3(\text{s})$  occurs at 825 °C. A phase transformation from  $\alpha\text{-Bi}_2\text{O}_3(\text{s})$  to  $\gamma\text{-Bi}_2\text{O}_3(\text{s})$  takes place at 730 °C but is not shown in Figure 6a since this data was not available in the HSC database. However, the transition was reported to occur by Irtyugo et al. [120].  $\text{ZnO}(\text{s})$  is stable in the temperature range shown in Figure 6a.

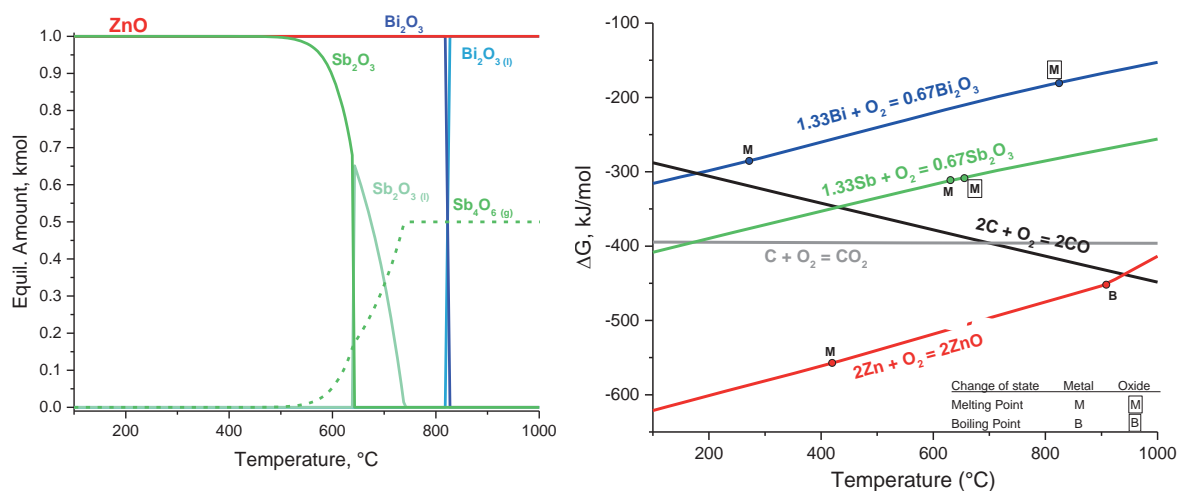


Figure 6: (a) Equilibrium composition for heat treated  $\text{Sb}_2\text{O}_3$ ,  $\text{Bi}_2\text{O}_3$ , and  $\text{ZnO}$  in an inert atmosphere [119]. (b) Ellingham diagram for oxidation of metals.  $P = 1$  atm.

An Ellingham diagram as shown in Figure 6b was used to determine the variation of  $\Delta G$  (compound stability) with temperature for the oxidation of a series of metals. The lower the position of a metal's line in the Ellingham diagram, the greater the stability of its oxide. For instance,  $\text{ZnO}$  is more stable than  $\text{Bi}_2\text{O}_3$ . In general, the stability of metal oxides decreases with temperature. A reduced metal, whose Gibbs free energy of formation is lower in the diagram at a given temperature, will reduce an oxide whose free energy of formation is higher in the diagram. For example, metallic zinc can reduce  $\text{Sb}_2\text{O}_3$  to metallic antimony, the zinc itself being oxidized to  $\text{ZnO}$ . Because the distance is greater between  $\text{Bi}_2\text{O}_3$  and  $\text{ZnO}$  as compared to  $\text{Sb}_2\text{O}_3$  and  $\text{ZnO}$ , Zn will be more effective as a reducing agent for  $\text{Bi}_2\text{O}_3$ .

The  $\Delta G$  of carbon dioxide ( $\text{CO}_2$ ) is almost independent of temperature, while that of carbon monoxide ( $\text{CO}$ ) has a negative slope and intersects the  $\text{CO}_2$  line near 700 °C. According to the Boudouard reaction (Eq. 36), carbon monoxide is the dominant oxide of carbon at higher temperatures ( $> 700$  °C), and the higher the temperature the more effective  $\text{CO}$  is as a reducing agent. It can be expected from thermodynamic calculations that  $\text{Sb}_2\text{O}_3$  will melt near 630 °C and the formation of  $\text{Sb}_4\text{O}_6(\text{g})$  upon further heating is also anticipated. During carbothermal reduction of  $\text{Sb}_2\text{O}_3$ , the reduction of  $\text{Sb}_2\text{O}_3$  is predicted to occur above 400 °C, while the reduction of  $\text{Bi}_2\text{O}_3$  occurs near 200 °C and volatilization of  $\text{ZnO}$  at 900 °C with equilibrium between  $\text{CO}$  and  $\text{ZnO}$  occurring at 940 °C.

## 4. MATERIALS & METHODS

### 4.1. MOV

The work started with the MOV as received from the supplier. It was pulverized, sieved into different size fractions, and characterized prior to and after comminution. A study on pH selective dissolution was done using four acids: acetic acid, hydrochloric acid, nitric acid, and sulfuric acid. Cementation studies were done to purify the MOV leachate, studying a variety of different parameters such as activator concentrations, temperature, pH, and zinc dust addition. The final step needed to produce zinc metal would be to use the purified zinc leachate as the electrolyte for zinc electrowinning. Electrolysis of zinc from the leachate is not discussed in this work. High temperature studies on  $\text{Sb}_2\text{O}_3$ ,  $\text{Bi}_2\text{O}_3$ ,  $\text{ZnO}$ , MOV, and leaching residue were done studying the effect of the heating rate and effect of carbon to residue ratio for carbothermal reduction reactions. Each type of experimental setup is described below.

The identification and composition of the additives in the specific type of MOV investigated needed to be determined as only the oxides of the major metals: zinc, bismuth, and antimony were known. Additives or impurities (any metal other than zinc or  $\text{ZnO}$ ) in the sample will have an impact on zinc leaching and the possible electrolytic process. The MOVs that were approximately 70 mm in diameter and weighing 1000 g were broken up into pieces approximately 2 cm in diameter. An impact mill (Siebtechnik) was used for further particle size reduction. The crushed MOV was mechanically sieved (CISA, 18, 30, 60, 120, 230 mesh) yielding the particle size fractions shown in Table 4. For all experiments material having a particle size smaller than  $63 \mu\text{m}$  was used (100 %, -250 mesh) because smaller particle sizes equate to higher surface to volume ratio and thus typically quicker leaching kinetics are observed.

Table 4: Particle size fraction by weight of pulverized MOV.

<b>Particle Size</b>	<b>Particle Size Weight Fraction</b>
> 1.0 mm	0.06
1 mm to > 500 $\mu\text{m}$	0.07
500 $\mu\text{m}$ to >250 $\mu\text{m}$	0.22
250 $\mu\text{m}$ to >125 $\mu\text{m}$	0.20
125 $\mu\text{m}$ to > 63 $\mu\text{m}$	0.11
< 63 $\mu\text{m}$	0.34

To determine the metal content in the pulverized MOV powder (< 63  $\mu\text{m}$ ), total dissolution of the MOV powder was performed in triplicate using concentrated hydrochloric acid (37 %) at  $70 \pm 3 \text{ }^\circ\text{C}$  while being continuously stirred using a magnetic stir bar. Before inductively coupled plasma – optical emission spectroscopy (ICP-OES, iCAP 6500, Thermo Fischer) analysis for the determination of metal concentrations, aliquots of the solutions were diluted with a 1 M nitric acid solution, prepared from concentrated stock solution (65 %, Suprapur®, Merck) and ultrapure water (Milli-Q, Millipore, >18  $\text{M}\Omega \cdot \text{cm}^{-1}$ ).

#### 4.1.1. Pretreatment

A large portion of the MOV consists of zinc oxide grains. For antimony recovery from the MOV, it is necessary to invoke a pretreatment step to separate the bulk zinc oxide from the antimony rich region. Therefore the pulverized MOV was leached in a straight wall, 150 mL capacity, titration vessel. The vessel was equipped with a pH electrode, a stir bar and a dosing device connected to a Metrohm 905 Titrande titrator connected to a computer for monitoring and controlling the acid addition. The leaching vessel is shown schematically in Figure 7. The pH was controlled using a silver/silver chloride (Ag/AgCl) glass electrode. Calibration of the pH electrode was done weekly using Metrohm® Ion analysis buffer solutions of pH 1, 4, 7, and 9. The temperature of the system was maintained at  $22\text{ }^{\circ}\text{C} \pm 1$ .

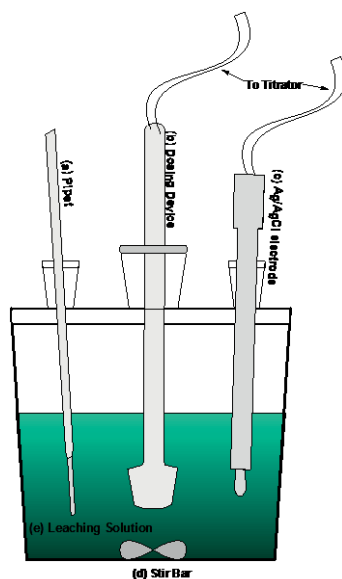


Figure 7: Titration vessel with (a) pipet, (b) dosing device, (c) Ag/AgCl pH electrode, (d) stir bar, and (e) leaching solution.

The acid leaching solutions were not initially prepared to the desired pH. The desired pH was entered into the titration program instead and a more concentrated acid solution was added to the water-MOV system until the desired pH of the system was reached. In total four acid solutions were used for the leaching studies prepared by mixing Milli-Q with: acetic acid ( $\geq 99.7\%$ , Sigma Aldrich), hydrochloric acid ( $37\%$ , Sigma Aldrich), nitric acid ( $65\%$ , Suprapur®, Merck) and sulfuric acid ( $95.0 - 98.0\%$ ). The acid solutions were titrated into the MOV-water mixture resulting in a leachate with a specified pH. The leaching experiments were carried out at a pH of 1, 3, and 5 for each acid solution with the exception of acetic acid in which leaching experiments were carried out having a pH 2, 3, and 5. The concentration of the metals leached as a function of time was determined using ICP-OES.

#### 4.1.2. Leachate Purification Using Cementation

The majority of zinc in the MOV was shown to be soluble therefore, bulk leaching experiments using 5 M H<sub>2</sub>SO<sub>4</sub> solution were started by mixing pulverized (< 63 μm) MOV to 400 mL water (MilliQ, Millipore, >18 MΩ/cm) in a straight wall, 1000 mL capacity beaker. The beaker was equipped with a pH electrode, a stir bar and a dosing device connected to a Metrohm 905 Titrando titrator linked to a computer for monitoring and controlling the acid addition similar as the setup shown in Figure 7 only on a larger scale. The 5 M sulfuric acid solution was made by the dilution of concentrated H<sub>2</sub>SO<sub>4</sub> (95.0 – 98.0 %) with milli-Q water. It was titrated into the MOV-water mixture resulting in a leachate with a pH of 3. The average volume of 5 M H<sub>2</sub>SO<sub>4</sub> added during the leaching experiments was 95.75 ± 0.04 mL. All leaching curves showed the same trend and very similar leaching results. After four hours, the pH remained constant at pH 3 indicating the solution had reached equilibrium. Once the bulk leaching was done, the leachate was separated from the insoluble residue. The concentration of the zinc leachate was determined by ICP-OES.

Activated cementation experiments were done using the zinc-sulfate leachate produced from the pretreatment step in order to remove unwanted impurities such as Co and Ni. Cementation experiments used the same setup as leaching experiments, as shown in Figure 7. To maintain a set pH, 0.1 M H<sub>2</sub>SO<sub>4</sub> solution was titrated into the reaction vial with cementation solution. Typical cementation experiments were carried out at 20 ± 1 °C. The stirring velocity was constant during all experiments at 600 RPM and nitrogen was bubbled through the cementation solution. Copper was added to the leachate as CuSO<sub>4</sub>·5H<sub>2</sub>O (Sigma Aldrich, > 99.0) as an activator for the cementation reactions. Antimony was added to the leachate in the form of soluble potassium antimony tartrate trihydrate (K<sub>2</sub>C<sub>8</sub>H<sub>4</sub>O<sub>12</sub>Sb<sub>2</sub>·3H<sub>2</sub>O, > 99.95, Sigma) also as an activator. 25 mL of leachate was used for each cementation experiment.

A known amount, typically 2 g·L<sup>-1</sup>, of zinc powder (325 mesh, 99.9 % Sigma Aldrich) was added to the reaction vessel in one portion initiating the cementation experiment (t = 0). From the time of the zinc dust addition (t = 0) samples were taken at t = 5, 10, 20, 30, 60, 90 and 120 minutes. Each sample was filtered and diluted prior to ICP-OES analysis.

#### 4.1.3. Cementation Product Morphology

Analytical grade chemicals were used in all experiments. Solutions were prepared using Milli-Q water. The standard 65 g·L<sup>-1</sup> zinc sulfate electrolyte used in all experiments was prepared by the dissolution of zinc sulfate heptahydrate, ZnSO<sub>4</sub>·7H<sub>2</sub>O, (>99 %, Sigma) in water, except for solutions being used in experiments to investigate the zinc ions effects in cobalt cementation. Into the standard 65 g·L<sup>-1</sup> zinc sulfate electrolyte, different chemicals were added for investigation purposes. Cobalt from cobalt sulfate heptahydrate, CoSO<sub>4</sub>·7H<sub>2</sub>O (>99 %, Sigma), copper from copper sulfate pentahydrate, CuSO<sub>4</sub>·5H<sub>2</sub>O (>99 %, Sigma), antimony from K<sub>2</sub>C<sub>8</sub>H<sub>4</sub>O<sub>12</sub>Sb<sub>2</sub>·3H<sub>2</sub>O (99.95 %, Sigma), and magnesium from magnesium sulfate heptahydrate, MgSO<sub>4</sub>·7H<sub>2</sub>O (>99.5 %, Sigma). The initial cobalt concentration was set at 100 mg·L<sup>-1</sup>. The ratio of cobalt concentration to activators concentration (Co:Cu:Sb) was 1:1:1. Before the addition of 2 g·L<sup>-1</sup> zinc dust, the pH was set at 4. In addition, zinc dust (325 mesh, 99.9 %) as the reducing agent was added to the electrolyte initiating the cementation. Magnesium was added into the solutions as an internal standard. As the magnesium reduction potential (E° = - 2.37 V) is more negative than the zinc (E° = - 0.76 V), it does not take part in the cementation reaction. The concentration of magnesium in the samples was used to calculate and correct for the evaporation taking place during each experiment. The selection of using 2 g·L<sup>-1</sup> of zinc dust in this study was based on the results made from previous studies [121].

Three different analytical measurements were used to investigate the characteristics of the cementation solution and cementation product. ICP-OES was used to monitor the change in metal ion concentration during cementation. The surface microstructure and morphology of the cementation product was investigated using a FEI Quanta 200 environmental scanning electron microscope (SEM) equipped with an Oxford Inca energy dispersive X-ray detector (EDX). Imaging was performed using accelerating voltages between 10 to 20 kV. A Bruker 2D Phaser X-ray diffractometer (XRD), equipped with a copper radiation source, and a scintillation detector was used to identify crystalline compounds present in the cementation product. Compound identification was made by comparisons with standards in the Joint Committee of Powder Diffraction Standards database [122].

Cementation experiments were conducted in a 150 mL glass vessel and lid with holes for sampling and instrumentation. For each experiment, 75 mL of the prepared electrolyte and  $2 \text{ g}\cdot\text{L}^{-1}$  of the zinc dust were used. The solution was stirred using a magnetic stir bar. The solution temperature was set to the desired temperature before the experiments began. A water bath was used for the raised-temperature experiments. A silver/silver chloride (Ag/AgCl) glass electrode was used to measure the pH. Prior to experiments, the pH electrode was calibrated using pH 2, 4, 7, and 10 standard. To keep the cementation solution at a constant pH, a 0.5 M  $\text{H}_2\text{SO}_4$  solution was dispensed into the reaction vessel using a Metrohm 905 Titrando titrator controlled the acid addition and pH. Nitrogen was bubbled through the cementation solution to remove dissolved oxygen. A schematic representation of the cementation setup is shown in Figure 7 with the addition of a port for nitrogen bubbling.

Two sets of experiments were performed. One to acquire the samples for determining the kinetics and to monitor the change in metal ion concentration during cementation. The second set of experiments was needed to isolate the cementation product for the morphology studies. Both experiments started with nitrogen bubbling, stabilizing the pH, and temperature adjustment of the cementation solution. Experiments for cementation kinetics analysis began once the Zn dust was added into the cementation solution and lasted for a period of 120 minutes. The first sample was collected before the zinc dust addition and the other samples were collected at 5, 10, 30, 60, 90, and 120 minutes. Each sample was filtered through  $0.45 \mu\text{m}$  polypropylene membrane and diluted with 0.1 M  $\text{HNO}_3$  for ICP-OES analysis of the metal ion concentration. Morphology experiments of the cementation product began once the Zn dust was added into the cementation solution and continued for a period of time, up to 90 minutes. Once the time had passes the cementation process was stopped by separating the product from the electrolyte using a Büchner funnel. The solution was forced through the filter paper leaving the solid product to be rinsed, collected, and analyzed. The filtered product was rinsed with Milli-Q water, then dried in an oven set at  $55 \text{ }^\circ\text{C}$  until analysis with SEM-EDX and XRD.

#### 4.1.4. Antimony Separation from the MOV Residue

The Sb rich residue resulting from bulk leaching experiments was used to study the effects of temperature on recovery of secondary antimony. Prior to high temperature experiments characterization was done on the residue which included ICP-OES and XRD analysis. Thermolysis and carbothermal reduction of the leaching residue and MOV were tested as well as  $\text{Sb}_2\text{O}_3$  (Sigma Aldrich, 99.9 %),  $\text{Bi}_2\text{O}_3$  (Regentplus®, 99.9 %), and ZnO (ACS reagent,  $\geq 99.0 \%$ ). Use of the thermal gravimetric analysis (TGA) was limited to temperatures below  $1000 \text{ }^\circ\text{C}$ . Typical operating parameters for TGA work are given in Table 5. Thermolysis curves were displayed as % weight loss vs. temperature or, when needed the derivative of the thermogravimetric curve. The TGA was calibrated with five high purity standards using their Curie points and peak inflection points as the calibration temperatures.

Table 5: Values of TGA operating parameters.

Variable	Value
Reaction temperature (°C)	100 - 1000
Balance Purge Rate (mL·min <sup>-1</sup> )	10
Sample Purge Rate (mL·min <sup>-1</sup> )	90
Sample Size (mg)	10
Heating Rate (°C·min <sup>-1</sup> )	10
Reaction Gas	N <sub>2</sub>

For experiments needing a controlled atmosphere and also requiring temperatures higher than 1000 °C a furnace within a glove box (Innovative Technology, Pure Lab HE) was used. The working gas in the glove box was argon (> 99.999 %) and the gas purification system ensured the atmosphere contained less than 1 ppm O<sub>2</sub> and H<sub>2</sub>O during all experiments unless otherwise noted. The glove box contained an integrated tube furnace with a maximum operating temperature of 1550 °C. The furnace contained a ceramic lining and was closed using formed aluminum silicate fibers as a cover. To monitor the temperature within the furnace a thermocouple was inserted through a bore in the aluminum silicate cover and placed as near to the sample as possible.

Two general types of experiments were performed: (1) thermal decomposition where the metal oxides as well as MOV residue were heated in a nitrogen atmosphere and (2) carbothermal reduction where charcoal was added to the metal oxides and MOV residue. It has been proven to work in zinc production [68] but the effect on the oxides of antimony and bismuth as well as the MOV residue are not as well known. For carbothermal reduction experiments, activated charcoal (DARCO®, -100 mesh) was mixed with the metal oxides and the MOV residue at multiple C/O molar ratios. Homogenization was done using a mortar and pestle. The C/O ratio for the MOV residue was determined by assuming the MOV residue to be composed of 85 % metals (determined by ICP-OES) with the remaining 15 % being oxygen and are given in Table 6.

Table 6: molar ratio of C/O used for carbothermal reduction.

Compound	C/O Ratio used
	1.4
MOV Residue	2.2
	8.6

#### 4.2. FLY ASH

The fly ash was taken from Amagerforbrænding, a grate-fired MSWI plant in Copenhagen, Denmark. One ash sample yielding two types of ash samples was investigated in this work; (1) the original, untreated fly ash sample and (2) the HALOSEP ash which underwent the HALOSEP treatment. The HALOGen SEPARation (HALOSEP) process is used to remove water soluble salts such as NaCl, KCl, CaCl<sub>2</sub>, and MgCl<sub>2</sub> and to alter the leaching properties of the fly ash with respect to metals such as Sb, Pb, and Zn [98]. The HALOSEP process has been shown to result in the reduction of fly ash weight by approximately 50-55 %, and most often the treated ash is stable enough to pass leaching tests [98]. However, one issue with the HALOSEP process which has been identified is that, although the leaching of most of the metals is significantly decreased, the mobility of antimony is in some cases too high to comply with non-hazardous waste landfill acceptance criteria. The untreated fly ash is a fine powder whereas the HALOSEP ash has been removed from the filter cakes and contains residual moisture from the wet HALOSEP treatment. It was then broken up and remained as large chunks 2 - 5 cm in diameter. The ash was stored inside in 200 liter polyethylene (PE) drums with a closed lid. The HALOSEP ash was treated 6 months after receiving it. Both the untreated and HALOSEP ash samples were stored indoor in PE drums with closed lids for approximately 2½ - 3 years before the leaching experiments were performed for this study.

Both ash samples were exposed to leaching at different pH values to investigate the effect of leaching pH on the mobility of, primarily antimony, but also of lead and zinc. The leaching setup was the same as previously described. Each leaching experiment used approximately 5 grams of ash and 100 mL of distilled water for an initial L/S of 20. The ash gave an alkaline solution upon addition to water, so 5 M hydrochloric acid (HCl) was added to the ash-water slurry to maintain the specific pH required in each experiment for a total of 23 hours. The 5 M HCl solution was made by the dilution of concentrated hydrochloric acid (ACS Reagent, > 37 %) and milli-Q water. For the HALOSEP fly ash a 5 M HCl solution was used for leaching within the pH interval 1 to 9, adding the ash to water resulted in a pH of 10.2 and therefore a base was needed above pH 10. In the pH interval 11 to 13, an NaOH solution was used for leaching. The concentration of metals in solution was determined by ICP-OES.

At the end of each leaching experiment the leachate was separated from the insoluble residue by filtration using a Büchner funnel. The residue was removed from the filter (Whatman, 1.6 $\mu$ m), dried in an oven at 60 °C for more than 4 hours and ground with a mortar and pestle. Tests to determine if the ash met the acceptance criteria for waste at landfills in the EU was done according to standard EN12457/1-4 part 2 (L/S = 10 l/kg, particle size < 4mm). The concentrations of elements in the ash samples were determined by an accredited lab.

## 5. RESULTS & DISCUSSION

This work covers a diverse range of techniques including leaching, cementation, and high temperature Sb extraction including carbothermal reduction. From start to finish the goal of this research project is to recycle the critical metal, antimony from waste. However, since  $\text{Sb}_2\text{O}_3$  is the most industrially important antimony compound and it is used as a starting material in the MOVs as well as starting material in plastics many of which end up in MSW, the thermal properties of  $\text{Sb}_2\text{O}_3$  was first investigated. There is limited and often conflicting data in literature regarding  $\text{Sb}_2\text{O}_3$  oxidation. Investigations into this were done to try and understand the confusion. In addition to a thermal investigation of  $\text{Sb}_2\text{O}_3$  the extraction of Sb from MOVs and MSW fly ash was also investigated. Since the major component of the MOV is zinc oxide, recycling of zinc could not be ignored and was also investigated. A process flow diagram is shown in Figure 8 for the experiments carried out in the work upon which this thesis is based.

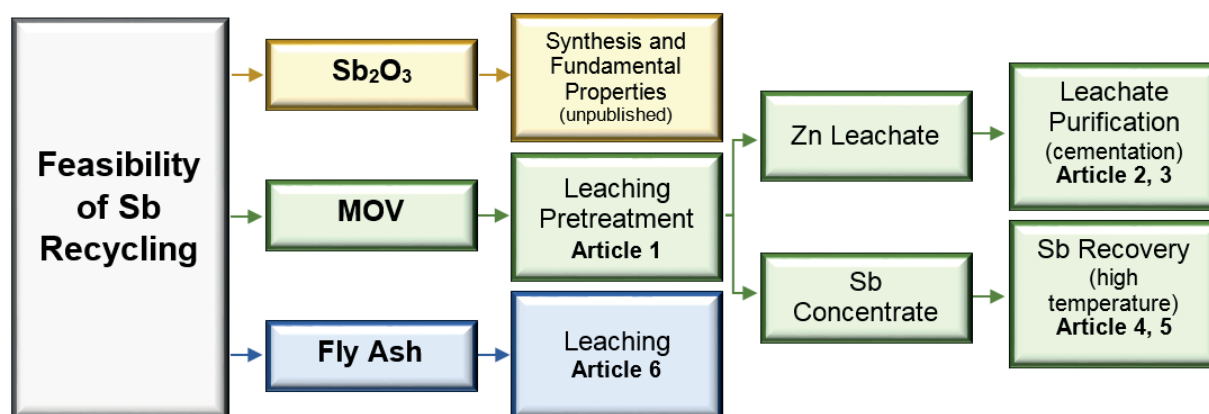


Figure 8: Flow diagram for work presented in this thesis.

Due to the low concentration of Sb in the MOV, several steps were needed to recover Sb. First an acid leaching pretreatment step was done in order to selectively separate the bulk zinc oxide grains from the minor antimony phase and is described in Paper I. Optimal zinc leaching would avoid co-leaching of antimony, bismuth and other minor metals present in the MOV making the leachate easy to integrate into an industrial zinc electrowinning process.

The original aim was to recycle antimony from the MOV. However, since an impure zinc sulfate stream was generated in the pretreatment step, it was logical to study how to purify this “waste” stream making it a valuable byproduct in the antimony recycling process. Paper II investigates if activated cementation could be used to produce a purified zinc electrolyte and also the optimal cementation conditions for cobalt removal from the MOV sulfuric acid leaching solution. Paper III examined the morphology of the cementation deposits under various conditions to determine what parameters influence cementation efficiency.

Due to the volatile nature of antimony compounds, the antimony rich insoluble residue from the pretreatment was heated in reducing and inert atmospheres to volatilize Sb and try to collect it as pure condensed phase. However, the temperature range needed for the liberation of Sb from the spinel and pyrochlore phases was not known. In order to determine this a series of thermolysis and carbothermal reduction experiments were performed. The heat treatment experiments are described in papers IV – V with the highlights given here.

Recycling of antimony from MSWI fly ash was done by examining the pH-dependent leaching behavior of antimony from two ash samples: untreated and HALOSEP treated ash as presented in Paper VI. HALOSEP is a salt removal treatment using a slightly acid HCl solution.

## 5.1. ANTIMONY RECOVERY FROM THE MOV

The MOV investigated in this work contained, in detectable amounts, the metals listed in Table 7 shown as milligrams of metal per gram of MOV.

Table 7: Chemical composition of MOV.

Metal	mg·g <sup>-1</sup>
Bi	45.9 ± 0.1
Co	6.9 ± 0.1
Mn	3.6 ± 0.1
Ni	6.1 ± 0.1
Sb	34.8 ± 1.1
Zn	762 ± 4

Due to production methods, the MOV does not consist strictly of the starting components ZnO, Bi<sub>2</sub>O<sub>3</sub>, Sb<sub>2</sub>O<sub>3</sub>, and other minor metal oxides. The microstructure of the MOV contains the three major phases summarized in Table 8. A SEM micrograph of a pulverized MOV particle is shown in Figure 9a with an overlay of EDX maps for zinc, antimony, and bismuth in Figure 9b.

Table 8: Description of major phases present in MOV.

Phase	Description	Compounds	Color in Figure 9
I - Zinc rich phase	most dominate phase, particles 20 to 140 μm	ZnO	Red
II - Antimony rich phase	small particles located around zinc oxide particles, 1-2 μm	Spinel: Zn <sub>2.33</sub> Sb <sub>0.67</sub> O <sub>4</sub> , Zn <sub>7</sub> Sb <sub>2</sub> O <sub>12</sub> Pyrochlore: Zn <sub>2</sub> Bi <sub>3</sub> Sb <sub>3</sub> O <sub>14</sub>	Green
III - Bismuth rich phase	crystalline, can change depending on cooling rate and the presence of transition metal oxides [59]	Bi <sub>2</sub> O <sub>3</sub>	Blue

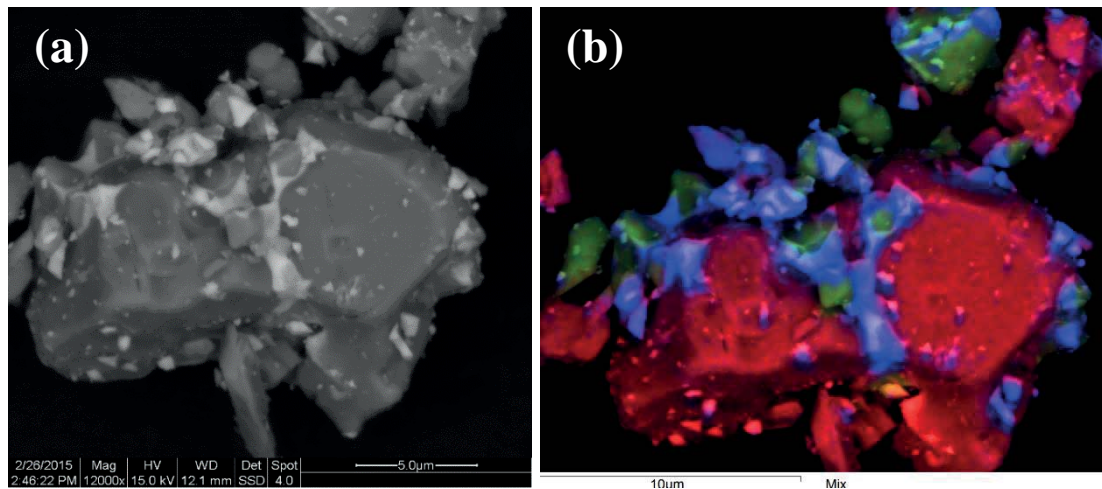


Figure 9: SEM-EDX micrograph of pulverized MOV having three phases: Phase I - zinc rich phase, Phase II – antimony rich phase, Phase III – bismuth rich phase. (a) SEM micrograph of pulverized MOV particle, (b) combined SEM micrograph and EDX map for zinc (red), antimony (green) and bismuth (blue).

During liquid phase sintering, antimony (III) oxide is oxidized to antimony (V) oxide near 530 °C [62]. By heating the antimony (V) oxide with zinc oxide a trirutile,  $ZnSb_2O_6$  phase forms [66]. It was shown by Leite et al. [62] that the trirutile phase is most likely an intermediate phase in the formation of the spinel phase. The spinel compound contains two structures: (1) cubic structure with chemical formula  $Zn_{2.33}Sb_{0.67}O_4$  and (2) orthorhombic structure having chemical formula  $Zn_7Sb_2O_{12}$  [123, 124]. Heating the trirutile phase, zinc oxide, and bismuth oxide forms pyrochlore ( $Zn_2Bi_3Sb_3O_{14}$ ) at sintering temperatures between 700 to 900 °C [58]. Further heating (900 to 1050 °C) of the pyrochlore phase with zinc oxide results in decomposition of the pyrochlore phase to spinel and the formation of liquid bismuth oxide phases [62] which promotes liquid phase sintering of the zinc oxide with liquid bismuth oxide. The  $Bi_2O_3$  phase is crystalline at room temperature, however, it can exist in several different crystalline forms depending on its thermal history and the presence of transition metal oxides [59].

Qualitative mineralogical analysis of the MOV using XRD confirmed the presence of  $ZnO$ ,  $Bi_2O_3$ ,  $Zn_{2.33}Sb_{0.67}O_4$ ,  $Zn_2Bi_3Sb_3O_{14}$ , and  $Zn_7Sb_2O_{12}$  [125]. Compounds containing cobalt, manganese and nickel were not confirmed due to their low concentrations. It has been suggested by Wong [65] that the octahedral crystal structure of the  $Zn_7Sb_2O_{12}$  spinel was doped with Mn and Co when Mn and Co were present during sintering. There was no peak correlation for antimony (III, V) oxide indicating that antimony is present in the spinel or pyrochlore phases.

#### 5.1.1. MOV Pretreatment - Concentrating the Antimony

Four acids were used as leachates in this study: acetic acid, which is a weak monoprotic organic acid, nitric, hydrochloric and sulfuric acid, each at three different pH levels. When possible pH 1, 3 and 5 were used except in the case of acetic acid where pH 1 was difficult to obtain without a substantial change to the solid to liquid ratio, which meant pH 2 was used instead. Acetic acid leaching results show that selective leaching of zinc from the MOV with respect to bismuth and antimony can be achieved using a leaching solution with a pH 5. However in acetic acid solutions at pH 5 some bismuth ( $1.3\% \pm 0.1$ ) was leached. In hydrochloric acid solutions zinc can be selectively leached from bismuth and antimony in pH 5 solutions. Similar results for selective leaching of zinc occur in nitric acid solutions with no bismuth or antimony detected in pH 5 solutions. With acetic, hydrochloric and nitric acid, the percent of zinc leached decreased with increasing pH. In all the acids at pH 1, 100 % of the zinc in the MOV was leached but at pH 5 the extraction of zinc decreased to 85 %, 81 %, and 78 % for acetic, hydrochloric, and nitric acid respectively [125].

Industrially, a sulfuric acid electrolyte is used in zinc production and it was therefore highlighted in this work. Leaching of the MOV in sulfuric acid solutions with pH 1, 3 and 5 gave results as shown in Figure 10. Sulfuric acid solutions were able to fully leach zinc at each pH level tested. Increasing the pH from 1 to 5 did not change the percent of zinc leached but rather the time (kinetics) needed for leaching will be longer. It is feasible to use pH 5 solutions to selectively leach zinc while avoiding co-leaching of antimony and bismuth. However, for further purification studies, the solution should be leached in pH 3 solutions to promote cementation of impurities in the leachate and decrease the time needed for leaching. Bismuth was leached when using pH 1 solution and the dominant species should be  $Bi^{3+}$  based on the  $E_h$ -pH diagrams [126]. In these conditions, less than 5 % of antimony was leached which is consistent with published data stating oxidizing, acidic solutions should not react with  $Sb_2O_3$  [126]. PHREEQC [127] calculations using the *minteq* database [128] showed that approximately 65 % of the zinc in the pH 1 leachate occurred as  $Zn^{2+}$  with the remaining 35 % of zinc in solution as  $ZnSO_4$  soluble complex. As the pH increased the fraction of zinc as  $Zn^{2+}$  ions decreased to 55 % for pH 5.

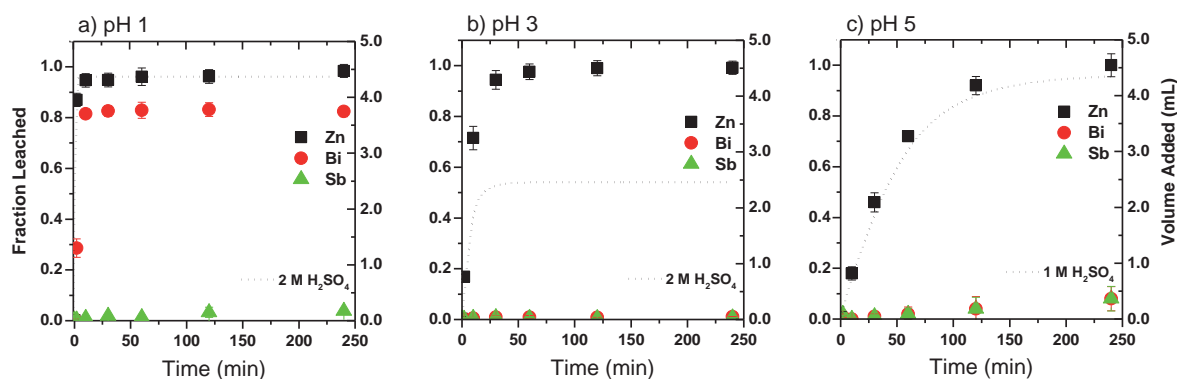


Figure 10: The leached fraction as given by the left ordinate for zinc (□), bismuth (○) and antimony (△) from the MOV in a) pH 1, b) pH 3, and c) pH 5 solutions. The volume and concentration of sulfuric acid ( $H_2SO_4$ ) added is shown as a solid black line corresponding to the right ordinate.

Minor metal impurities in the zinc-sulfate leachate include Co, Mn, and Ni with the leaching fraction of each versus time is shown in Figure 11. Approximately 65 % of Co and 25 % of Mn and Ni were leached independent of the pH studied here for the sulfate system.

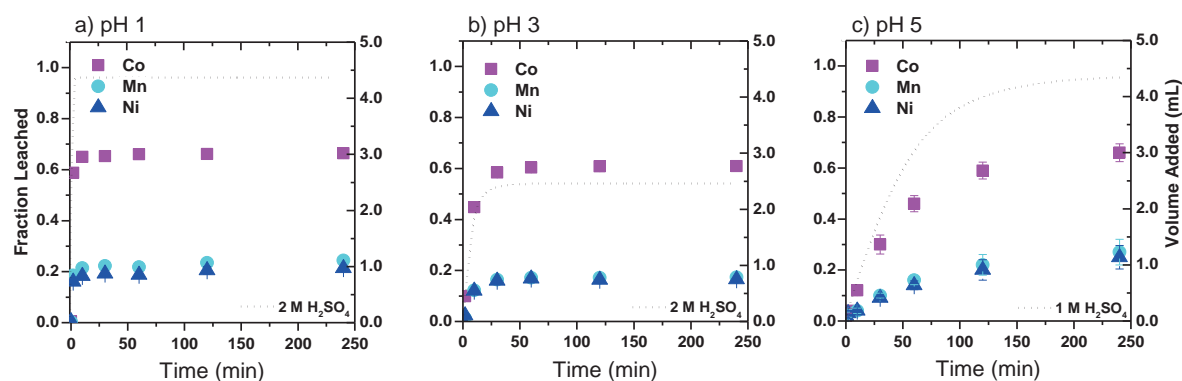


Figure 11: The leached fraction for cobalt (□), manganese (○) and nickel (△) from MOV in a) pH 1, b) pH 3, and c) pH 5 sulfate solutions. The volume and concentration of sulfuric acid ( $H_2SO_4$ ) added is shown as a dotted black line corresponding to the right ordinate.

Minor metal co-leaching at pH 5 is summarized in Table 9 for all acids. This data shows that leaching with  $HNO_3$  gives the lowest co-leaching percentage of the minor metals present in the MOV but industrially it is not used in zinc production. The four acids give similar results when it comes to co-leaching of other metals with Zn. The amount of cobalt co-leached was around 66 %, while Mn and Ni were co-leached at 27 % and 25 % respectively. The minor metal impurities would have to be removed before zinc electrowinning.

Table 9: Percentage of minor metals co-leached with zinc in pH 5 leaching solutions.

Acid	Co	Mn	Ni
$CH_3COOH$	$74.5 \pm 0.4$	$23.4 \pm 0.1$	$19.6 \pm 0.3$
HCl	$72.6 \pm 5.5$	$23.1 \pm 2.9$	$18.5 \pm 0.9$
$HNO_3$	$63.3 \pm 0.7$	$19.7 \pm 0.3$	$17.0 \pm 0.2$
$H_2SO_4$	$66.4 \pm 3.5$	$27.1 \pm 5.0$	$24.8 \pm 4.6$

Results of leaching with acetic acid, hydrochloric acid, and nitric acid are described in detail in Paper I [125]. The results for all acids are similar, in that zinc can be leached, but not selectively with respect to minor metals no matter the leachate used: acetic, hydrochloric, nitric, or sulfuric acid. However, since zinc is industrially electrowon from sulfate solution it is viewed as the preferred leachate. Further purification of the zinc-sulfate leachate is required if the leachate is to be used for industrial electrowinning of zinc. Purification by activated cementation could be effective for removing antimony, bismuth, nickel, and cobalt from the leaching solution. The added benefit of the use of antimony is that in the presence of copper it acts as an activator, increasing the kinetics of the cementation reaction [109].

XRD analysis results for the pH 1 sulfuric acid leaching residue is shown in Figure 12 as a solid black line (—). The majority of the peaks can be identified as originating from antimony containing compounds, such as  $Zn_{2.33}Sb_{0.67}O_4$  (□),  $Zn_7Sb_2O_{12}$  (■),  $ZnCo_{1.33}Sb_{0.67}O_4$  (○), and  $Zn_{1.66}Ni_{0.67}Sb_{0.67}O_4$  (●). Also present in the MOV is  $Zn_2Bi_3Sb_3O_{14}$  (★) and  $Bi_2O_3$  (◆) both having identical peaks. It is logical based on characterization and literature data that pyrochlore ( $Zn_2Bi_3Sb_3O_{14}$ ), spinel both cubic ( $Zn_{2.33}Sb_{0.67}O_4$ ) and orthorhombic ( $Zn_7Sb_2O_{12}$ ) as well as some residual  $Bi_2O_3$  are present in the sample. It is also probable that cobalt, nickel, and manganese are present in the sample. However, the chemical form of those metals is not known. The residue can be compared to the starting material, dashed gray line (- - -) in Figure 12. The diffractogram for the starting material contained prominent peaks for ZnO whereas no ZnO peaks were present in the diffractogram for the leaching residue. It can be concluded from leaching data and XRD spectrum that it will be difficult to solubilize the zinc present in the combined zinc-antimony oxides.

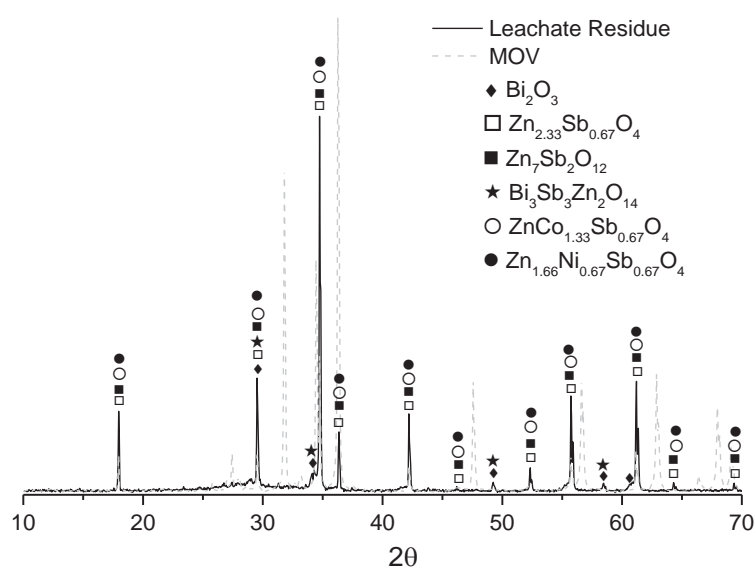


Figure 12: XRD diffractogram (—) of leaching residue (pH 1, sulfuric acid) compared to diffractogram of non-leached starting material (- - -).

A comparison of the pulverized MOV material before and the insoluble residue after sulfuric acid leaching is shown in Figure 13a and b respectively. In the original MOV material the dominating phase was zinc oxide while all that remains in the leached residue is the antimony-rich phase in particles approximately 2  $\mu m$  in diameter with some residual, undissolved bismuth-rich phase attached to them.

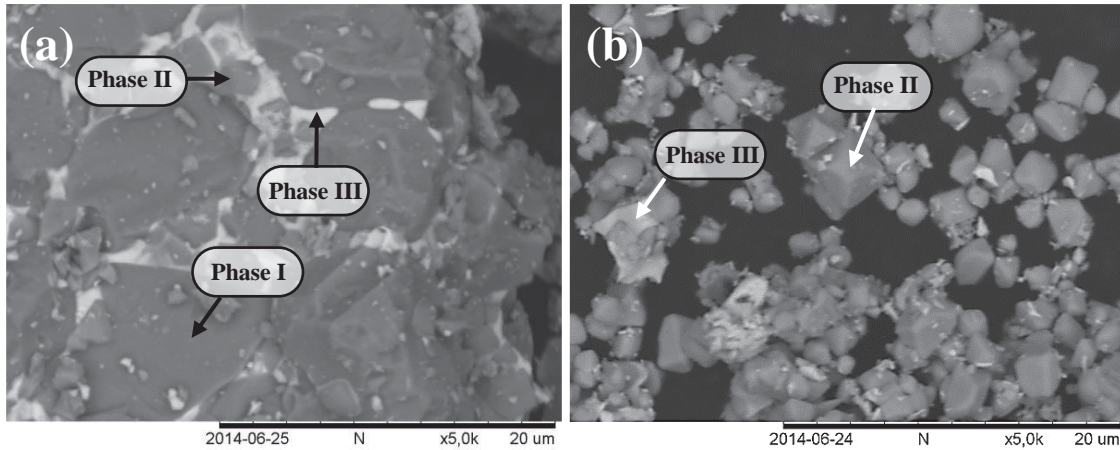


Figure 13: (a) SEM micrograph of the MOV prior to leaching showing all three phases: phase I – zinc oxide grains, phase II – antimony rich phase, and phase III – bismuth rich phase. (b) SEM micrograph of pulverized MOV post leaching in pH 1 sulfuric acid solution for 240 minutes. The antimony-rich phase (phase II) remains along with some of the undissolved bismuth-rich phase (phase III).

### 5.1.2. Leachate Purification Using Activated Cementation

The cementation solution being investigated was produced from dilute, sulfuric acid leaching of pulverized MOV at pH 3 having the metal concentrations given in Table 10. The aim was to investigate the feasibility of using cementation as a means for MOV leachate purification to make it suitable for zinc electrowinning. For comparison, typical metal concentrations in a metal solution prepared for industrial zinc electrowinning by cementation are also shown in Table 10 as well as the concentration of metal prior to cementation. For the MOV leachate to be easily integrated into an industrial zinc electrowinning process, significant amounts of impurities need to be removed. It has been reported that  $15 \text{ mg}\cdot\text{L}^{-1}$  of cobalt, nickel, and copper can reduce the current efficiency by 10 %, 15 % and 40 % respectively in this process [70].

Table 10: Concentration of metals in leachate for the elements found in the MOV along with industrial zinc electrowinning solution concentrations before and after cementation.

Element	MOV leachate ( $\text{mg}\cdot\text{L}^{-1}$ )	Industrial electrolyte before cementation [70] ( $\text{mg}\cdot\text{L}^{-1}$ )	Industrial electrolyte after cementation [70] ( $\text{mg}\cdot\text{L}^{-1}$ )
Bi	0	0	0
Co	$437 \pm 8$	15	1 – 0.05
Cu	0	1000	0.1 – 0.15
Mn	$68 \pm 1$	0	0
Ni	$106 \pm 2$	0	0
Sb	0	0	0.01 – 0.02
Zn	$81,100 \pm 1590$	$\sim 150,000$	$\sim 150,000$

Experiments were carried out at temperatures of 20, 30, 40, 50, 60 °C. Cementation results are shown in Figure 14 as the dimensionless unit of  $C/C_0$  where  $C$  is the total concentration in solution at any time and  $C_0$  is the initial concentration. The cementation solutions contained copper and antimony as activators with a concentration of  $0.4 \text{ g}\cdot\text{L}^{-1}$  each of which were completely removed from the solution within the first 5 minutes.

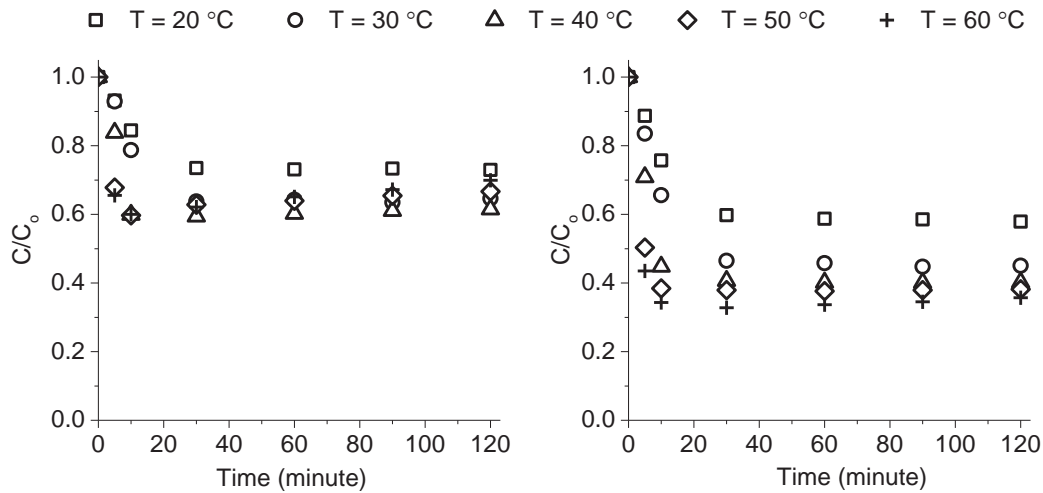


Figure 14: Influence of temperature ( $T = 20, 30, 40, 50, 60$  °C) on the cementation of cobalt and nickel with copper and antimony concentrations of  $0.4 \text{ g}\cdot\text{L}^{-1}$ , pH 4, and  $2 \text{ g}\cdot\text{L}^{-1}$  zinc dust.

Elevated temperatures did not have a significant effect on the amount of cobalt and nickel cemented from solution but the kinetics increased with temperature as indicated in Figure 14. Literature suggested the optimal temperature for cobalt cementation was near  $80$  °C. However, our system was not effective at this temperature due to severe evaporation. Cementation of cobalt at higher ( $T > 40$  °C) temperatures resulted in the occurrence of a maximum in cobalt removal after 10 minutes. A maximum of  $169 \text{ mg}\cdot\text{L}^{-1}$  of cobalt and  $55 \text{ mg}\cdot\text{L}^{-1}$  of nickel were removed from the solution after 30 minutes at  $40$  °C. While after 120 minute at  $40$  °C,  $160 \text{ mg}\cdot\text{L}^{-1}$  of cobalt and  $56 \text{ mg}\cdot\text{L}^{-1}$  of nickel were removed. There are several reasons for the maxima: higher temperatures resulting in an increased rate of hydrogen production at the zinc surface, evaporation of leachate, and cobalt re-dissolution at elevated temperatures [109, 129].

In addition to temperature, the effect of pH on the cementation reactions was investigated between pH 3.0 and 5.5 with the results for cobalt and nickel removal shown in Figure 15. A cementation solution maintained at a pH between pH 5.0 and 5.5 gave the most effective removal of cobalt and nickel with  $218 \text{ mg}\cdot\text{L}^{-1}$  of cobalt and  $74 \text{ mg}\cdot\text{L}^{-1}$  of nickel removed. Using a pH higher than 6.0 had a negative impact on cementation most likely due to hydrolysis and the formation of basic zinc salts. If the pH of the solution is too high (typically higher than pH 5.0), the formation of basic zinc sulfate or zinc hydroxide inhibits the reaction kinetics by forming a passivating layer on the zinc powder [72, 129, 130].

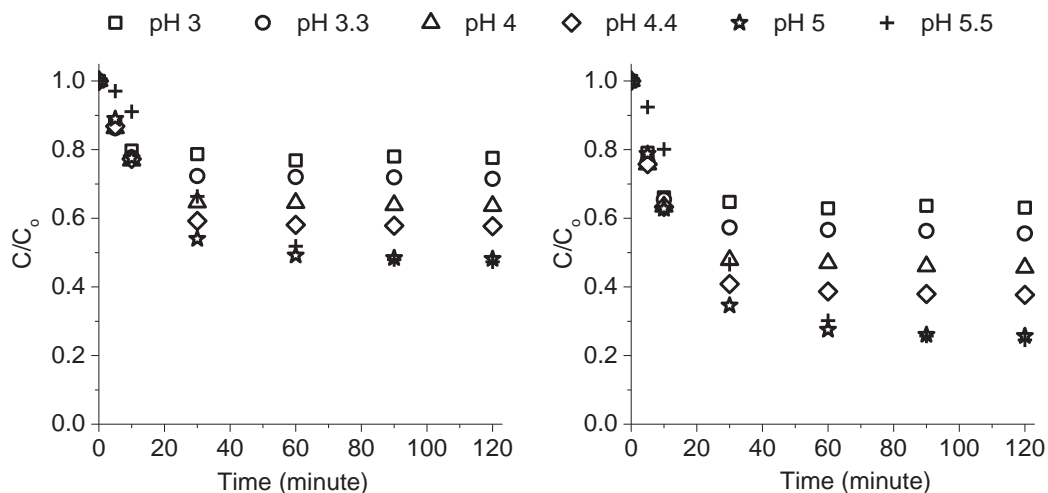


Figure 15: Results for the influence of solution pH on cementation cobalt and nickel with copper and antimony concentrations of  $0.4 \text{ g}\cdot\text{L}^{-1}$  at  $T = 20$  °C, pH 4, and  $2 \text{ g}\cdot\text{L}^{-1}$  zinc dust.

In addition to the effects of temperature and pH on cementation, other studied parameters can be found in Paper II. However, it was found that for the MOV leachate system that the optimized Co cementation conditions for copper concentration, antimony concentration, zinc dust addition, temperature and pH were  $0.8 \text{ g}\cdot\text{L}^{-1}$  Sb,  $0.4 \text{ g}\cdot\text{L}^{-1}$  Cu,  $T = 40 \text{ }^\circ\text{C}$ , and  $0.2 \text{ g}\cdot\text{L}^{-1}$  Zn addition in a solution of pH 5.0. These conditions were applied to obtain the results in Figure 16. Over 90 % of Ni and nearly 60 % of the Co were removed from the zinc-sulfate leachate by cementation. Even though copper and antimony were added to the cementation solution as activators they were easily removed and caused no contamination to the leachate. The starting and final concentration of metals in the leachate at  $20 \text{ }^\circ\text{C}$  and  $40 \text{ }^\circ\text{C}$  are shown in Table 11.

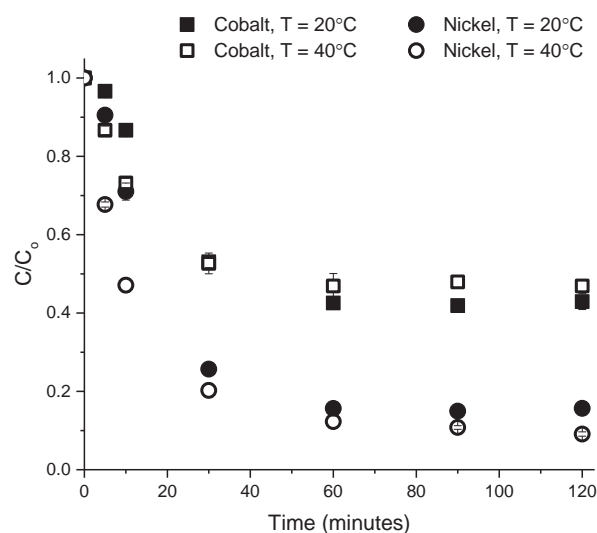


Figure 16: Cementation with addition of  $0.8 \text{ g}\cdot\text{L}^{-1}$  Sb,  $0.4 \text{ g}\cdot\text{L}^{-1}$  Cu,  $2 \text{ g}\cdot\text{L}^{-1}$  Zn, at pH 5.

Table 11: Concentration of metals in MOV leachate before and after optimized cementation.

Metal	Pre-cementation	Post-cementation	
	Metal concentration ( $\text{mg}\cdot\text{L}^{-1}$ )	Metal concentration at $T = 20 \text{ }^\circ\text{C}$ ( $\text{mg}\cdot\text{L}^{-1}$ )	Metal concentration at $T = 40 \text{ }^\circ\text{C}$ ( $\text{mg}\cdot\text{L}^{-1}$ )
Co	$423 \pm 14$	$186 \pm 7$	$194 \pm 9$
Cu	$378 \pm 24$	$0.1 \pm 0.7$	$0.0 \pm 0.7$
Mn	$60.7 \pm 2.1$	$57.9 \pm 0.6$	$62.1 \pm 0.5$
Ni	$96.8 \pm 5.7$	$15.5 \pm 1.1$	$8.6 \pm 0.6$
Sb	$765 \pm 40$	$0.7 \pm 0.2$	$1.4 \pm 0.1$

The kinetics for cobalt cementation were fast during the first 10 minutes of cementation. Similarly in the cementation experiments it was seen that all dissolved copper and antimony was consumed within 10 minutes which suggests that the cemented Cu/Sb alloy on the zinc dust surface also influences Co cementation. To improve Co removal, the batch addition of the two activators (Sb/Cu) along with zinc dust were performed after 60 minutes yielding the results shown in Figure 17. The solution initially contained  $0.8 \text{ g}\cdot\text{L}^{-1}$  of antimony and  $0.4 \text{ g}\cdot\text{L}^{-1}$  of copper.  $2 \text{ g}\cdot\text{L}^{-1}$  of zinc dust was added at  $t = 0$ . The cementation reaction proceeded for 60 minutes and was stopped by filtering the solution and removing the cementation product. To the filtered solution,  $0.8 \text{ g}\cdot\text{L}^{-1}$  of antimony and  $0.4 \text{ g}\cdot\text{L}^{-1}$  copper were again added to the solution as well as  $2 \text{ g}\cdot\text{L}^{-1}$  of zinc dust.

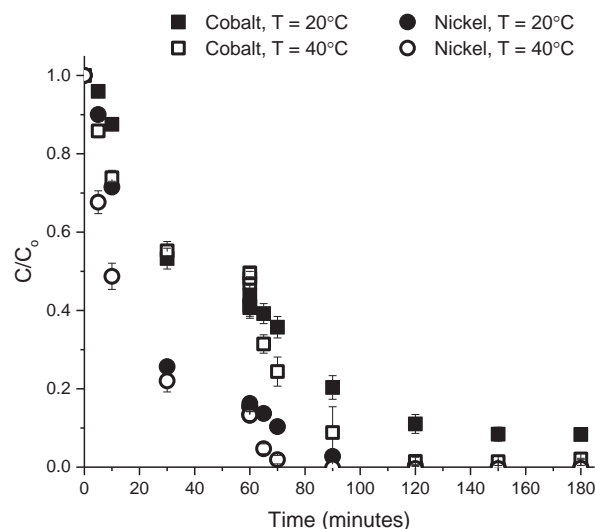


Figure 17: Cementation with two batch additions of  $0.8 \text{ g}\cdot\text{L}^{-1}$  Sb,  $0.4 \text{ g}\cdot\text{L}^{-1}$  Cu,  $2 \text{ g}\cdot\text{L}^{-1}$  Zn, at pH 5.

Batch addition of the activators at  $40^\circ\text{C}$  resulted in the removal of metals summarized in Table 12. The batch cementation process resulted in complete removal of the copper and antimony activator along with nickel and 98 % of the cobalt from the MOV leachate. The remaining cobalt could be removed by adding a third cementation step or possibly by increasing the temperature.

Table 12: Concentration of metals in MOV leachate before and after batch additions under optimized cementation conditions for  $40^\circ\text{C}$ .

Metal	Batch 1		Batch 2		% change
	Pre-cementation concentration ( $\text{mg}\cdot\text{L}^{-1}$ )	Post-cementation concentration ( $\text{mg}\cdot\text{L}^{-1}$ )	Pre-cementation concentration ( $\text{mg}\cdot\text{L}^{-1}$ )	Post-cementation concentration ( $\text{mg}\cdot\text{L}^{-1}$ )	
Co	$414 \pm 14$	$200 \pm 7$	$194 \pm 6$	$8.6 \pm 0.7$	98
Cu	$381 \pm 22$	$4.6 \pm 0.8$	$389 \pm 22$	$0.0 \pm 0.6$	100
Mn	$59.3 \pm 1.0$	$60.3 \pm 1.1$	$58.4 \pm 0.2$	$61.4 \pm 1.6$	3.6
Ni	$97.4 \pm 2.5$	$13.2 \pm 1.3$	$12.9 \pm 1.1$	$0.0 \pm 0.4$	100
Sb	$759 \pm 5$	$8.9 \pm 0.1$	$772 \pm 15$	$1.6 \pm 1.7$	100

This investigation has shown that it is possible to purify the MOV leachate of 98 % cobalt and all nickel using cementation. However, the economics of this method were not investigated but are important if this method is to be used to recycle zinc from the MOVs. This research shows that a pure zinc sulfate stream can be successfully produced from discarded MOV by sulfuric acid leaching followed by activated cementation of pulverized MOV's.

### 5.1.3. Cementation Product Morphology

Thus far purification of the zinc sulfate leachate by cementation has been shown to be successful. But this is not the whole story. More information is needed such as what factors influence Co cementation. To investigate this the morphology of the cementation product was studied and the results are discussed in Paper III. A study on the residues formed during cobalt cementation are of importance to understanding the cementation process. Therefore the residues produced studying the effects of temperature, pH, and zinc ion concentration were evaluated.

A zinc sulfate solution containing only Co as an impurity was used to study the cementation product morphology. The effect of temperature on cobalt cementation can be seen in Figure 18 where the dimensionless fraction of cobalt remaining in the electrolyte is divided by the initial cobalt concentration versus time. These results are similar to the results obtained for the MOV leachate system shown in Figure 14. Increasing the temperature of the cementation solution increased the rate of cobalt removal significantly. This is to be expected according to the Arrhenius equation where higher temperatures result in a larger rate constant or faster reaction rate. The maximum amount of Co removal was 45 % occurring at 70 °C. Increased temperature also resulted in the re-dissolution of cobalt after 30 minutes. Bøckman and Østvold [129] determined that there are two cobalt reactions occurring during cementation. First the formation of the cobalt alloy on the zinc dust surface, second the formation of basic cobalt salts due to localized high pH levels due to hydrogen evolution. When the core of the zinc dust particle, cementation surface, is consumed hydrogen evolutions stops and the localized pH becomes that of the bulk solution causing dissolution of the cobalt salts. Hydrogen evolution is detrimental not only because it causes dissolution of the deposited products [131] but also because the electrons from zinc oxidation are used to promote hydrogen evolution and are not used to reduce metals from solution.

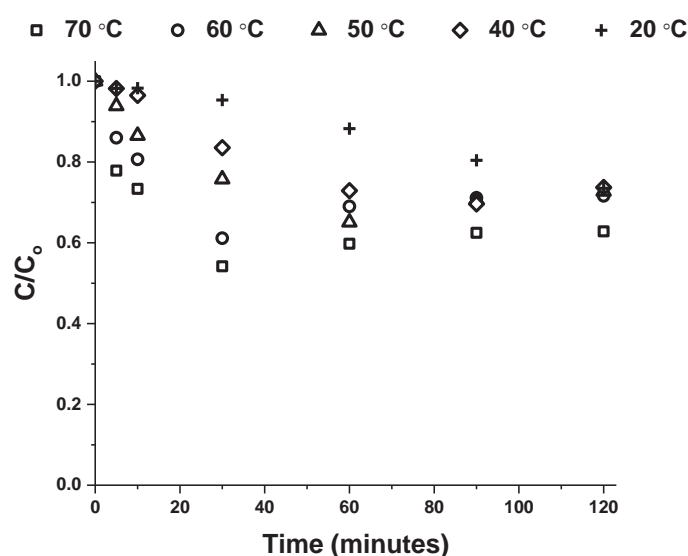


Figure 18: Effect of temperature on cobalt cementation: pH 4, 65 g·L<sup>-1</sup> Zn, 100 mg·L<sup>-1</sup> Co, 100 mg·L<sup>-1</sup> Cu, 100 mg·L<sup>-1</sup> Sb, Temperature = 20 °C, 40 °C, 50 °C, 60 °C, 70 °C.

At elevated temperatures, there are two interesting regimes in Figure 18 the first rate regime, which occurs between 0 and 30 minutes, represents the cementation of cobalt and dissolution of zinc dust, while the second rate regime, greater than 30 minutes, is cobalt cementation coupled with cobalt dissolution. From the first rate regime, which is a linear function of cementation over time, it is possible to calculate the cementation activation energy. Figure 19a shows the Arrhenius plot for the first rate regime of cobalt cementation, while Figure 19b gives reaction rate constants versus the inverse of the reaction temperature. From the slope in Figure 19b, the activation energy,  $E_A$  was determined to be 45 kJ·mol<sup>-1</sup>.

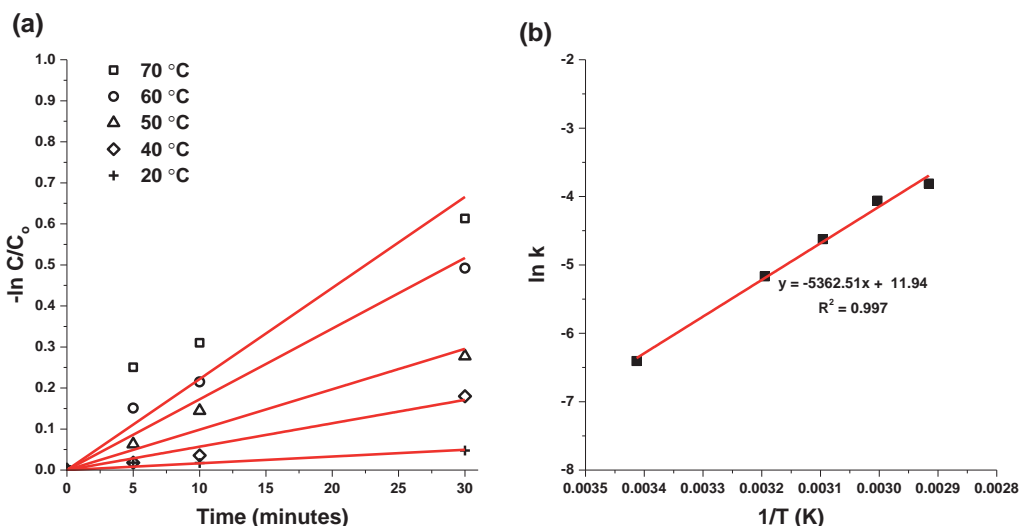


Figure 19: (a) The negative log of the ratio of cobalt concentration as a function of time and temperature during cobalt cementation from zinc sulfate electrolyte at solution pH 4. (b) Arrhenius plot for cobalt cementation.

When the  $E_A > 40 \text{ kJ}\cdot\text{mol}^{-1}$ , the reaction is said to be chemically or electrochemically controlled while  $E_A < 10 \text{ kJ}\cdot\text{mol}^{-1}$  is typically a diffusion controlled processes [132]. From the activation energy it can be said that cobalt cementation within the first 30 minutes is a chemically controlled process. The activation energy determined in this study is smaller than the activation energy reported by Lew [114] where the activation energy was determined to be  $86.6 \text{ kJ}\cdot\text{mol}^{-1}$ . However, activation energies between  $39 - 115 \text{ kJ}\cdot\text{mol}^{-1}$  have been reported [70, 100, 102]. All studies conclude that the rate of cobalt cementation is chemically or electrochemically controlled.

The cementation residues were collected after 30 minutes because the maximum removal of cobalt occurred at this time. The micrographs of the unreacted zinc dust are shown in Figure 20a and the cementation product collected at 20 °C and 70 °C is shown Figure 20b and c respectively. The original, unreacted, zinc dust are spherical particles less than 20  $\mu\text{m}$  in diameter. It has been reported that, in general, smaller zinc dust particles result in faster kinetics and higher cobalt concentration yield [103]. At 20 °C, the cementation product is shown as a dendritic layer covered in a mossy deposit. The dendrites are the reduced Cu-Sb-Co metals whereas the mossy deposits were determined to be either zinc oxide or zinc hydroxide according to the relatively higher concentration of zinc and oxygen with EDX analysis. The dissolution of zinc dust is accompanied by hydrogen evolution. As hydrogen evolves, the localized pH in the vicinity of the active sites on the zinc dust increases and promotes the formation of zinc hydroxide that can be observed by the presence of thin layers (mossy and platelet) surrounding the dendritic deposits. The formation of zinc hydroxides retards cobalt cementation by forming a passivating layer. As the temperature is increased the cementation product becomes more compact and the zinc hydroxide changes from a mossy layer to a platelet morphology as seen in Figure 20c. Børve and Østvold [103] suggest the platelets are  $\text{ZnSO}_4$ . EDX data collected here also agree with Børve and Østvold. In that the sulfur in addition to zinc was detected on the hexagonal deposits collected at 70 °C but was not detected at 20 °C. XRD analysis suggests a Zn-Co-O ( $\text{Zn}_{0.998}\text{Co}_{0.002}\text{O}$ ) as well as zinc to be present at 20 °C (Figure 20b) while at 70 °C (Figure 20c) zinc sulfate in addition to Cu-Sb compounds ( $\text{Cu}_2\text{Sb}$ ,  $\text{Cu}_3\text{Sb}$ ) were possible.

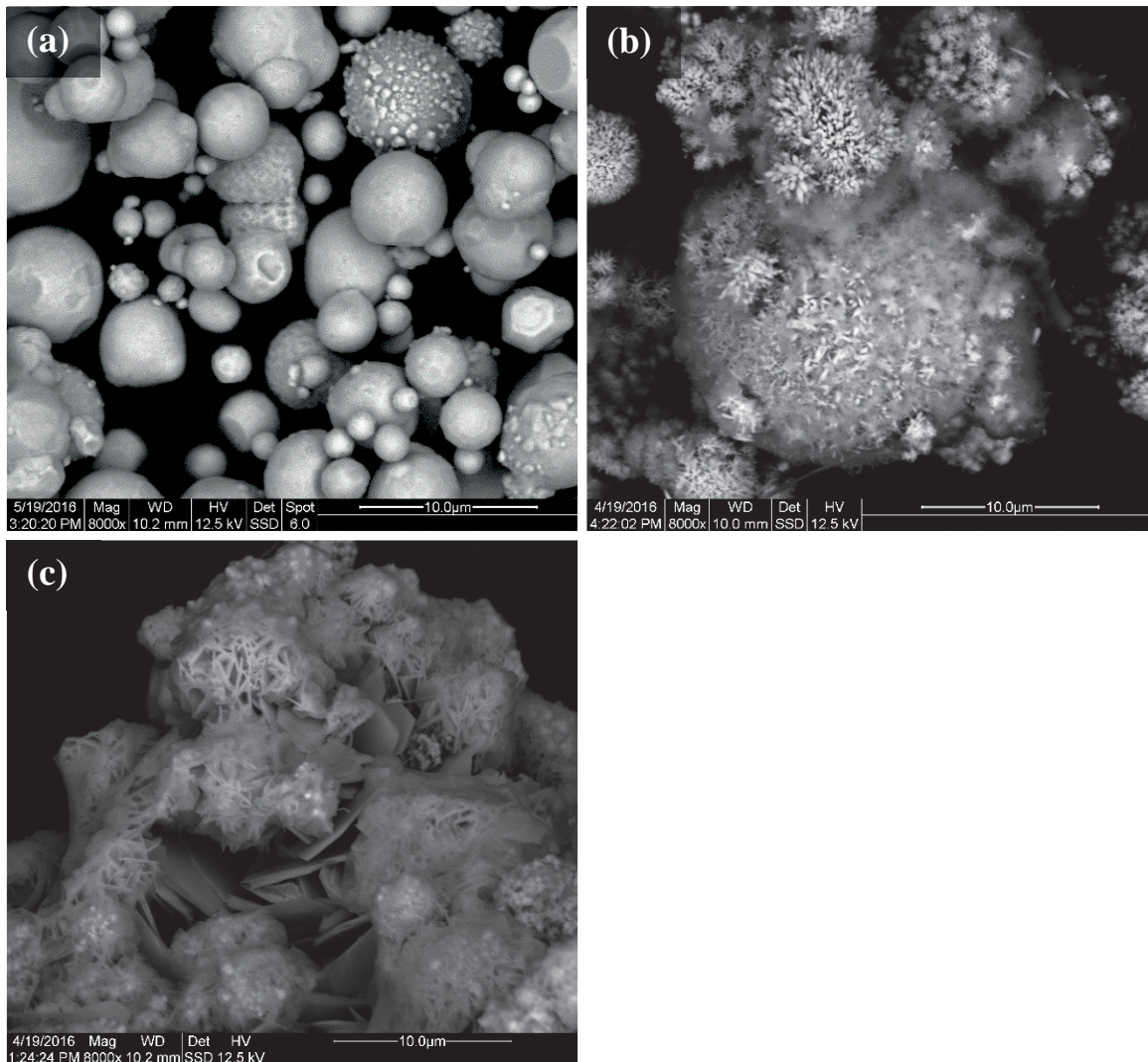


Figure 20: SEM image of (a) zinc dust prior to cementation and cementation product collected after 30 minutes at (b) 20 °C and (c) 70 °C.

An abundance of protons in the electrolyte causes lower cobalt reduction because the electrons from the dissolution of zinc are consumed in hydrogen evolution. According to Van der Pas and Dreisinger [133], when the hydrogen evolution becomes more significant, up to 98 % of the cathodic current is used for this detrimental reaction. The formation of zinc hydroxides that is preceded by the increase in solution pH due to the hydrogen evolution also contributes to the inhibition of cobalt removal at higher solution pH. These passivating substances become more significant in terms of their inhibiting effect when the pH is relatively high.

Figure 21 shows the effect of the solution pH on the cementation rate of cobalt with respect to time. As the solution pH increases, the amount of cobalt being removed from the solution increases. The highest reaction rate for cobalt cementation, represented by rate constants, is observed at solution pH 3 in the first 10 minutes. However, performing cobalt cementation at pH 4 yields more removal of cobalt. This may be because oxidation of zinc dust and thus hydrogen evolution are slower at the higher pH increasing the time it takes for the passivating layer to form.

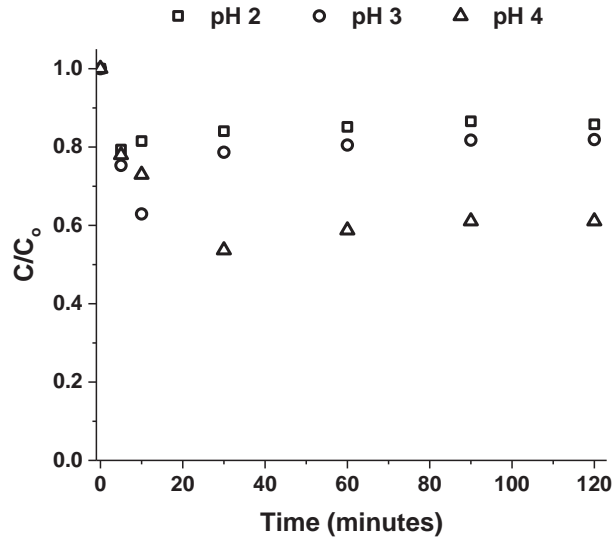


Figure 21: Dimensionless cobalt concentration as a function of time and solution pH during cobalt cementation from zinc sulfate electrolyte.  $T = 70\text{ }^{\circ}\text{C}$ ,  $65\text{ g}\cdot\text{L}^{-1}\text{ Zn}$ ,  $100\text{ mg}\cdot\text{L}^{-1}\text{ Co}$ ,  $100\text{ mg}\cdot\text{L}^{-1}\text{ Cu}$ ,  $100\text{ mg}\cdot\text{L}^{-1}\text{ Sb}$ .

The cementation deposits after 2 minutes and 90 minutes at pH 2 and pH 4 are shown in Figure 22. After 2 minutes of cementation, the passivating zinc hydroxide phase is clearly visible at both pH values studied. The zinc hydroxide was detected by XRD and EDX analysis, where the hexagonal crystals contained high amounts of Zn and O with 60 % and 10 % content respectively. In addition to Zn and O, sulfur was also detected. This is reasonable since cementation was done in a zinc-sulfate electrolyte and would suggest that the salts forming during cementation are not only zinc hydroxide but also zinc sulfate salts. EDX analysis of the cementation product after 90 minutes showed significantly lower levels of Zn, O, and S than after 2 minutes. From ICP-OES data it was shown that the Cu and Sb activators deposited on the zinc dust surface instantaneously after which cobalt cementation occurs.

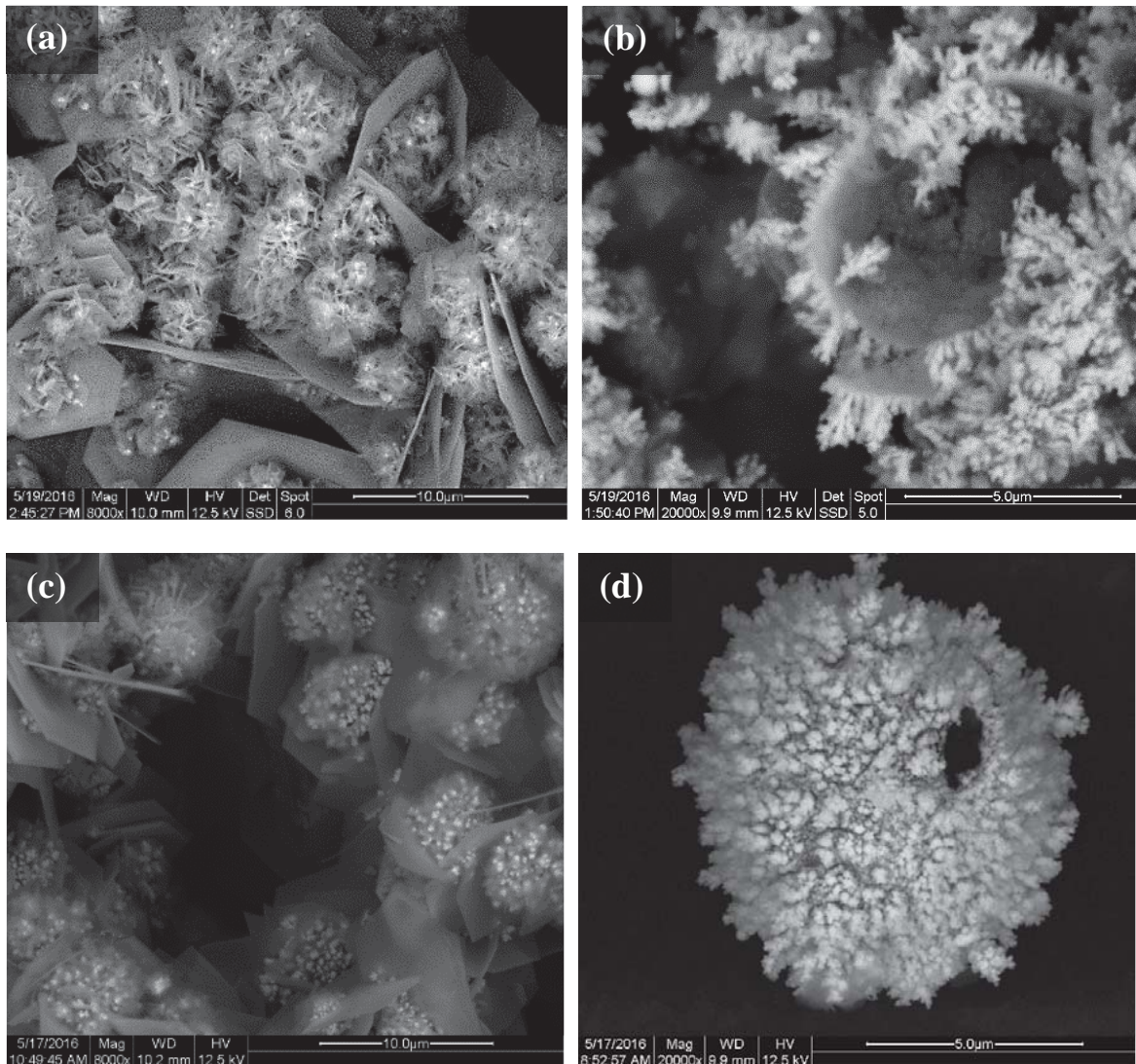


Figure 22: Cementation deposits at pH 2 after (a) 2 minutes and (b) 90 minutes and at pH 4 after (c) 2 minutes and (d) 90 minutes.  $T = 70\text{ }^{\circ}\text{C}$ ,  $65\text{ g}\cdot\text{L}^{-1}\text{ Zn}$ ,  $100\text{ mg}\cdot\text{L}^{-1}\text{ Co}$ ,  $100\text{ mg}\cdot\text{L}^{-1}\text{ Cu}$ ,  $100\text{ mg}\cdot\text{L}^{-1}\text{ Sb}$ .

After 90 minutes, hollow-spheres were observed containing Cu, Sb, and Co. These hollow-spheres are caused by the total dissolution of internal zinc dust. In all spectrums of the EDX, the amount of the zinc element was less than 25 wt% while the rest were copper and antimony with content between 30 and 45 wt% for each element respectively. The morphology after 90 minutes at pH 2 (Figure 22b) appears less dense than the cementation product at pH 4 (Figure 22d). This is most likely due to the lower amount of hydrogen gas forming at higher solution pH. The mean concentration of Co detected by EDX was 11 wt% at pH 4 and 3 wt% at pH 2 in the cementation product collected after 90 minutes.

It is known that the removal of cobalt from a zinc sulfate solution requires the addition of a reducing agent in this case zinc dust. However, the concentration of zinc ions in solution can inhibit the cobalt cementation process as seen in Figure 23. The absence of zinc ions nearly yields the complete removal of cobalt with some re-dissolution of the cobalt occurring once the zinc dust was consumed. Zinc ions cause polarization due to the abundance of cations surrounding the zinc dust [134] the repulsion of the charges prevents the migration of cobalt ions to the zinc dust surface. Very little difference in cobalt removal was observed in solutions containing  $33 - 131\text{ g}\cdot\text{L}^{-1}\text{ Zn}$ .

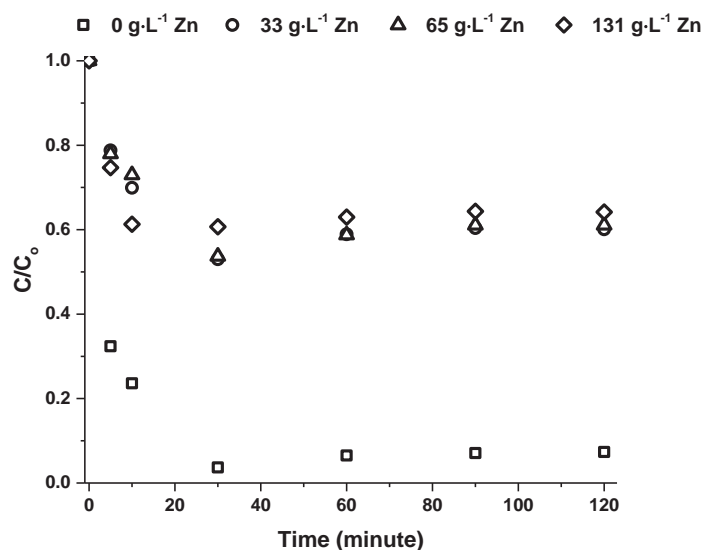


Figure 23: Dimensionless cobalt concentration as a function of time and initial zinc ion concentration during cobalt cementation from zinc sulfate electrolyte.  $T = 70\text{ }^{\circ}\text{C}$ ,  $\text{pH } 4$ ,  $100\text{ mg}\cdot\text{L}^{-1}\text{ Co}$ ,  $100\text{ mg}\cdot\text{L}^{-1}\text{ Cu}$ ,  $100\text{ mg}\cdot\text{L}^{-1}\text{ Sb}$ .

The morphology of the cementation residue after 2 and 90 minutes is given in Figure 24a-d. When zinc ions were not present, dense, mossy deposits were observed as shown in Figure 24a. EDX analysis, determined the Co content was 12 wt% after 2 minutes and over 40 wt% after 90 minutes, this is in reference to Figure 24a and b respectively. EDX also showed a low concentration of zinc,  $< 10\%$ , in the cementation product. The addition of Zn ions caused the formation of zinc hydroxide or zinc sulfate as seen in Figure 24c which have been shown and reported to block/cover the active surface needed for cobalt cementation. After 90 minutes, the zinc dust was dissolved in both sample leaving the cementation product as hollow spheres. The cementation product appears to be more compact when there is no zinc in the starting electrolyte while the  $131\text{ g}\cdot\text{L}^{-1}\text{ Zn}$  solution yielded a more dendritic morphology.

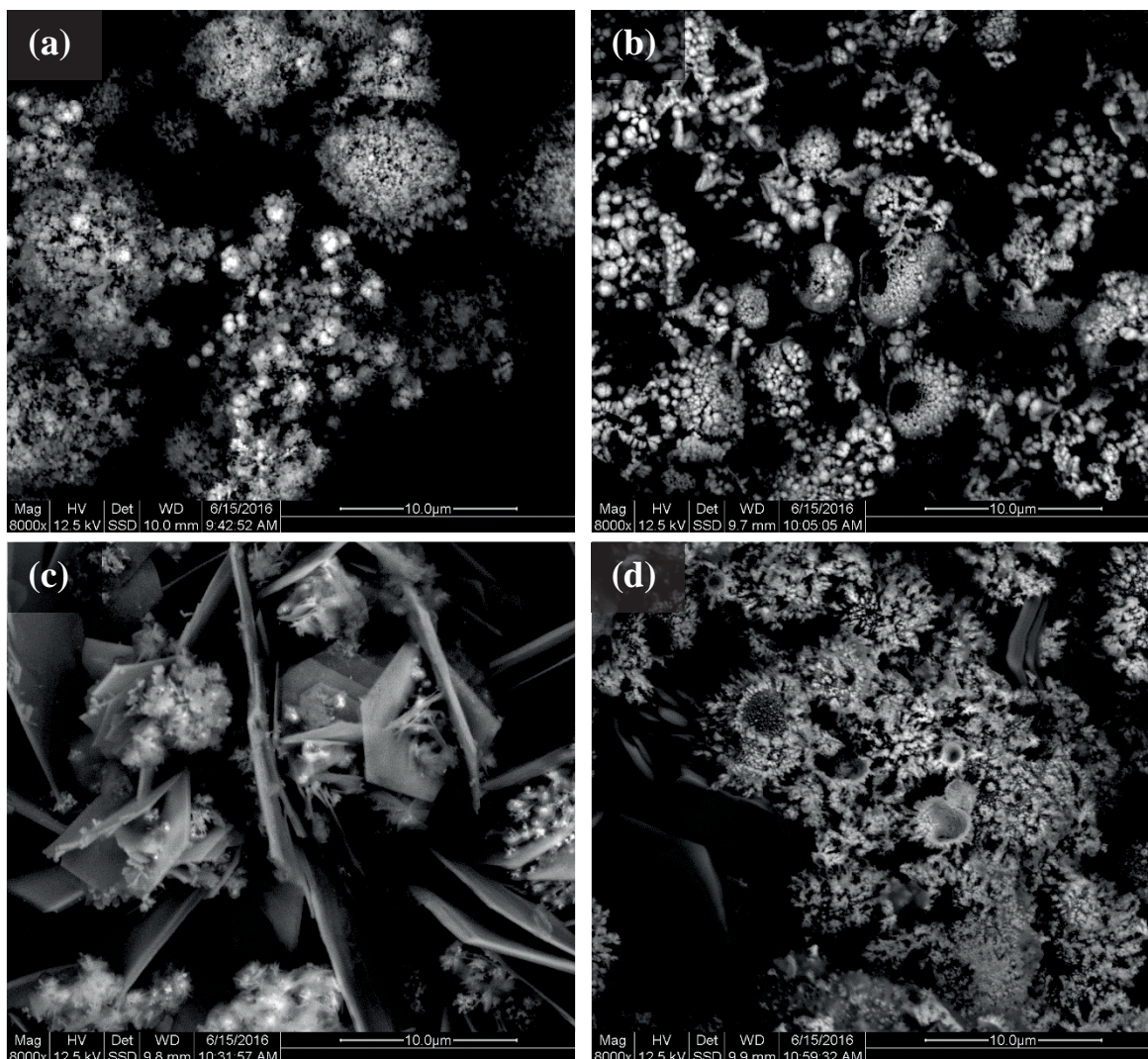


Figure 24: Cementation residue in electrolyte with no initial zinc in solution after (a) 2 minutes and (b) 90 minutes. Cementation residue with  $131 \text{ g}\cdot\text{L}^{-1}$  Zn initial zinc concentration after (c) 2 minutes and (d) 90 minutes.  $T = 70 \text{ }^\circ\text{C}$ ,  $\text{pH } 4$ ,  $100 \text{ mg}\cdot\text{L}^{-1}$  Co,  $100 \text{ mg}\cdot\text{L}^{-1}$  Cu,  $100 \text{ mg}\cdot\text{L}^{-1}$  Sb.

From the morphology studies, it can be concluded that higher temperatures increase the cobalt cementation kinetics, and consequently the cobalt content in the deposited alloy. Increasing the temperature causes the redissolution of cobalt. Cobalt cementation is a chemically controlled process with an activation energy of  $45 \text{ kJ}\cdot\text{mol}^{-1}$ . Increasing the temperature also caused the formation of  $\text{ZnSO}_4$  platelets which were not seen at room temperature. The solution pH plays a significant role in determining which reaction is more favorable. At low solution pH ( $< 4$ ), more hydrogen evolution was thought to occur and the cobalt cementation was very poor. At high solution pH ( $> 4$ ), the formation of the passivating substances, such as zinc hydroxide were observed. The presence of zinc ions in the electrolyte itself inhibits the cobalt cementation due to the cation repulsion effect that blocks/inhibits cobalt ions to move closer to the cathodic surface. Nearly all the copper and antimony cements within the first 90 seconds, however cobalt starts depositing with copper and antimony acting as the preferential substrates for cobalt and also as a stabilizer for the deposited cobalt to not redissolve. From EDX data it can be concluded that cobalt deposits as an alloy with antimony and copper when it is reduced from the zinc sulfate electrolyte and not as a concentrated Co product.

### 5.1.4. Antimony Separation from the MOV Residue

The composition of the leached MOV residue is given in Table 13 as milligrams of metal per gram of MOV residue. Before leaching the amount of antimony in the MOV was 35 mg and after leaching there is 186 mg of antimony in the residue, i.e. sulfuric acid leaching as a pretreatment step increased the antimony concentration over 5 times.

Table 13: Composition of the solid leaching residue given in  $\text{mg}\cdot\text{g}^{-1}$ .

Metal	$\text{mg}\cdot\text{g}^{-1}$
Bi	$247 \pm 1$
Co	$11.8 \pm 0.1$
Mn	$14.7 \pm 0.1$
Ni	$25.9 \pm 0.1$
Sb	$186 \pm 2$
Zn	$360 \pm 1$

Prior to the leaching pretreatment, the MOV consisted of three main phases: firstly, the bulk zinc oxide phase, which accounted for nearly 90 % of the MOV; secondly, the bismuth oxide phase, found in the region between the zinc oxide grains, and lastly the phase containing antimony compounds such as spinel-like ( $\text{Zn}_7\text{Sb}_2\text{O}_{12}$ ) and pyrochlore ( $\text{Zn}_2\text{Bi}_3\text{Sb}_3\text{O}_{14}$ ). The bulk zinc oxide phase seen in Figure 9 was dissolved during the leaching pretreatment with sulfuric acid leaving the bismuth and antimony phases as an insoluble residue.

The remaining zinc is no longer present as zinc oxide but is found within the non-leachable spinel and pyrochlore compound having the chemical compositions  $\text{Zn}_{2.33}\text{Sb}_{0.67}\text{O}_4/\text{Zn}_7\text{Sb}_2\text{O}_{12}$  and  $\text{Zn}_2\text{Bi}_3\text{Sb}_3\text{O}_{14}$  respectively. Bismuth is present as  $\text{Bi}_2\text{O}_3$ . The remaining metals are most likely substituted into the spinel lattice. This is to be expected as the MOV is sintered during manufacturing and several products can be formed during this process. The XRD diffractogram of the residue shown in Figure 25 supports this conclusion where peaks are seen for Zn-Co-Sb-O and Zn-Ni-Sb-O compounds. XRD data are in good correlation to ICP-OES data.

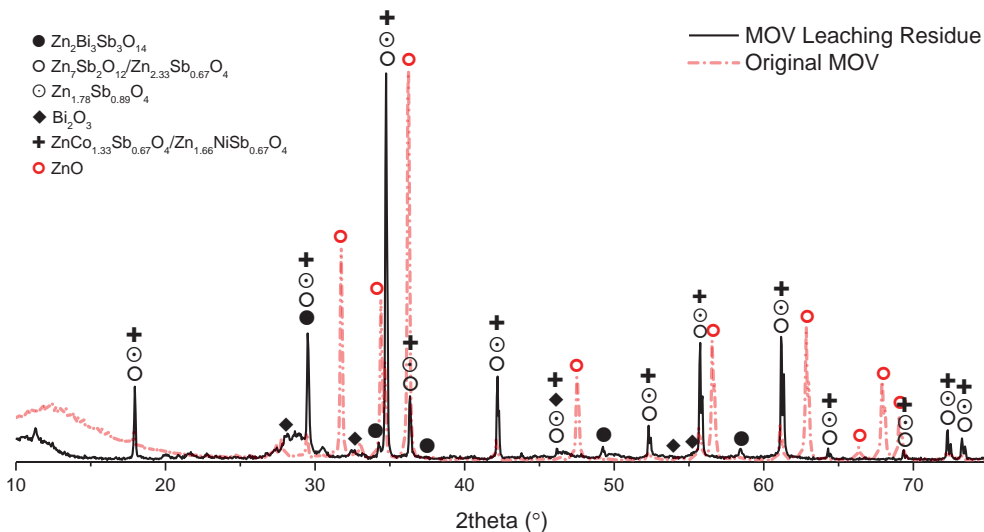
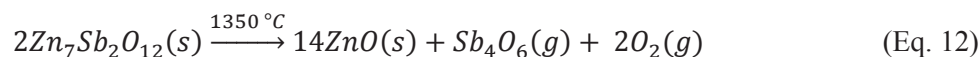


Figure 25: XRD diffractogram of the original (unleached) MOV and the MOV leaching residue.

There are two polymorphous forms of the  $Zn_7Sb_2O_{12}$  compound. The cubic  $\alpha$ - $Zn_7Sb_2O_{12}$  which has a crystal structure of the inverse spinel and orthorhombic  $\beta$ - $Zn_{2.33}Sb_{0.67}O_4$ , in which the crystal structure is not understood. Since antimony is not found as  $Sb_2O_3$  but within the spinel and pyrochlore compounds, the fate of antimony during thermal treatment of the MOV residue is not clear. The spinel compound has been reported to be stable up to 1350 °C [74]. Filipek et al. 2008 have suggested thermal decomposition of spinel occurs according to the reaction in Equation 12.



Thermal decomposition of the MOV residue in the absence of carbon in the present work resulted in less than 5 % mass loss. The addition of carbon to the MOV residue had a large effect on the mass loss as seen in Figure 26. For all samples containing carbon, there are four inflections indicating several stages of decomposition occurring in the MOV residue-carbon samples. The mass loss increased with temperature due to thermal decomposition, representing the mass of volatile matter removed from the sample. The decomposition regions are labeled in Figure 26 and correspond to the decomposition reactions given in Equation 37 - 39. The decomposition mechanisms proposed are based on this research, literature data, and mass balance calculations.

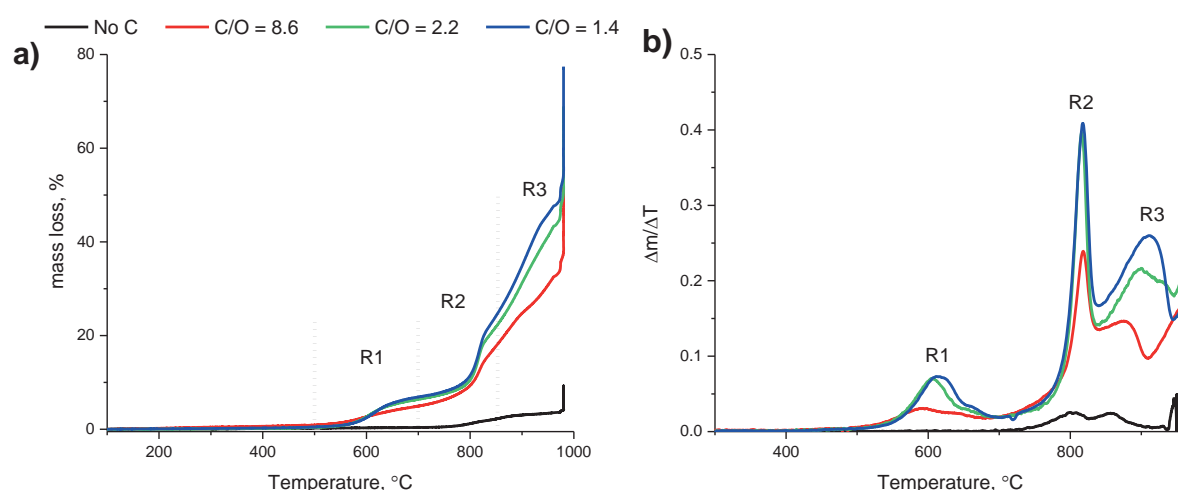


Figure 26: (a) Effect of C/O molar ratio on mass loss of MOV residue during heating to 980 °C, heating rate 10 °C·min<sup>-1</sup>. (b) Derivative curve for mass loss as a function of temperature.

Region	Temperature	Reaction	Equation
R1	500 – 700 °C	$Bi_2O_3(s) + 3C(s) \rightarrow 2Bi(s) + 3CO(g)$	Eq. 39
R2	700 – 850 °C	$2Zn_7Sb_2O_{12}(s) + 4C(s) \rightarrow 14ZnO(s) + Sb_4O_6(g) + 4CO(g)$	Eq. 38
R3	~ 900 °C	$ZnO(s) + C(s) \rightarrow Zn(s) + CO(g)$	Eq. 37

The first reaction is the loss of oxygen forming liquid Bi (R1) occurring at 600 °C. In the presence of carbon, R2 has been proposed as the decomposition mechanism for  $Zn_7Sb_2O_{12}$ . The complete decomposition of  $Zn_7Sb_2O_{12}$  would result in a theoretical mass loss of approximately 65.7 % when the C/O = 1.4. The experimental mass loss between 700 – 980 °C was 71.5 %, indicating that the decomposition of spinel occurs in this range. In addition it is possible that a portion of the Bi was also volatilized in this range explaining why the experimental mass loss is higher than the theoretical mass loss.

Since it is known that ZnO decomposed according to R3 near 900 °C, the reaction near 800 °C is assumed to be the volatilization of Sb<sub>4</sub>O<sub>6</sub>(g). The theoretical weight loss is 22.8 %, while the experimental weight loss for the vaporization of Sb<sub>4</sub>O<sub>6</sub>(g) plus the formation of CO was 17.3 %. The difference in values is expected due to multiple reactions occurring near 900 °C. This is depicted in Figure 26b, where the derivative curve does not return to baseline before the ZnO(s) reduction reaction (R3) begins.

The calculated and experimentally determined weight losses for Equations 37 - 39 are given in Table 14. Theoretical weight loss calculations were made using the following assumptions and the composition of the MOV residue given in Table 13.

1. All Bi in the sample is in the form of Bi<sub>2</sub>O<sub>3</sub>.
2. All Sb in the sample is in the form Zn<sub>7</sub>Sb<sub>2</sub>O<sub>12</sub>. This also accounts for 97 % of the Zn in the sample.
3. Liquid Bi, Co, Ni, Mn remain as a solid in the residue.
4. The C used is calculated according to Eq. 37 - 39.

There are small deviations between the theoretical and experimental data. From the derivative curves in Figure 26b, it is seen that decomposition in R2 is not complete before decomposition in R3 begins. Multiple reactions occur simultaneously; therefore the experimental mass loss should only be viewed as an estimate from an explicit decomposition reaction. Simultaneous reactions will cause deviation between theoretical and experimental data. Also, the volatilization of Bi could not be accounted for in the theoretical calculations and therefore the mass loss will always be slightly lower than the experimentally obtained data.

Table 14: Theoretical mass loss, in wt%, from mass balance calculations and experimental mass loss for Equations 37 - 39.

Region	Theoretical			Experimental		
	C/O = 8.6	C/O = 2.2	C/O = 1.4	C/O = 8.6	C/O = 2.2	C/O = 1.4
R1	2.5	4.0	4.3	4.6	6.3	6.8
R2	13.2	21.2	22.8	12.7	15.5	17.3
R3	24.9	39.9	42.9	34.2	46.9	54.2
<i>Subtotal</i>	<i>40.7</i>	<i>65.1</i>	<i>70.0</i>	<i>51.5</i>	<i>68.7</i>	<i>78.3</i>
Co, Ni, Mn	2.6	4.2	4.5			
Bi	12.3	19.7	21.2			
C	44.9	11.8	5.1			
<b>Total</b>	<b>109.1</b>	<b>103.0</b>	<b>102.3</b>			

Metals such as cobalt, nickel, and manganese make up less than 5 % of the MOV residue and are not accounted for in the mass balance calculations. Since they are substituted into the spinel lattice they are believed to remain after the decomposition and volatilization of zinc and antimony. In Table 14, Subtotal refers to total mass loss from reactions given in Equations 37 - 39, Total accounts for the other metals (Co, Ni, Mn), liquid bismuth, and unreacted carbon. The Bi, unreacted carbon, and other metals are assumed to remain in the solid phase and do not contribute to mass loss.

It has been reported once that molten bismuth will volatilize at high temperatures. This was observed when reducing pure Bi<sub>2</sub>O<sub>3</sub> [135]. The weight loss curve above 700 °C is smooth with no sharp inflection points, indicating the slow kinetics of bismuth volatilization. It can be concluded that some of the bismuth remained in the sample and some was volatilized. This would also explain the deviation between theoretical and experimental mass loss. From the TGA data, it can be concluded that antimony in the form of Sb<sub>4</sub>O<sub>6</sub> can be collected by carbothermal reduction of the MOV leach residue and condensation with some bismuth as an impurity between 700 - 850 °C.

### 5.1.5. MOV Residue Morphology During Thermolysis and Carbothermal Reduction

Studying the phase change during thermolysis and carbothermal reduction called for higher temperatures and a larger sample size. Therefore reduction experiments requiring temperatures exceeding the range of the TGA were performed in a furnace in an argon atmosphere glovebox which also allowed for larger MOV residue samples to be used and subsequently characterized. It has been shown that it is possible to liberate antimony from the  $Zn_7Sb_2O_{12}$  structure at temperatures higher than 1350 °C if performed in air [74] and higher than 1115 °C are needed in an argon atmosphere [75].

Thermolysis experiments were done using six temperatures. Results from ICP-OES analysis of the MOV residue remaining after thermal reduction are shown in Table 15. The amount of each metal remaining after thermolysis is given in milligrams per gram of MOV residue. Heating to 1100 °C resulted in over 50 % weigh loss of the sample, the majority being bismuth and antimony. These results indicate that nearly 80 % of the antimony can be separated from the MOV residue and eventually collected in the gaseous phase between 900 – 1100 °C.

Table 15: ICP-OES analysis of the MOV residue samples after thermolysis. Results given in mg of metal per gram of MOV residue.

Sample Temp.	Weight loss	Bismuth	Cobalt	Manganese	Nickel	Antimony	Zinc
°C	%	mg·g <sup>-1</sup>					
500	3.2	196	10	12	24	146	257
700	4.1	223	12	15	27	170	313
825	6.1	187	12	15	27	165	318
900	11.1	126	12	15	28	171	312
1100	57.6	0	11	13	26	33	241
1300	81.7	3	10	11	25	8	72

The crystalline compounds identified by XRD analysis in three thermolysis residue samples are shown in Figure 27. Based on the diffractogram, no change occurred in the leaching residue when heated from room temperature to 500 °C. Heating from 500 °C to 700 °C causes a change in the crystal structure of  $Bi_2O_3$  and at temperatures over 900 °C  $Bi_2O_3$  has been separated from the leach residue. For the sample treated at 900 °C, peaks were confirmed for pyrochlore ( $Zn_2Bi_3Sb_3O_{14}$ ), spinel ( $Zn_{2.33}Sb_{0.67}O_4$  and  $Zn_7Sb_2O_{12}$ ), and phases containing Zn-Co-Sb-O and Zn-Ni-Sb-O such as  $ZnCo_{1.33}Sb_{0.67}O_4$  and  $Zn_{1.33}NiSb_{0.67}O_4$ . Antimony containing compounds such as spinel and pyrochlore were destroyed when heated from 900 to 1100 °C separating antimony from the remaining MOV leaching residue. At 1100 °C, XRD peaks for ZnO are present while no peaks for the spinel or pyrochlore compounds are detected. However, a new compound,  $ZnSb_2O_4$ , as well as an Sb-Co alloy are indicated by the diffractogram at 1100 °C as well as an Sb-Co alloy. At 1300 °C peaks for ZnO and an Ni-Sb alloy were seen along with peaks for CoO or Cobalt (II) Aluminate which was also indicated by the blue color of the residue in the alumina crucible.

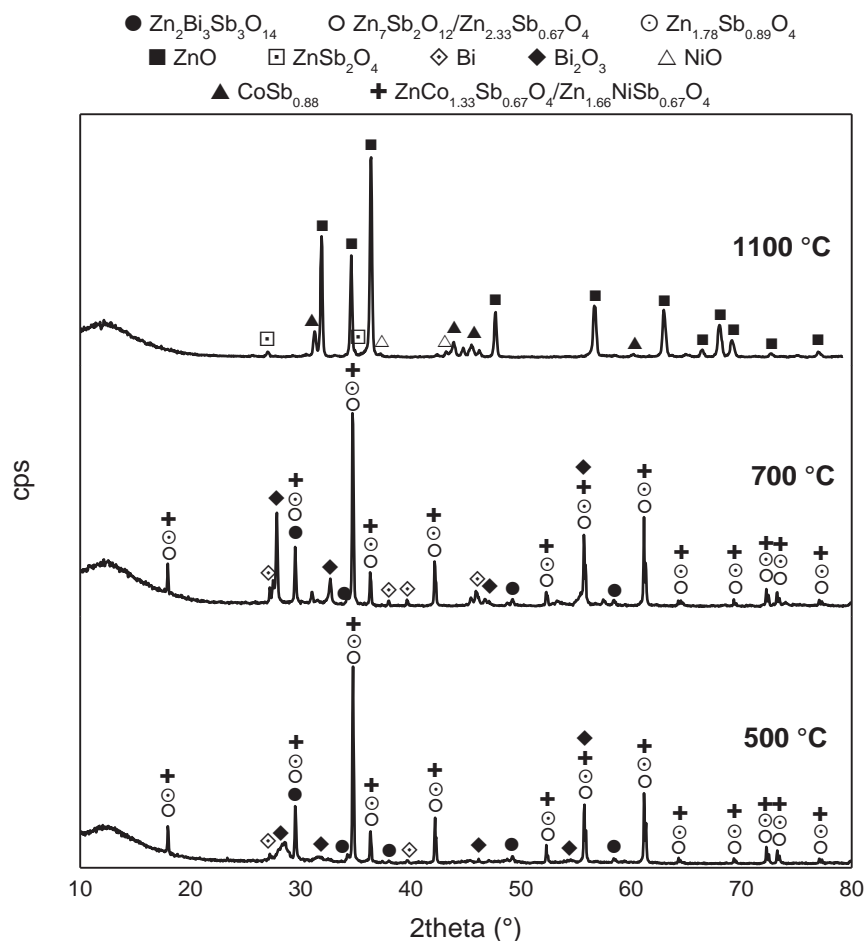


Figure 27: XRD spectra for thermolysis of MOV leaching residue in argon atmosphere at temperatures of 500, 700, and 1100 °C.

Thermolysis results of the MOV leaching residue show that antimony within the  $Zn_7Sb_2O_{12}$  compound can no longer be detected in material treated above 1100 °C. This differs from other work where temperatures higher than 1115 °C were used to break down the  $Zn_7Sb_2O_{12}$  compound [75]. Antimony was not completely separated from the MOV leaching residue at 1100 °C, however as seen in Table 15 a significant amount was removed.

Following XRD analysis, each sample was imaged and analyzed with SEM-EDX and the micrographs are shown in Figure 28a-f for each leaching residue. Heating to 500 °C causes no change in the residue. At 700 °C some changes occurred in the bismuth phase and small balls of bismuth oxide formed. It has been reported that between 710 - 740 °C bismuth changes from  $\alpha$ - $Bi_2O_3$  to  $\delta$ - $Bi_2O_3$  [136]. The antimony phase remained unaffected as confirmed by XRD and ICP-OES. The bismuth oxide phase is collected into larger spheres; leaving the antimony rich phase mostly unaffected at 825 °C as seen in Figure 28c.

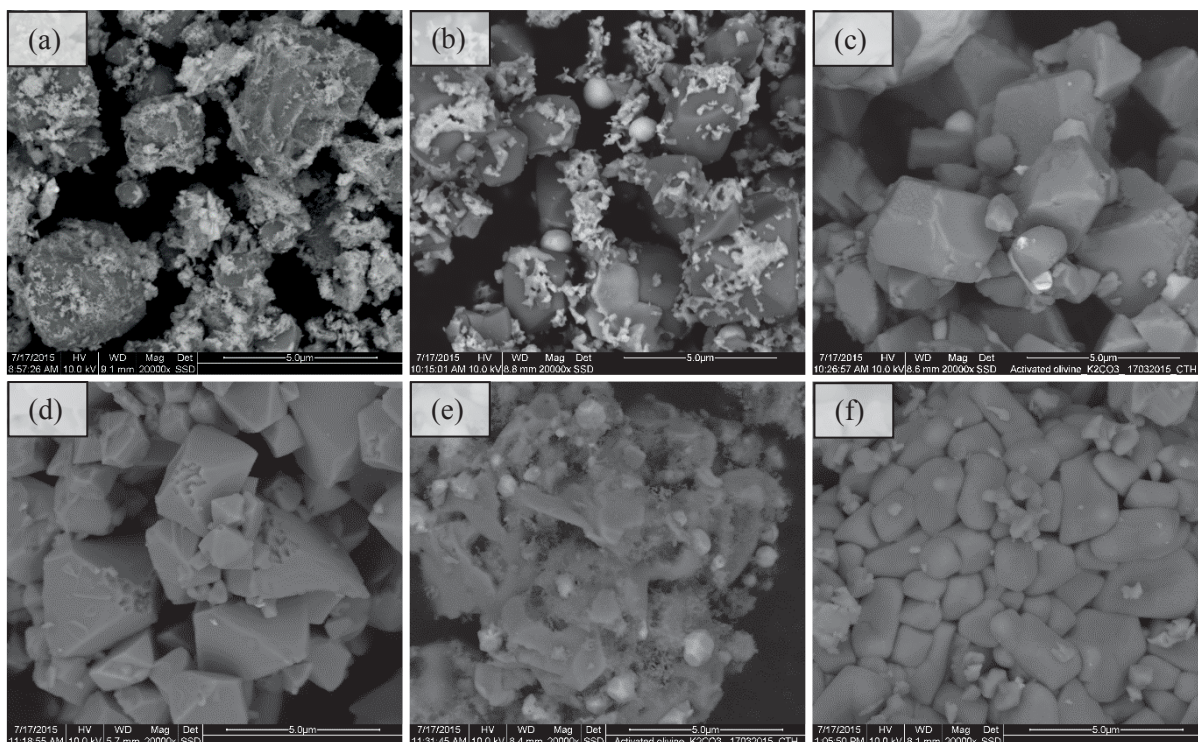


Figure 28: SEM micrographs of heat treated MOV residue at (a) 500 °C, (b) 700 °C, (c) 825 °C, (d) 900 °C, (e) 1100 °C, (f) 1300 °C.

At 900 °C decomposition of the antimony phase was seen from the cavities occurring in the crystals shown in Figure 28d. The antimony phase is fully decomposed at 1100 °C (Figure 28e). Decomposition of the antimony phase either reveals or causes formation of a nickel-antimony compound seen in Figure 28e as small, lighter in color particles, less than 1 μm in diameter. EDX analysis of the remaining sample in Figure 28f shows what remains of the MOV residue after heating to 1300 °C, EDX suggests it contains mainly cobalt and nickel, this is in good agreement with ICP-OES data.

From XRD, ICP, SEM-EDX and measurement of weight loss of the heat treated MOV residue it can be concluded that approximately 80 % of the antimony was separated/volatilized between 900 - 1100 °C. The antimony can be collected and condensed to produce a secondary source of antimony. However, a small amount of antimony remains in the residue alloyed with cobalt or nickel.

Further investigations on antimony separation by carbothermal reduction were performed. ICP-OES analysis on the carbothermal reduction samples are given in Table 16 which provides the weight loss experienced by each sample during heating, as well as the amount, in milligrams of metal remaining after reduction per gram of MOV residue and carbon mixture. It was concluded that zinc was separated from the MOV leaching residue above 900 °C and bismuth was separated above 1000 °C. Nearly 70 % of the antimony in the sample was separated when the MOV residue was heated to 1000 °C. However, some antimony remained along with cobalt, nickel, and manganese at temperatures up to 1100 °C.

Table 16: ICP-OES analysis of carbothermal reduction residue samples. Results given in mg of metal per gram of MOV residue.

Sample Temp.	Weight Loss	Bismuth	Cobalt	Manganese	Nickel	Antimony	Zinc
°C	%	mg·g <sup>-1</sup>					
500	2.2	214	11	14	26	162	270
700	8.8	213	11	13	25	161	276
825	20.2	172	12	13	28	161	294
900	32.5	172	11	12	25	142	214
1000	75.5	79	4	8	10	50	0
1100	92.1	1	4	4	8	24	0

XRD analysis on three carbothermal reduction samples after heat treatment are shown in Figure 29. No change in XRD pattern was seen when heating the MOV leaching residue up to 500 °C. At 500 °C the XRD pattern was shown to contain peaks for spinel ( $Zn_{2.33}Sb_{0.67}O_4$  and  $Zn_7Sb_2O_{12}$ ), pyrochlore ( $Zn_4Bi_3Sb_2O_{12}$ ) and phases containing Zn-Co-Sb-O and Zn-Ni-Sb-O compounds, such as  $ZnCo_{1.33}Sb_{0.67}O_4$  and  $Zn_{1.33}NiSb_{0.67}O_4$  were also present. At 700 °C the presence of bismuth metal or a Bi-Sb alloy such as  $Bi_{0.97}Sb_{0.03}$  or  $Bi_{0.92}Sb_{0.07}$  appeared. In addition the peaks for spinel, pyrochlore, Zn-Co-Sb-O, and Zn-Ni-Sb-O remained.

Heating the MOV leach residue to 825 °C destroyed the spinel phase leaving detectible amounts of ZnO, pyrochlore, CoSb and Bi or a Bi-Sb alloy such as  $Bi_{0.97}Sb_{0.03}$  or  $Bi_{0.92}Sb_{0.07}$ . No change was seen in the XRD diffractogram when the sample had been heated from 825 °C to 900 °C. However, significant changes occurred at 1000 °C where ZnO and pyrochlore were reduced. The XRD data for the 1000 °C sample shows the existence of a Bi-Sb alloy, CoSb, and a Ni-Sb alloy such as NiSb and NiSb<sub>2</sub>. The residue remaining after heating the MOV leaching residue to 1100 °C showed peaks corresponding to CoSb, CoO, Ni-Sb, and possibly  $Zn_{1.67}Mn_{1.33}O_4$ . The peaks for bismuth or bismuth containing compounds were not present.

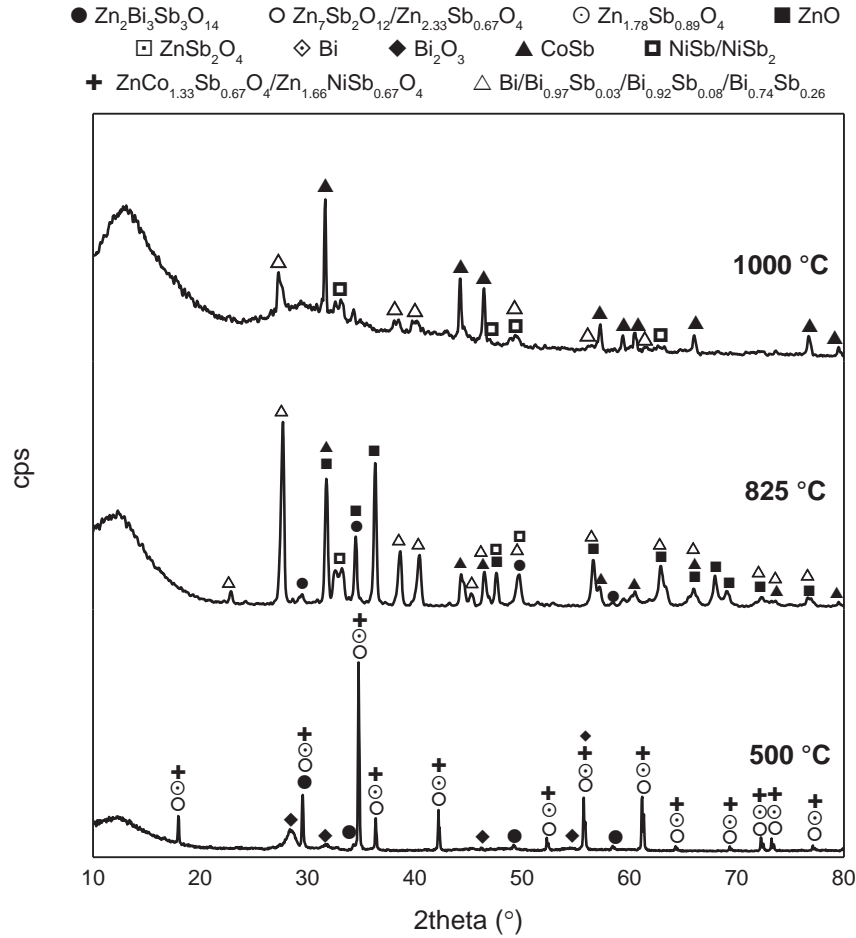


Figure 29: XRD spectra for carbothermal reduction of MOV leaching residue in argon at temperatures of 500, 825, and 1000 °C.

From the micrographs in Figure 30 and diffractograms in Figure 29, it can be concluded that at 500 °C no change has occurred to the leaching residue. The bismuth oxide phase and the antimony rich phases are present. Heating the leaching residue to 700 °C causes a change in the bismuth phase, most likely melting or phase separation, [137] as seen by the bismuth rich spheres in Figure 30b. The bismuth spheres contain small amounts of antimony as indicated by EDX. The antimony rich phase appears unaffected as seen from XRD and SEM. Further heating to 825 °C caused thermal degradation of the antimony containing spinel compounds,  $Zn_{2.33}Sb_{0.67}O_4$  and  $Zn_7Sb_2O_{12}$  phases yielding small particles of Zn-Ni-Co-Sb-O in a zinc oxide matrix according to EXD results.

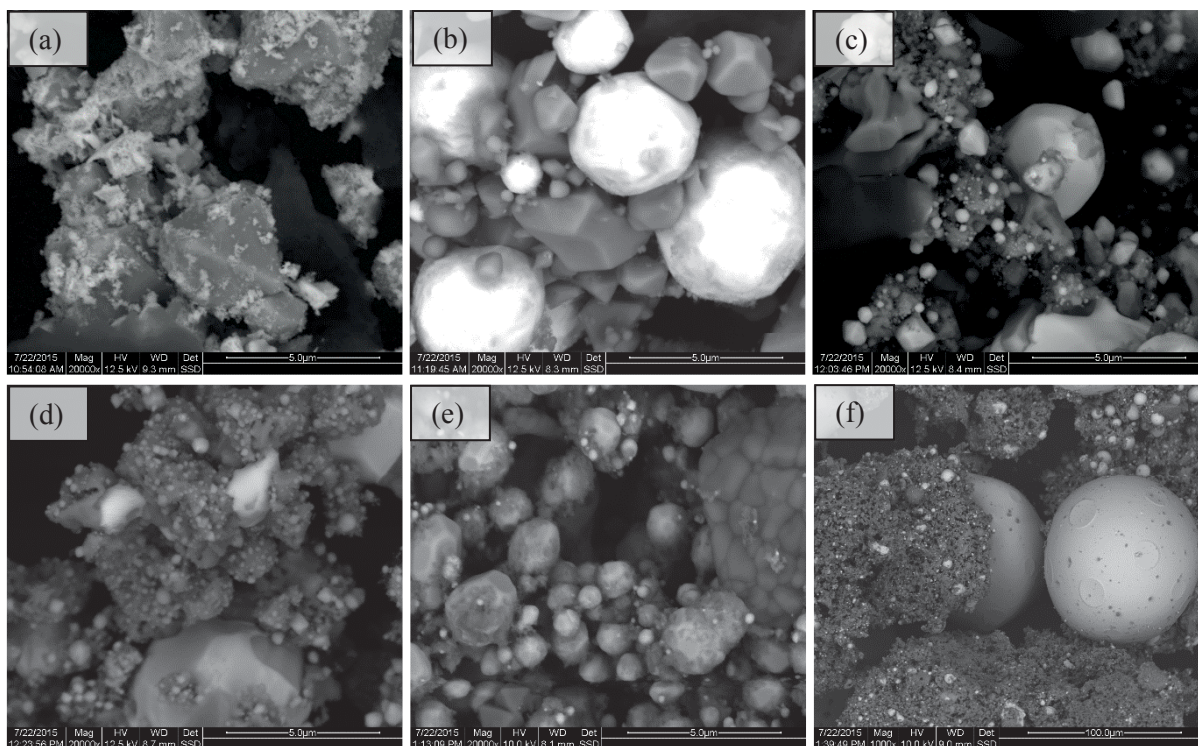


Figure 30: SEM micrographs of MOV residue after carbothermal reduction at (a) 500 °C, (b) 700 °C, (c) 825 °C, (d) 900 °C, (e) 1000 °C, (f) 1100 °C.

It could not be concluded from SEM-EDX that any change had occurred during heating from 825 °C to 900 °C and the XRD spectra for these two samples were similar. ZnO volatilized and is no longer detectable in the residue from treatment at temperatures above 900 °C which is expected. The reduction of zinc oxide in the presence of carbon is reported to occur at 907 °C [138]. At temperatures higher than 1000 °C, round particles originating from a melt and composed of Sb-Ni-Co as seen in Figure 30e and Figure 30f were formed. These structures probably are composed of the alloys CoSb and NiSb/NiSb<sub>2</sub> that were identified by XRD. The “spongy” structures in Figure 7f made up of partially sintered, small particles consist of different Ni-Sb, Co-Sb or Bi-Sb alloys as indicated in Figure 29.

The low temperature, thermodynamically stable, orthorhombic  $\beta$ -Zn<sub>7</sub>Sb<sub>2</sub>O<sub>12</sub> undergoes reversible transition to high temperature cubic  $\alpha$ -Zn<sub>7</sub>Sb<sub>2</sub>O<sub>12</sub> at 1225 °C [75]. The compound  $\alpha$ -Zn<sub>7</sub>Sb<sub>2</sub>O<sub>12</sub> is stable up to 1350 °C, above which it decomposes to ZnO releasing Sb<sub>4</sub>O<sub>6</sub>(g) and O<sub>2</sub>(g). However, it was observed that in the presence of carbon, Zn<sub>7</sub>Sb<sub>2</sub>O<sub>12</sub> can be destroyed at temperatures between 700 - 825 °C. In the present work, SEM-EDX, ICP-OES and XRD results from carbothermal reduction of the MOV leaching residue show that nearly 70 % of the antimony can be separated from the MOV leaching residue by vaporization at temperatures between 900-1000 °C.

## 5.2. ANTIMONY RECOVERY FROM MSWI FLY ASH

The aim of this research was to give information on the pH-dependent leaching behavior of antimony in MSWI ash focusing on the possibility of extracting and recovering it from the ash in its original form, and after a salt removal treatment (HALOSEP) using a slightly acid HCl solution. Such information is scarce in scientific and technical literature today. Since hydrochloric acid waste solutions are available as byproducts from the flue gas cleaning in many MSWI plants, dilute HCl was used for the leaching experiments here.

The concentrations of elements in the ash samples are given in Table 17 and were determined by an accredited lab. As was expected, the chloride concentration had been significantly decreased in the HALOSEP ash. Due to the removal of salts, the concentration of metals should be increased and that was also the case. Antimony, lead, and zinc all show an increase in concentration after the HALOSEP process.

Table 17: Element concentrations in each ash sample.

Element	Untreated Fly Ash, mg·kg <sup>-1</sup>	HALOSEP Fly Ash, mg·kg <sup>-1</sup>	Uncertainty in the analytical method, %
Aluminum	18,000	38,000	20
Antimony	550	850	15
Arsenic	140	180	25
Barium	530	980	20
Beryllium	1.1	2.9	20
Cadmium	96	74	30
Calcium	290,000	250,000	20
Chloride, Cl <sup>-</sup>	147,800	2674	10
Chromium	200	620	20
Cobalt	11	21	30
Copper	430	880	20
Iron	4200	15,000	20
Lead	2400	4700	20
Magnesium	8300	16,000	20
Manganese	290	580	20
Mercury	9.2	21	25
Molybdenum	< 11	< 11	20
Nickel	29	73	35
Phosphorus	3300	6900	20
Potassium	25,000	7700	20
Scandium	< 1.1	2.2	20
Silicon	45,000	130,000	20
Sodium	27,000	8400	20
Strontium	390	410	20
Sulfate, SO <sub>4</sub> <sup>2-</sup>	83,200	173,600	10
Sulfur	41,000	78,000	25
Tin	610	920	20
Titanium	2900	9600	20
Vanadium	26	57	20
Yttrium	6.3	13	20
Zinc	13,000	21,000	25
Zirconium	52	170	20
LOI, loss on ignition (%)	17	4.1	

XRD analysis made on the original untreated fly ash showed the presence of  $\text{Ca}(\text{OH})_2$ ,  $\text{CaSO}_4$ ,  $\text{NaCl}$ ,  $\text{KCl}$ ,  $\text{Mg}(\text{OH})_2$ , and  $\text{CaCO}_3$ . The HALOSEP treated ash was shown to contain  $\text{CaSO}_4 \cdot \text{H}_2\text{O}$  as its main crystalline component in addition to  $\text{CaCO}_3$  and possibly traces of ettringite ( $\text{Ca}_6\text{Al}_2(\text{SO}_4)_3(\text{OH})_{12} \cdot 26\text{H}_2\text{O}$ ) and  $\text{NaCl}$ . The sodium chloride most likely remained inside the pore structure of the ash particles. The amount of  $\text{NaCl}$  in the HALOSEP ash sample is very small if it is there at all. Ettringite is a hydration product which occurs in Portland cement and super-sulfated residues [139]. It was shown by Antao et al. [139] that when ettringite is heated, the short range order is disrupted and it becomes XRD amorphous and may be the reason it is not easily detected.

Thermodynamic calculations do not model the real processes exactly, since strong simplifying assumptions have to be made (ideal thermodynamic conditions, homogeneous distribution of the elements, chemical equilibrium, etc.), which can be far from reality in some systems. Nevertheless, thermodynamic models can be powerful tools for understanding chemical behavior. Only the Eh-pH diagrams using the untreated ash sample are shown because only minor differences were seen when comparing the untreated and HALOSEP treated samples. Indications from the Eh-pH diagrams shown in Figure 31 suggest that antimony is not leachable between pH 1 – 12 or at least the dominant antimony species in the pH range will not be that of a soluble antimony compound. For antimony to be soluble, a pH < -1 or in excess of pH 12 would be necessary although it is not seen in Figure 31. At neutral and higher pH values, antimony could react with calcium to form  $\text{Ca}_3(\text{SbO}_4)_2$ .

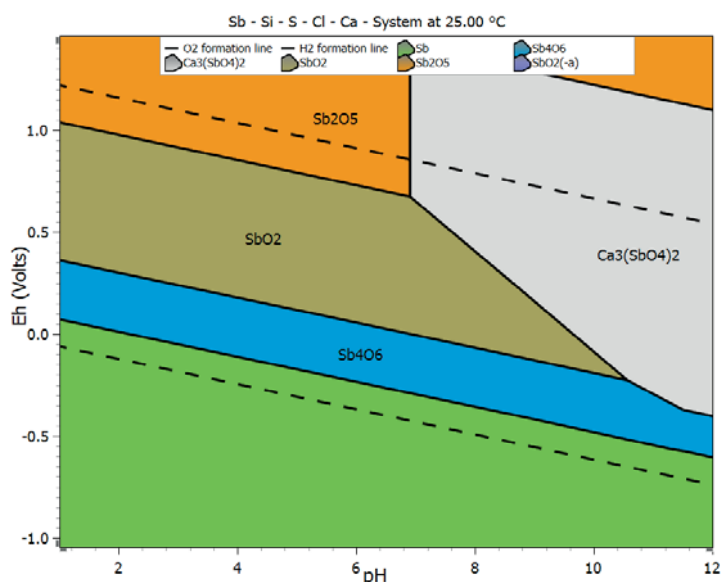


Figure 31: Eh-pH diagrams for antimony modeled using elements and concentrations present in the untreated ash.

Experimental results for HCl leaching of antimony from untreated MSWI fly ash are shown in Figure 32a. The low pH range 1 – 4, extracted the most antimony, approximately 20 % from what is available in the ash. The antimony concentration in the untreated fly ash is  $550 \text{ mg} \cdot \text{kg}^{-1}$  ash and  $850 \text{ mg} \cdot \text{kg}^{-1}$  in the HALOSEP treated fly ash. Assuming total recovery from the ash, it would take 1176 tons of ash to recover 1 ton of antimony from the HALOSEP ash. The amount of antimony extracted decreased as the pH of leaching was increased. Water leaching of the untreated fly ash resulted in a slurry having pH 12.5 and the amount of antimony leached from that treatment was below the detection limit or less than 1.5 % ( $10 \text{ mg} \cdot \text{kg}^{-1}$ ) of the total antimony concentration.

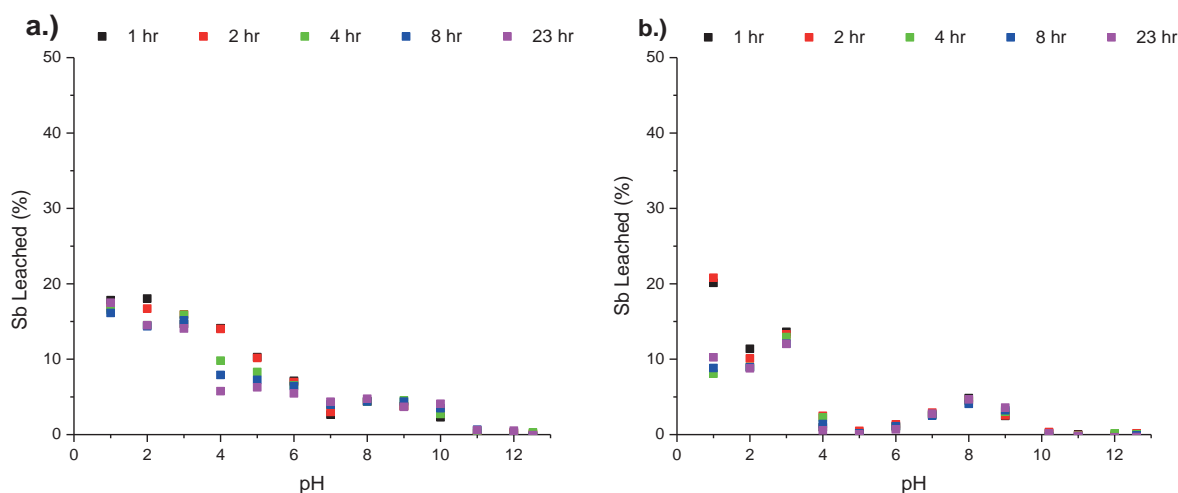


Figure 32: The effect of pH on Sb leaching from a) untreated fly ash leached with HCl solution and water (pH 12.5); b) treated fly ash leached with HCl solution (pH 1-10), water (pH 10.2) and NaOH solution (pH 11 - 12.6). Initial L/S = 20.

Leaching with an HCl solution at a pH 1 to 3 released up to 20 % ( $170 \text{ mg}\cdot\text{kg}^{-1}$ ) of Sb from the ash. From pH 4 to 9, less than 5 % of the antimony was leached. Above pH 9, no antimony removal from the ash was detected. The results for antimony leaching from the treated sample are shown in Figure 32b. From these results it can be concluded that the pH range in which antimony can be recovered is smaller for the HALOSEP treated ash (pH < 3) compared to for the untreated ash (pH < 5). However, in the pH range 6 to 12, both ash samples leach less than 5 % of their total antimony content. Soluble antimony compounds were not indicated from the Eh-pH diagram because less than 50 % of the antimony was soluble and thus not the dominant phase.

The behavior of antimony in these experiments is probably due to the formation of secondary calcium minerals formed either during the HALOSEP salt removal process and the following storage time or, for the original, untreated ash, during the leaching experiments carried out in the present work. It has been shown by others that calcium-bearing minerals and the presence of amorphous hydrated calcium silicates such as those formed during the hydration of cement, play an important role in the mechanisms controlling antimony leaching from ash [82, 140]. In their experiments, the binding of antimony to those compounds occurred either by formation of surface complexes or as proper chemical bonding in an ettringite like compound. XRD analysis confirmed the presence of  $\text{CaCO}_3$ ,  $\text{CaSO}_4$ , and  $\text{Ca}(\text{OH})_2$  in both ash samples and possibly ettringite ( $\text{Ca}_6\text{Al}_2(\text{SO}_4)_3(\text{OH})_{12}\cdot 26\text{H}_2\text{O}$ ) in the treated ash. When the pH < 10,  $\text{Ca}(\text{OH})_2$  and ettringite dissolve leaving  $\text{CaCO}_3$ ,  $\text{CaSO}_4$ , of which  $\text{CaSO}_4$  has no interaction with Sb [141]. Therefore at neutral pH values, the interaction of  $\text{CaCO}_3$  with antimony to form calcium antimonites and antimony solubility are believed to have the largest influence on retarding antimony extraction in this region. The treated ash shows two more pronounced leaching minimums occurring at pH 5 and 10. Antimony leaching from uncarbonated bottom ash by Cornelis et al. [141] showed similar minimums in antimony leaching occurring at pH 5 and 10. Similarly when the bottom ash underwent accelerated carbonation, the minimum in leaching was less pronounced such as the case for the untreated fly ash in this study.

The untreated ash released more antimony at each pH used compared to the HALOSEP ash. This may be due to the presence of soluble antimony bearing calcium compounds, in particular calcium antimonite,  $\text{Ca}(\text{Sb}(\text{OH})_6)_2$  and  $\text{Ca}(\text{Sb}(\text{OH})_6)_2\cdot 6\text{H}_2\text{O}$ , which have been shown to be present in bottom ash and suggested for fly ash [10, 83]. From Eh-pH diagrams and leaching results, it can be concluded that to increase the leaching efficiency of antimony from the fly ash, a more concentrated HCl solution (pH < 1) should be used.

The amount, in wt%, of ash leached at each pH is dominated by calcium for the untreated ash. However, for the treated ash, dissolution of magnesium and aluminum account for the major leached fraction in pH levels up to 3, at which point calcium has the highest leaching efficiency as seen in Figure 33. There may be a correlation between the leaching of the major metals (Al, Ca, Mg, S and Si) and that of the minor metals. Figure 33 shows the pH-dependent leaching behavior of the major metals from both ash samples during 23 over hours. Aluminum and silicon show similar leaching trends with respect to pH but different leaching efficiencies for each ash due to the presence of aluminum silicates [89]. The silicates may have formed cement like hydrated compounds that are less soluble. Magnesium showed similar leaching efficiencies for the two ash samples, probably due to  $Mg(OH)_2$  as detected by XRD.

There was a significant decrease in the leaching of, most notably, calcium but also silicon from the treated ash. This is most likely due to the pH 4 HALOSEP treatment during which the calcium that was easily available was removed from the ash leaving the calcium enclosed in ash particles or in non-leachable compounds. Ettringite dissolution can be seen in Figure 33a as a sharp decrease in leaching efficiency near pH 10. This is in good agreement with Astrup et al. [142], who determined that when  $pH > 9.5$ , Ca is controlled by ettringite, while at  $pH < 9.5$ , gypsum ( $CaSO_4 \cdot 2H_2O$ ) was a better predictor of the Ca concentration in solution. This is not seen for the HALOSEP ash due to the acid rinse done in the HALOSEP process causing dissolution of any ettringite present.

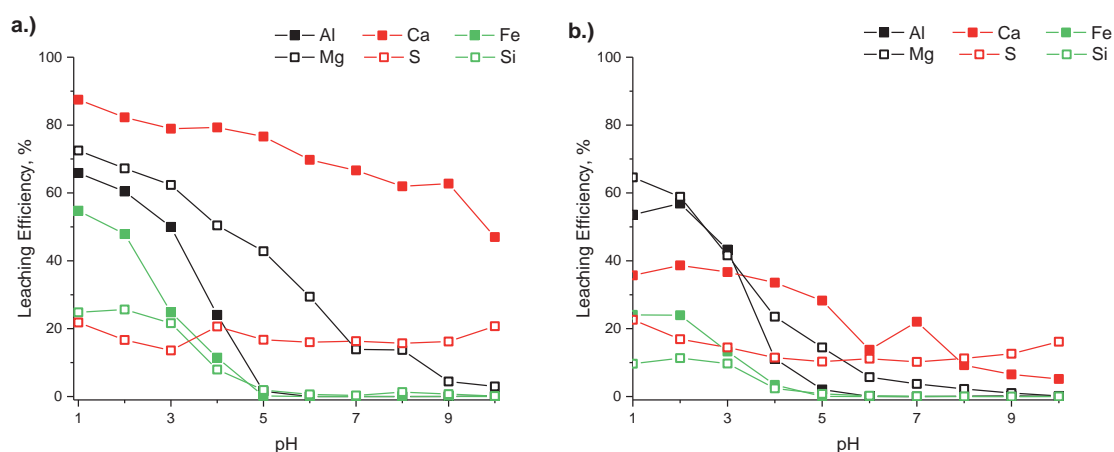


Figure 33: Leaching efficiency for the major metals present in a) untreated and b) treated fly ash.

Because the treated ash was received as large pieces, the sample was milled to reduce the particles size. It is possible that upon milling the HALOSEP treated ash, unleached surfaces were exposed causing an increase in leaching efficiency. Thus, the leaching data presented in this article for treated ash can be viewed as a worst case with respect to how this ash would comply with landfilling acceptance criteria.

During leaching experiments at pH 1 to 4 with the untreated ash, a gel formation was observed. This could be the formation of silica gel, which has also been reported by Steenari and Björefors [143]. Their work on metal recovery from ash concluded that at pH 2 and 4, the leachates were oversaturated with respect to silica and some silicates. However in this case, it seems more logical that the gel formation is associated with calcium dissolution as seen by the Ca concentration given in Table 17, and the pH-dependent leaching behavior shown in Figure 34. To investigate this further, the ash was analyzed using SEM to give information on how the HALOSEP treatment had influenced the ash particles. The untreated ash in Figure 34a shows small conglomerates on the particle surfaces, whereas the treated ash in Figure 34b shows distinct crystalline compounds, most likely gypsum as indicated by XRD. The HALOSEP process removed most of the soluble chloride salts from the ash as well as some calcium. Since leaching is affected by particle size, it is logical that the amorphous calcium compounds would more easily leach than crystalline  $CaSO_4$ , as shown in Figure 33. No gel formation was seen in leachates from the HALOSEP treated ash.

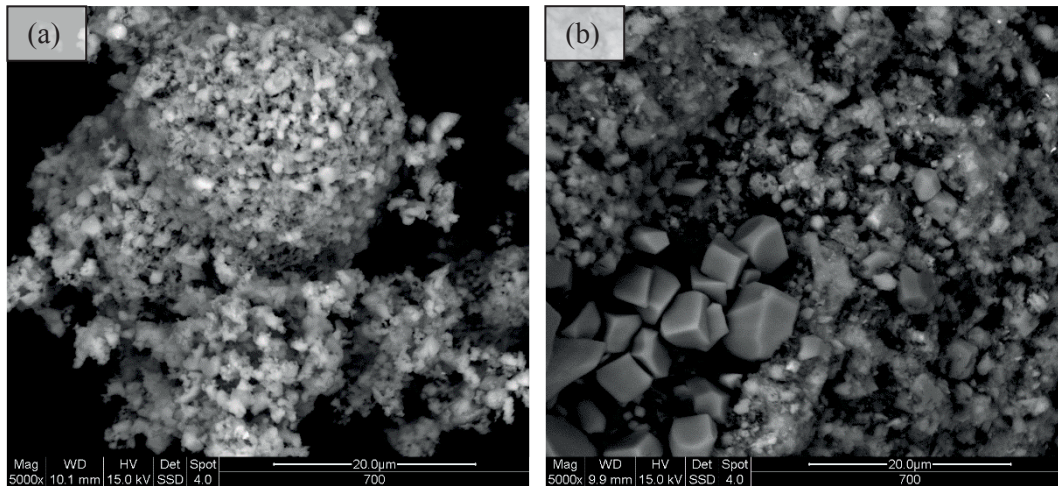


Figure 34: SEM images of the (a) untreated ash and (b) treated ash.

The pH-dependent leaching results show that approximately 20 % of the antimony could be extracted using a pH 1 hydrochloric acid solution with an L/S of 20 for both ash samples, and the amount of antimony leached decreased with increasing pH. There was no clear difference in antimony leaching between the original ash and the ash after HALOSEP treatment. There was not enough research done on extraction and recovery of secondary antimony from the MSWI fly ash to propose a process flow for this system.

## 6. SUMMARY & CONCLUSIONS

Because there is a limited amount of antimony currently being recycled today, this work set out to determine if antimony could be recycled from waste more specifically metal oxide varistors (MOVs) and MSWI fly ash. Several techniques were investigated for antimony extraction and recovery including leaching and thermal treatment. From the studies presented here it can be concluded that antimony oxide can be recovered from MOV's using a hybrid hydro- and pyro- metallurgical process. Initially the composition of the MOV was determined in order to quantify the metals within the MOV. It was shown that the MOV contained three main phases: (1) the bulk zinc oxide phase, (2) the bismuth rich phase, and (3) the antimony rich phase. In order to concentrate the antimony, pH selective dissolution was needed to remove the bulk zinc oxide phase.

The leaching study determined that it was possible to selectively leach Zn from the MOV without significant co-leaching of bismuth and antimony by selecting a suitable pH, mainly higher than 3 in all acids investigated. Sulfuric acid leaching of zinc is preferred because nearly 80 % of zinc is produced by electrowinning from sulfate solutions, and the MOV sulfuric acid leachate could be incorporated in an already existing industrial process. Independent of the pH values studied here, sulfate leaching removed 100 % of the zinc oxide from the MOV, making this the ideal selective leaching solution from which it is easy to (1) concentrate antimony and (2) produce a semi-pure zinc sulfate leachate. It was not possible to leach zinc without co-leaching minor amounts of manganese, cobalt, and nickel. The leachate contained impurities of cobalt ( $\sim 400 \text{ mg}\cdot\text{L}^{-1}$ ) and nickel ( $\sim 100 \text{ mg}\cdot\text{L}^{-1}$ ) which needed to be removed to make the leaching solution suitable for zinc electrowinning. Therefore, reductive precipitation also called cementation was investigated as a way to remove nickel and cobalt to produce a purified zinc sulfate electrolyte from sulfuric acid leaching of MOVs. This process, leaching then purification, would create a process suitable for recycling the zinc from the MOV.

Results indicated that increasing the temperature does not significantly increase the amount of cobalt and nickel cemented from the leachate but mainly increases the cementation kinetics. At temperatures above  $40 \text{ }^\circ\text{C}$  the cemented Co started to redissolve thus lowering the removal efficiency. It was seen that adjusting the pH of the cementation had the largest influence on the amount of impurities cemented from solution with pH 5.0 being the most effective. At pH 5, 52 % of cobalt and 74 % of nickel was removed from the MOV leachate. If the pH was higher than 5, the kinetics of cementation were slower. From the results obtained by studying different cementation parameters an optimization study was done at  $20 \text{ }^\circ\text{C}$  and  $40 \text{ }^\circ\text{C}$ . The optimum conditions were shown to be  $0.4 \text{ g}\cdot\text{L}^{-1}$  copper,  $0.8 \text{ g}\cdot\text{L}^{-1}$  antimony,  $2 \text{ g}\cdot\text{L}^{-1}$  zinc dust and a solution pH of 5. Results showed that 56 % of cobalt and 90 % of nickel could be removed using these optimized conditions. To further improve the amount of cobalt cemented from solution, higher temperatures ( $> 60 \text{ }^\circ\text{C}$ ) should be used. A study on the effect of a two-step batch addition of zinc dust was done to see if the amount of cobalt and nickel removed from the solution can be improved. It was shown that it is possible to purify the MOV leachate of 98 % cobalt and all nickel using a two-step cementation process.

In a separate study on the cementation residue morphology, it was shown that formation of zinc hydroxides and zinc sulfates retard cobalt removal by forming a passivating layer. The formation of zinc hydroxides and zinc sulfate salts is due to a localized high pH created by the evolution of hydrogen. The formation of basic salts occurs only until the zinc dust particle has completely dissolved, thus generation of hydrogen stops, and the localized pH is that of the bulk solution causing redissolution of the basic salts. Formation of the salts can be influenced by temperature, pH and zinc concentration, however, its formation could not be prevented using the parameters studied here.

In addition to determining a suitable leachate for concentrating antimony, characterization of the MOV powder before and after leaching determined that the bulk ZnO grains were dissolved, leaving the bismuth oxide ( $\text{Bi}_2\text{O}_3$ ) and antimony phases ( $\text{Zn}_{2.33}\text{Sb}_{0.67}\text{O}_4$ ,  $\text{Zn}_7\text{Sb}_2\text{O}_{12}$ ,  $\text{Zn}_2\text{Bi}_3\text{Sb}_3\text{O}_{14}$ ) in the insoluble residue. The leaching “pretreatment” of the MOV in a dilute sulfuric acid solution increased the concentration of antimony from 35 mg of antimony per gram of MOV to 186 mg of antimony per gram of MOV residue making it more feasible to recover antimony from the MOV.

Thermogravimetry was used to investigate the weight loss and rate of weight change of simple metal oxides ( $\text{Sb}_2\text{O}_3$ ,  $\text{Bi}_2\text{O}_3$ ,  $\text{ZnO}$ ) as well as those of the MOV leaching residue as a function of temperature in inert and reducing conditions. Simple metal oxides were used as a reference to help predict the behavior of the sintered metal oxide compounds ( $\text{Zn}_7\text{Sb}_2\text{O}_{12}$ ,  $\text{Zn}_{2.33}\text{Sb}_{0.67}\text{O}_4$ , and  $\text{Zn}_2\text{Bi}_3\text{Sb}_3\text{O}_{14}$ ) present in the MOV residue. The thermal treatment of the simple metal oxides suggested that sublimated antimony oxide could be separated from a mixture of  $\text{Sb}_2\text{O}_3$ ,  $\text{Bi}_2\text{O}_3$ , and  $\text{ZnO}$  by heating to  $650\text{ }^\circ\text{C}$  and collected by distillation. The addition of carbon causes volatilization and reduction of  $\text{Sb}_2\text{O}_3$ . It also lowered the volatilization kinetics most likely due to the presence of metallic antimony which is less volatile than  $\text{Sb}_2\text{O}_3$ . Carbothermal reduction of  $\text{Bi}_2\text{O}_3$  and subsequent volatilization of  $\text{Bi(l)}$  occurred at nearly the same temperature. For the separation of bismuth and zinc, once antimony was volatilized, carbon could be added to lower the reduction temperature for their recovery.

Thermal decomposition of the MOV residue in the absence of carbon resulted in less than 5 % mass loss below  $1000\text{ }^\circ\text{C}$ . This was expected as it was reported that thermal decomposition of  $\text{Zn}_7\text{Sb}_2\text{O}_{12}$  occurred near  $1350\text{ }^\circ\text{C}$  yielding  $\text{ZnO}$  and  $\text{Sb}_4\text{O}_6$ . To lower this temperature carbon was added to the MOV residue which increased the mass loss significantly. The first reaction, occurring around  $600\text{ }^\circ\text{C}$ , was the reduction of  $\text{Bi}_2\text{O}_3$  from the MOV, while near  $800\text{ }^\circ\text{C}$ , volatilization of  $\text{Sb}_4\text{O}_6$  occurred. The theoretical weight loss was 22.8 % while the experimental weight loss for  $\text{Sb}_4\text{O}_6$  was 17.3 %. At temperatures above  $900\text{ }^\circ\text{C}$ , zinc was reduced then volatilized. Thermal treatment and carbothermal reduction of  $\text{Bi}_2\text{O}_3$  showed that once reduced, Bi metal was slowly volatilized. This is also believed to occur during carbothermal reduction of the MOV residue. Therefore, antimony can be collected from the vapor phase between  $700 - 850\text{ }^\circ\text{C}$  with a small amount of bismuth present.

It was determined from a TGA investigation that a simple thermal treatment of the MOV residue below  $1000\text{ }^\circ\text{C}$  did not have a significant effect on antimony removal, however, carbothermal reduction resulted in nearly 80 % weight loss of the MOV residue. TGA investigations lead to two conclusions: (1) higher temperatures were needed for thermal separation of antimony and (2) the residue needed to be characterized in order to determine the temperature at which antimony recovery takes place. The composition of the residue after thermolysis experiments concluded that up to  $900\text{ }^\circ\text{C}$  antimony compounds were stable in the residue. Between  $900 - 1100\text{ }^\circ\text{C}$ , decomposition of antimony containing compound with inverse spinel structure ( $\text{Zn}_7\text{Sb}_2\text{O}_{12}$ ,  $\text{Zn}_{2.33}\text{Sb}_{0.67}\text{O}_4$ ) occurred and 80 % of the antimony was volatilized from the sample. This indicates that it is possible to separate the antimony from the MOV leaching residue and eventually collect the majority of antimony from the gaseous phase. Addition of carbon to the MOV residue showed that nearly 70 % of antimony could be separated from the residue below  $1000\text{ }^\circ\text{C}$  with decomposition of the antimony phases starting below  $825\text{ }^\circ\text{C}$ . The remaining antimony formed an alloy with nickel and cobalt.

The surge arrester in which the MOV is housed must first be disassembled while the MOV consists of chemical compounds that must be separated metallurgically. The complexity of the MOV is the same throughout. Thus, in order to extract antimony the matrix or bulk phase in this case  $\text{ZnO}$  needs to be separated to concentrate the valuable component, antimony. From the results generated in Papers I – VI it is now possible to put together a recycling process to recover antimony from MOVs and MSWI fly ash. The general flowsheet to recover secondary antimony from the MOVs is presented in Figure 35.

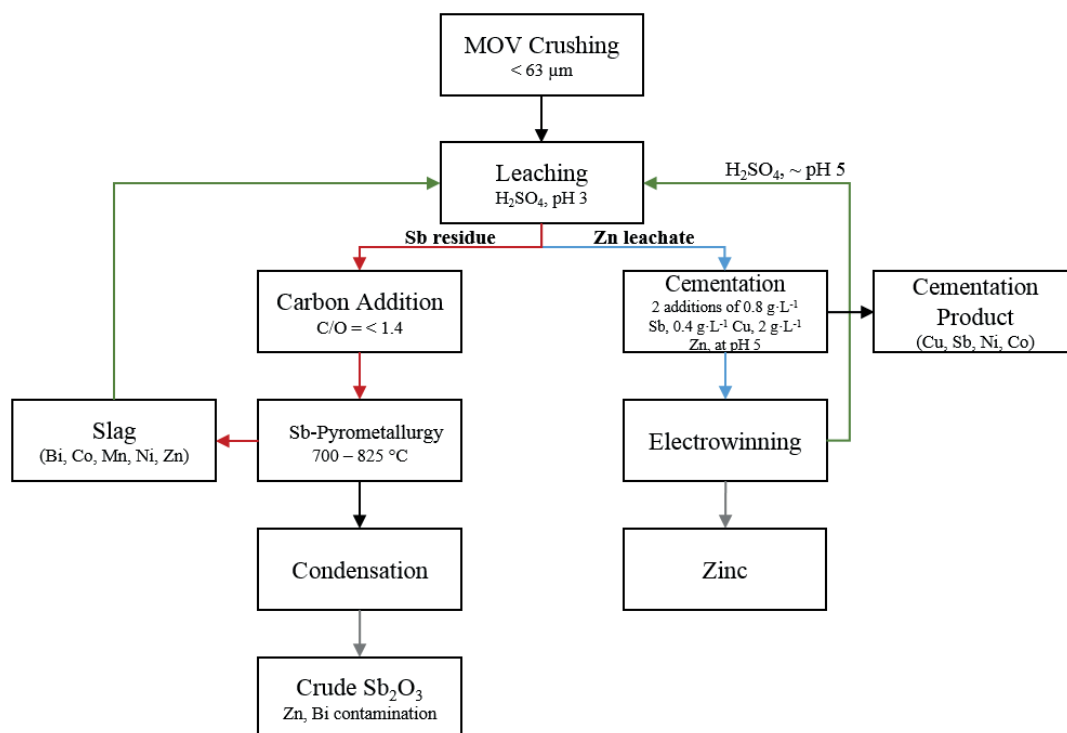


Figure 35: Process layout for recovery of antimony oxide from MOVs based on the research discussed in this thesis.

The feed material for the process shown in Figure 35 are crushed MOVs. The MOV is a brittle material and can be broken by compression of impact to produce fine particles. Screens can be used to separate the size fractions (vibrating deck screens, roller, gyrator, and trammel screens). Zinc can be leached from the crushed MOVs in one hour at room temperature using dilute sulfuric acid. A separation step, such as filtering, needs to be added in order to separate the zinc sulfate leachate from the concentrated antimony residue. Once the solid phase has been removed 98 % of the cobalt and all nickel can be removed from the zinc sulfate leachate by a two-step batch addition of  $0.8 \text{ g}\cdot\text{L}^{-1}$  Sb,  $0.4 \text{ g}\cdot\text{L}^{-1}$  Cu, and  $2 \text{ g}\cdot\text{L}^{-1}$  Zn dust at pH 5. The concentrated antimony rich phase separated from the sulfuric acid leachate can be mixed with carbon with a  $\text{C/O} = 1.4$  or lower and heat treated at  $800 \text{ }^\circ\text{C}$  causing decomposition of the antimony compounds and volatilization of  $\text{Sb}_4\text{O}_6$ . The  $\text{Sb}_4\text{O}_6$  can be collected by condensation. From TGA results it is reasonable to assume that less than 5 % of the Bi and ZnO phases will volatilize at this temperature [135]. A mass balance is shown for this process in Table 18 using the parameters discussed in this research.

Table 18: Concentration of metals, given in kilograms (kg) at each stage (feed material, leachate, post-cementation, cementation product, leaching residue, and after carbothermal reduction) of the antimony recycling process. When processing 1 ton of MOV.

	MOV feed material	Zinc Sulfate Leachate <sup>a</sup>	Leachate After Cementation <sup>b</sup>	Cement Product <sup>c</sup>	Sb-rich Residue <sup>d</sup>	Carbothermal Reduction at 800 °C <sup>e</sup>
Bi	45.9 ± 0.1	nd	nd	0	41.3 ± 0.3	0.05
Co	6.9 ± 0.1	4.14 ± 0.10	0.08 ± 0.01	4.05	2.0 ± 0.2	0
Mn	3.6 ± 0.1	0.64 ± 0.01	0.64 ± 0.02	0.00	2.5 ± 0.2	0
Ni	6.1 ± 0.1	0.94 ± 0.02	0.000 ± 0.001	0.94	4.3 ± 1.8	0
Sb	34.8 ± 1.1	nd	nd	15.1	31.3 ± 1.8	25.1
Zn	762 ± 4	760 ± 15	799 ± 15	0	60.1 ± 0.2	3.0
Cu				7.5		
C						26.2

<sup>a</sup> nd = not detected < 0.04g

<sup>b</sup> 1.6 g/L Sb, 0.4 g/L Cu, 2 g/L Zn were added for cementation, all Zn dust is reduced

<sup>c</sup> Sb, Cu, Ni were completely cemented along with 98 % of Co

<sup>d</sup> leaching 1 ton of MOV resulted in 167 kg of residue

<sup>e</sup> C/O = 1.4, 80 % of Sb is assumed recovered along with 5 % of the Bi and Zn in the condensed phase

This was a feasibility study to see if antimony could be recovered from MOV's. It was shown that by processing 1 ton of MOV's it is possible to recover nearly 30 kg of Sb<sub>2</sub>O<sub>3</sub> (25 kg of Sb). However, this process can be further developed to increase the amount and purity of antimony recovered. From the currently proposed process, it would require approximately 34 tons of MOV's to recover 1 ton of secondary antimony oxide. To put that in perspective it would require 1176 tons of MSWI fly ash or 1,000,000 tons of ore to recover 1 ton of Sb.

Sustainable design can be incorporated into the antimony recovery process. Since H<sub>2</sub> gas is generated during cementation, it could be possible to use the air/H<sub>2</sub> mixture originating from the cementation step as a reducing agent when heating the Sb-rich residue. Replacing carbon with a hydrogen gas mixture would also lower the CO<sub>2</sub> emissions for this process. To increase the circular flow of materials, Co, Cu, Ni, and Sb can be recovered from the cementation product or sold as a metal mixture. Bismuth is listed as a critical material by the European Union. Bi<sub>2</sub>O<sub>3</sub> could be recovered in the first leaching pretreatment step by sulfuric acid leaching at pH 1 (Figure 10) and then precipitation forming Bi<sub>2</sub>O<sub>3</sub>. There are many alterations that could be made to this process and the research thus far is a solid starting point from which adjustments/improvements can be made.

The next phase of this research would be to investigate the collection of antimony from the condensed gas phase as well as to optimize heating methods and parameters to make the process as sustainable as possible. In addition, this research showed that zinc can be successfully recycled from discarded MOV by leaching pulverized MOV's. Cementation can be used to purify the leaching solution followed by electrolysis to recover metallic zinc. However, the economics of this method were not investigated but are important if this method is to be used to recycle zinc from the MOVs.

Recovery of antimony from MSWI fly ash by leaching was not ideal and proved to be difficult. The chemical nature of the antimony species found in fly ash is not known. In addition, the species will vary depending on the incineration conditions and furnace feedstock. However, leaching did cause the concentration of antimony in the dry residue to increase. Leaching at pH 4 showed an increase in the antimony concentration from 550 mg·kg<sup>-1</sup> to 1435 mg·kg<sup>-1</sup> in the untreated ash and 850 mg·kg<sup>-1</sup> to 1242 mg·kg<sup>-1</sup> in the HALOSEP treated ash. This suggests that a two-step recovery process could be preferable for antimony recovery where insoluble antimony is concentrated in the residue and recovered by another leaching step using an organic acid such as tartaric acid. There was not enough research done on extraction and recovery of secondary antimony from the MSWI fly ash to propose a process flow for this system.

## 7. FUTURE WORK

There are many areas of interesting studies to be continued with respect to this work. A more fundamental understanding of chemical processes and reaction mechanisms associated with antimony recovery would be interesting for this work and also for the electronics industry, which includes determining the exact phases formed, composition and structure including bond lengths of the antimony compounds formed in the MOV using EXAFS. In addition a life cycle assessment (LCA) comparing production of primary antimony and secondary antimony would be interesting.

An investigation into the kinetics of MOV leaching is needed to get data for optimization. Some parameters would need to be modified and alkaline leaching would be included to find out if it results in a selective leaching of antimony directly from the MOV. Experiments to determine if leaching of the MOV was a chemically controlled process or a diffusion controlled process are of importance and need to be developed. The determination of the activation energy of leaching system is also interesting because the rate of the reaction can be determined at a given temperature.

One thing that should be researched more is the mechanism by which cementation occurs when removing contaminating metals from the zinc sulfate solution produced by leaching the MOV. It would be relevant to this work but also to industrial zinc production and not much work has been done in this area which means the reactions are still largely unknown. There are other means of leachate purification such as solvent extraction which might be better suited for the MOV leachate purification process and should also be investigated.

High temperature separation of antimony from the MOV seems to be promising but requires temperatures between 800 and 1100 °C for thermolysis and carbothermal reduction. It would be interesting to investigate what parameters can be changed to lower the antimony recovery temperature. This could include things such as changing the environment by purging with a reducing gas. It would be very interesting to determine the reaction mechanism for the liberation of antimony or antimony species from the pyrochlore and spinel structures respectively. This would be useful in both the recycling of old and the production of new MOV.

In general the reaction mechanisms of antimony compounds in the MOV system are not well-known and often conflicting data exists. It would be scientifically interesting to investigate more chemical reactions of antimony, antimony oxides and mixed metal antimony oxides found in this and other industrial systems such as MSWI fly ash.

## 8. ACKNOWLEDGMENTS

There are many people and organizations to thank but to list them all would be endless. So if you are reading this, the author would like to thank you. In addition the author of this work would like to sincerely thank:

- Chalmers Area of Advance - Production and Stena Metal AB for providing research funding.
- Supervisor Britt-Marie Steenari for her time, guidance, patience, and help.
- The Examiner, Prof. Christian Ekberg, and the committee members.
- Henrik Jilvero and Christer Forsgren from Stena for your help with the ash work.
- Mikael, the most interesting person I have ever met and a really wonderful husband. Also, our beautiful cat Katherine who has recently been my therapy kitty, her cuddles helped me through the PhD process.
- Yuda Columbus for your excellent lab work, energy, and ideas. You were a really great Masters student and your hard work is very much appreciated.
- All of my colleagues (present and former) at Nuclear Chemistry/Industrial Materials Recycling. Among them especially Anna and Filip for being incredible office mates. I have enjoyed our conversations and our continued friendship.
- Stellan Holgersson for maintaining and fixing lab equipment thus making it possible to keep doing research.
- I would also like to thank colleagues Habib, Nico, Henrik, and Sebastian from OOMK for help with experiments and equipment.
- The friends I have made in the US and Sweden for the really good times and unforgettable memories.
- My Mom, she taught me to be a strong, independent woman. She has been and always will be my guiding light no matter what situation I put myself in. She will always be someone I look up to and admire.
- Last and most importantly my family! You are all so much fun and really great people. You have taught me the most important things in life and I love you.

Thank You All!  
Toni Karlsson

## 9. REFERENCES

1. *Sustainable Development Goals*. 17 Goals to Transform our World 2017 [cited 2017 08-15]; Available from: <http://www.un.org/sustainabledevelopment/>.
2. *Waste Framework Directive*, in *Directive 2008/98/EC on waste*, E. Commission, Editor. 2008.
3. Brundtland, G., M. Khalid, S. Agnelli, S. Al-Athel, B. Chidzero, L. Fadika, V. Hauff, I. Lang, M. Shijun, M. Morino de Botero, M. Singh, S. Okita, and A. Others, *Our Common Future ('Brundtland report')*. 1987: Oxford University Press, USA.
4. Sekula, R., M. Wnek, and S. Slupek, *Potential Utilization Method of Scrap Ceramic Insulators*. *Journal of Solid Waste Technology and Management*, 1999. **26**(2): p. 6.
5. Grimes, S., J. Donaldson, and D.C. Gomez, *Report on the environmental benefits of recycling*. 2008, Bureau of International Recycling (BIR).
6. Carlin, J.F., *ANTIMONY*, in *U.S. Geological Survey, Mineral Commodity Summaries, January 2013*. 2013, Department of the Interior: Washington, DC. p. 2.
7. Sverdrup, H.U., K.V. Ragnarsdottir, and D. Koca, *An assessment of metal supply sustainability as an input to policy: security of supply extraction rates, stocks-in-use, recycling, and risk of scarcity*. *Journal of Cleaner Production*, 2017. **140, Part 1**: p. 359-372.
8. Guberman, D.E., *Mineral Information Antimony*, in *2017*, USGS, Editor. 2017, US Geological Survey, Mineral Commodity Summaries: Washington D.C.
9. Kirk-Othmer, *Kirk-Othmer Encyclopedia of Chemical Technology*. 1992, John Wiley & Sons: New York. p. 367-407.
10. Paoletti, F., P. Sirini, H. Seifert, and J. Vehlow, *Fate of antimony in municipal solid waste incineration*. *Chemosphere*, 2001. **42**(5-7): p. 533-543.
11. van Velzen, D., H. Langenkamp, and G. Herb, *Antimony, its sources, applications and flow paths into urban and industrial waste: a review*. *Waste Management & Research*, 1998. **16**(1): p. 32-40.
12. Takaoka, M., T. Yamamoto, T. Tanaka, N. Takeda, K. Oshita, and T. Uruga, *Direct speciation of lead, zinc and antimony in fly ash from waste treatment facilities by XAFS spectroscopy*. *Physica Scripta*, 2005. **2005**(T115): p. 943.
13. Wang, L., Q. Chen, I.A. Jamro, R. Li, Y. Li, S. Li, and J. Luan, *Geochemical modeling and assessment of leaching from carbonated municipal solid waste incinerator (MSWI) fly ash*. *Environmental Science and Pollution Research*, 2016. **23**(12): p. 12107-12119.
14. Johansson, I., E. Sahlin, B.v. Bahr, J. Björkmalm, and J.T. Olsson, *Kritiska metaller i svenska avfallsaskor*, in *The content of critical elements in residues from Swedish waste-to-energy plants*. 2013, SP Sveriges Tekniska Forskningsinstitut: Waste Refinery.
15. IAWG (International Ash Working Group: A.J. Chandler, T.T.E., J. Hartle'n, O. Hjelm, D. Kosson, S.E. Sawell, H.A. van der Sloot, J. Vehlow), *Municipal Solid Waste Incinerator Residues, Studies in Environmental Science*. Elsevier Science, 1997. **67**.
16. Rombach, E. and B. Friedrich, *Chapter 10 - Recycling of Rare Metals*, in *Handbook of Recycling*, E. Worrell and M.A. Reuter, Editors. 2014, Elsevier: Boston. p. 125-150.
17. Hultgren, H., *Varistor Material Information*. 2014: Personal Communication.
18. AGENCY, S.E.P., *From waste management to resource efficiency Sweden's Waste Plan 2012-2017*, in *Report 6560*. 2012, SWEDISH ENVIRONMENTAL PROTECTION AGENCY. p. 115.
19. Eurostat. *Municipal waste by waste operations*. [Webpage] 2017-03-06 [cited 2017 2017-05-24]; Waste Statics]. Available from: <http://appsso.eurostat.ec.europa.eu/nui/submitViewTableAction.do>.
20. *Swedish Waste Management 2016*. Avfall Sverige AB: Malmö, Sweden.
21. Karlfeldt Fedje, K., C. Ekberg, G. Skarnemark, and B.-M. Steenari, *Removal of hazardous metals from MSW fly ash—An evaluation of ash leaching methods*. *Journal of Hazardous Materials*, 2010. **173**(1-3): p. 310-317.
22. CRM-EU. *Critical Raw Materials for the EU - Report of the Ad-hoc Working Group on defining critical raw materials*. 2010; Available from: [http://ec.europa.eu/enterprise/policies/rawmaterials/documents/index\\_en.htm](http://ec.europa.eu/enterprise/policies/rawmaterials/documents/index_en.htm).

23. NDS, *Reconfiguration of the National Defense Stockpile (NDS) Report to Congress*. 2009, <https://www.scribd.com/document/16483302/Reconfiguration-of-the-National-Defense-Stockpile-Report-to-Congress>; Washington, DC. p. 87.
24. Guberman, D.E., *U.S. Geological Survey, Mineral Commodity Summaries*, in *Antimony*. 2014. p. 196.
25. USGS. *Antimony Statics and Information*. 1991-2017 2017-07-07; Available from: <https://minerals.usgs.gov/minerals/pubs/commodity/antimony/>.
26. CRM-EU, *REPORT ON CRITICAL RAW MATERIALS FOR THE EU*, in *Report of the Ad hoc Working Group on defining critical raw materials*. 2014, European Commission: <http://ec.europa.eu/DocsRoom/documents/10010/attachments/1/translations>.
27. Anderson, C.G., *Hydrometallurgically treating antimony-bearing industrial wastes*. JOM, 2001. **53**(1): p. 18-20.
28. Nakamura, K., S. Kinoshita, and H. Takatsuki, *The origin and behavior of lead, cadmium and antimony in MSW incinerator*. Waste Management, 1996. **16**(5-6): p. 509-517.
29. *International Antimony Association VZW*, in *Safe use of antimony catalysts in PET*. (2014) <http://www.antimony.com/en/publications.aspx>.
30. Commission, E., *Annex V to the Report of the Ad-hoc Working Group on defining critical raw materials*. 2010.
31. Anderson, C.G., *The metallurgy of antimony*. Chemie der Erde - Geochemistry, 2012. **72**, **Supplement 4**(0): p. 3-8.
32. Norman, N.C., *Chemistry of Arsenic, Antimony and Bismuth*. 1998: Springer.
33. Filella, M., P.A. Williams, and N. Belzile, *Antimony in the environment: knowns and unknowns*. Environmental Chemistry, 2009. **6**(2): p. 95-105.
34. Venugopal, B. and T.D. Luckey, *Metal toxicity in mammals. Volume 2. Chemical toxicity of metals and metalloids*. 1978: Plenum Press.
35. Filella, M. and P.M. May, *Computer simulation of the low-molecular-weight inorganic species distribution of antimony(III) and antimony(V) in natural waters*. Geochimica et Cosmochimica Acta, 2003. **67**(21): p. 4013-4031.
36. Habashi, F., *Handbook of Extractive Metallurgy Primary Metals*, ed. F. Habashi. Vol. 2. 1997, Weinheim, Federal Republic of Germany: VCH Verlagsgesellschaft. 641-681.
37. Cody, C.A., L. DiCarlo, and R.K. Darlington, *Vibrational and thermal study of antimony oxides*. Inorganic Chemistry, 1979. **18**(6): p. 1572-1576.
38. Golunski, S.E., T.G. Nevell, and M.I. Pope, *Thermal stability and phase transitions of the oxides of antimony*. Thermochemica Acta, 1981. **51**(2-3): p. 153-168.
39. Centers, P.W., *Sublimation-controlled oxidation of antimony trioxide*. Journal of Solid State Chemistry, 1988. **72**(2): p. 303-308.
40. Weast, R.C., *Handbook of Chemistry and Physics*. 57 ed. 1976, Cleveland, Ohio: CRC Press.
41. Svensson, C., *Refinement of the crystal structure of cubic antimony trioxide, Sb<sub>2</sub>O<sub>3</sub>*. Acta Crystallographica Section B, 1975. **31**(8): p. 2016-2018.
42. Svensson, C., *The crystal structure of orthorhombic antimony trioxide, Sb<sub>2</sub>O<sub>3</sub>*. Acta Crystallographica Section B, 1974. **30**(2): p. 458-461.
43. Agrawal, Y.K., A.L. Shashimohan, and A.B. Biswas, *Studies on antimony oxides: Part I*. Journal of thermal analysis, 1975. **7**(3): p. 635-641.
44. Pokrovski, G.S., A.Y. Borisova, J. Roux, J.-L. Hazemann, A. Petdang, M. Tella, and D. Testemale, *Antimony speciation in saline hydrothermal fluids: A combined X-ray absorption fine structure spectroscopy and solubility study*. Geochimica et Cosmochimica Acta, 2006. **70**(16): p. 4196-4214.
45. Sharutin, V.V. and O.K. Sharutina, *Bis(tetraphenylantimony) succinate, malate, and tartrate: Syntheses and structures*. Russian Journal of Coordination Chemistry, 2014. **40**(9): p. 643-647.
46. Schwarzmann, E., H. Rumpel, and W. Berndt, *Antimony Oxides, High Pressure Synthesis*. Zeitschrift für Naturforschung B, 1977. **32B**: p. 617-618.
47. Graedel, T.E. and B.K. Reck, *Chapter 3 - Recycling in Context*, in *Handbook of Recycling*, E. Worrell and M.A. Reuter, Editors. 2014, Elsevier: Boston. p. 17-26.

48. EPA, *Advancing Sustainable Materials Management: 2014 Fact Sheet*, in *Assessing Trends in Material Generation, Recycling, Composting, Combustion with Energy Recovery and Landfilling in the United States*. 2016, Unites States Environmental Protection Agency: <https://www.epa.gov/smm/advancing-sustainable-materials-management-facts-and-figures-report>.
49. Berndt, D. and S.C. Nijhawan, *Lead-acid batteries with low antimony alloys*. Journal of Power Sources, 1976. **1**(1): p. 3-15.
50. Johnson, C.A., H. Moench, P. Wersin, P. Kugler, and C. Wenger, *Solubility of Antimony and Other Elements in Samples Taken from Shooting Ranges*. Journal of Environmental Quality, 2005. **34**(1): p. 248-254.
51. Nakamura, K., S. Kinoshita, and H. Takatsuki, *The origin and behavior of lead, cadmium and antimony in MSW incinerator*. Waste Management, 1996. **16**(5): p. 509-517.
52. Levinson, L.M., Philipp, H.R., *Zinc Oxide Varistors - A Review*. Ceramic Bulletin, 1986. **65**(4): p. 639-646.
53. Kemikalieinspektionen. *Flödesanalyser för kemiska ämnen*. Antimontrioxid 2015 [cited 2017 11/5/2017].
54. ABB, *High Voltage Surge Arresters, Buyer's Guide, ABB High Voltage Products Surge Arrestors*. 2014: Ludvika, Sweden.
55. Ashraf, M.A., A.H. Bhuiyan, M.A. Hakim, and M.T. Hossain, *Microstructure and electrical properties of Ho<sub>2</sub>O<sub>3</sub> doped Bi<sub>2</sub>O<sub>3</sub>-based ZnO varistor ceramics*. Physica B: Condensed Matter, 2010. **405**(17): p. 3770-3774.
56. Olsson, E., *Interfacial Microstructure in ZnO Varistor Materials*, in *Physics*. 1988, Chalmers University of Technology: Göteborg, SE. p. 50.
57. Bernik, S., S. Maček, and A. Bui, *The characteristics of ZnO–Bi<sub>2</sub>O<sub>3</sub>-based varistor ceramics doped with Y<sub>2</sub>O<sub>3</sub> and varying amounts of Sb<sub>2</sub>O<sub>3</sub>*. Journal of the European Ceramic Society, 2004. **24**(6): p. 1195-1198.
58. Arefin, M.L., F. Raether, D. Dolejš, and A. Klimera, *Phase formation during liquid phase sintering of ZnO ceramics*. Ceramics International, 2009. **35**(8): p. 3313-3320.
59. Kim, J.C. and E. Goo, *Morphology and Formation Mechanism of the Pyrochlore Phase in ZnO Varistor Materials*. Journal of Materials Science, 1989. **24**(1): p. 76-82.
60. Huang, Y., M. Liu, Y. Zeng, and C. Li, *The effect of secondary phases on electrical properties of ZnO-based ceramic films prepared by a sol–gel method*. Journal of Materials Science: Materials in Electronics, 2004. **15**(8): p. 549-553.
61. Huang, Y.Q., L. Meidong, Z. Yike, L. Churong, X. Donglin, and L. Shaobo, *Preparation and properties of ZnO-based ceramic films for low-voltage varistors by novel sol-gel process*. Materials Science and Engineering: B, 2001. **86**(3): p. 232-236.
62. Leite, E.R., M.A.L. Nobre, E. Longo, and J.A. Varela, *Microstructural development of ZnO varistor during reactive liquid phase sintering*. Journal of Materials Science, 1996. **31**(20): p. 5391-5398.
63. Sekula, R., T. Ruemenapp, M. Ljuslinder, and B. Doser, *For a better environment: recycling opportunities for insulating components* in *ABB Review*, P. Terwiesch, et al., Editors. 2009, ABB Asea Brown Boveri Ltd: Zurich Switzerland.
64. Gutknecht, T., Y. Colombus, and B.-M. Steenari, *Recycling Zinc from Metal Oxide Varistors Through Leaching and Cementation of Cobalt and Nickel*. Journal of Sustainable Metallurgy, 2017. **3**(2): p. 239-250.
65. Wong, J., *Microstructure and phase transformation in a highly non–Ohmic metal oxide varistor ceramic*. Journal of Applied Physics, 1975. **46**(4): p. 1653-1659.
66. Kim, J., T. Kimura, and T. Yamaguchi, *Sintering of Zinc Oxide Doped with Antimony Oxide and Bismuth Oxide*. Journal of the American Ceramic Society, 1989. **72**(8): p. 1390-1395.
67. Miles, G.C. and A.R. West, *Pyrochlore phases in the system ZnOBi<sub>2</sub>O<sub>3</sub>Sb<sub>2</sub>O<sub>5</sub>: II. Crystal structures of Zn<sub>2</sub>Bi<sub>3</sub>.08Sb<sub>2</sub>.92O<sub>14</sub>+ $\delta$  and Zn<sub>2</sub>+ $x$ Bi<sub>2</sub>.96–( $x$ – $y$ )Sb<sub>3</sub>.04– $y$ O<sub>14</sub>.04+ $\delta$* . Solid State Sciences, 2006. **8**(12): p. 1422-1429.
68. Gordon, R.B., T.E. Graedel, M. Bertram, K. Fuse, R. Lifset, H. Rechberger, and S. Spatari, *The characterization of technological zinc cycles*. Resources, Conservation and Recycling, 2003. **39**(2): p. 107-135.

69. Bard, A. and M. Stratmann, *Encyclopedia of Electrochemistry*, in *Electrochemical Engineering*, D. MacDonald and P. Schmuki, Editors. 2007, WILEY-VCH Verlag GmbH & Co. KGaA: Federal Republic of Germany.
70. Nelson, A., W. Wang, G.P. Demopoulos, and G. Houlachi, *The Removal of Cobalt from Zinc Electrolyte by Cementation: A Critical Review*. Mineral Processing and Extractive Metallurgy Review, 2000. **20**(4-6): p. 325-356.
71. Yang, D., G. Xie, G. Zeng, J. Wang, and R.-x. Li, *Mechanism of cobalt removal from zinc sulfate solutions in the presence of cadmium*. Hydrometallurgy, 2006. **81**(1): p. 62-66.
72. Dreher, T.M., A. Nelson, G.P. Demopoulos, and D. Filippou, *The kinetics of cobalt removal by cementation from an industrial zinc electrolyte in the presence of Cu, Cd, Pb, Sb and Sn additives*. Hydrometallurgy, 2001. **60**(2): p. 105-116.
73. Rydberg, J., M. Cox, C. Musikas, and G.R. Choppin, *Solvent Extraction Principles and Practice*. 2004, New York, NY: Marcel Dekker, Inc.
74. Filipek, E. and G. Dąbrowska, *Unknown thermal properties of ZnSb<sub>2</sub>O<sub>6</sub> and Zn<sub>7</sub>Sb<sub>2</sub>O<sub>12</sub> compounds*. Journal of Thermal Analysis and Calorimetry, 2008. **94**(1): p. 195-201.
75. Filipek, E. and G. Dąbrowska, *Phase relations up to the solidus line in the part of the Sb-Zn-O system*. Central European Journal of Chemistry, 2009. **7**(2): p. 192-196.
76. Rosenqvist, T., *Reduction of Metal Oxides in Principles of extractive metallurgy*, B.J. Clark, Editor. 1974, McGraw-Hill: New York. p. 264-298.
77. Jung, C.H., T. Matsuto, N. Tanaka, and T. Okada, *Metal distribution in incineration residues of municipal solid waste (MSW) in Japan*. Waste Management, 2004. **24**(4): p. 381-391.
78. Belevi, H. and H. Moench, *Factors Determining the Element Behavior in Municipal Solid Waste Incinerators. I. Field Studies*. Environmental Science & Technology, 2000. **34**(12): p. 2501-2506.
79. Wiles, C.C., *Municipal solid waste combustion ash: State-of-the-knowledge*. Journal of Hazardous Materials, 1996. **47**(1): p. 325-344.
80. Karlfeldt, K. and B.M. Steenari, *Assessment of metal mobility in MSW incineration ashes using water as the reagent*. Fuel, 2007. **86**(12-13): p. 1983-1993.
81. Tang, J. and B.-M. Steenari, *Leaching optimization of municipal solid waste incineration ash for resource recovery: A case study of Cu, Zn, Pb and Cd*. Waste Management, 2016. **48**: p. 315-322.
82. Cornelis, G., T.V. Gerven, and C. Vandecasteele, *Antimony leaching from MSWI bottom ash: Modelling of the effect of pH and carbonation*. Waste Management, 2012. **32**(2): p. 278-286.
83. Cornelis, G., C.A. Johnson, T.V. Gerven, and C. Vandecasteele, *Leaching mechanisms of oxyanionic metalloid and metal species in alkaline solid wastes: A review*. Applied Geochemistry, 2008. **23**(5): p. 955-976.
84. Paoletti, F., H. Seifert, J. Vehlow, and P. Sirini, *Oxyanions forming elements in waste combustion- partitioning of antimony*. Waste Management & Research, 2000. **18**(2): p. 141-150.
85. Klein, J., S. Dorge, G. Trouvé, D. Venditti, and S. Durécu, *Behaviour of antimony during thermal treatment of Sb-rich halogenated waste*. Journal of Hazardous Materials, 2009. **166**(2-3): p. 585-593.
86. Van Der Hoek, E.E., J.T. Van Elteren, and R.N.J. Comansi, *Determination of As, Sb and Se Speciation in Fly-Ash Leachates*. International Journal of Environmental Analytical Chemistry, 1996. **63**(1): p. 67-79.
87. Pitts, J.J., P.H. Scott, and D.G. Powell, *Thermal decomposition of antimony oxychloride and mode in flame retardancy*. Journal of Cellular Plastics, 1970. **6**(1): p. 35-37.
88. Paoletti, F., H. Seifert, J. Vehlow, and P. Sirini, *Oxyanions forming elements in waste combustion -partitioning of antimony*. Waste Management and Research, 2000. **18**(2): p. 141-150.
89. Fedje, K.K., S. Rauch, P. Cho, and B.-M. Steenari, *Element associations in ash from waste combustion in fluidized bed*. Waste Management, 2010. **30**(7): p. 1273-1279.
90. Eighmy, T.T., J.D. Eusden, J.E. Krzanowski, D.S. Domingo, D. Staempfli, J.R. Martin, and P.M. Erickson, *Comprehensive Approach toward Understanding Element Speciation and*

- Leaching Behavior in Municipal Solid Waste Incineration Electrostatic Precipitator Ash.* Environmental Science & Technology, 1995. **29**(3): p. 629-646.
91. Tella, M. and G.S. Pokrovski, *Antimony(III) complexing with O-bearing organic ligands in aqueous solution: An X-ray absorption fine structure spectroscopy and solubility study.* Geochimica et Cosmochimica Acta, 2009. **73**(2): p. 268-290.
  92. C. F. Baes and R. S. Mesmer: *The Hydrolysis of Cations.* John Wiley & Sons, New York, London, Sydney, Toronto 1976. 489 Seiten, Preis: £ 18.60. Berichte der Bunsengesellschaft für physikalische Chemie, 1977. **81**(2): p. 245-246.
  93. Tostar, S., E. Stenvall, A. Boldizar, and M.R.S.J. Foreman, *Antimony leaching in plastics from waste electrical and electronic equipment (WEEE) with various acids and gamma irradiation.* Waste Management, 2013. **33**(6): p. 1478-1482.
  94. Hong, K.J., S. Tokunaga, Y. Ishigami, and T. Kajiuchi, *Extraction of heavy metals from MSW incinerator fly ash using saponins.* Chemosphere, 2000. **41**(3): p. 345-352.
  95. *Establishing Criteria and Procedure for the Acceptance of Waste at Landfills Pursuant to Article 16 of and Annex II to Directive 1999/31/EC*, in *Article 16 of and Annex II to Directive 1999/31/EC*, T.C.O.T.E. UNION, Editor. 2003: <http://eur-lex.europa.eu/legal-content/EN/TXT/?uri=CELEX%3A32003D0033>.
  96. Stenberg, G., *Salt Recovery from Waste to Energy Incineration Fly Ash*, in *Department of Civil and Environmental Engineering*. 2016, CHALMERS UNIVERSITY OF TECHNOLOGY. p. 64.
  97. Rasmussen, E., *A method for treatment of flue gas cleaning products*, in *European Patent Office*. 2004: Europe.
  98. Rasmussen, E., *Sambehandling af RGA og scrubbervæske fra forbrændingsanlæg med HALOSEP processen*. 2015, Miljøstyrelsen: Stena Metall A/S.
  99. Wadge, A. and M. Hutton, *The leachability and chemical speciation of selected trace elements in fly ash from coal combustion and refuse incineration.* Environmental Pollution, 1987. **48**(2): p. 85-99.
  100. Lew, R., *The removal of cobalt from zinc sulphate electrolytes using the copper-antimony process*, in *Materials Engineering*. 1994, The University of British Columbia: Vancouver, Canada.
  101. Bratsch, S.G., *Standard Electrode Potentials and Temperature Coefficients in Water at 298.15 K.* Journal of Physical and Chemical Reference Data, 1989. **18**(1): p. 1-21.
  102. van der Pas, V. and D.B. Dreisinger, *A fundamental study of cobalt cementation by zinc dust in the presence of copper and antimony additives.* Hydrometallurgy, 1996. **43**(1-3): p. 187-205.
  103. BØrve, K. and T. Østvold, *Norzink removal of cobalt from zinc sulphate electrolytes*, in *Hydrometallurgy '94*. 1994, Springer Netherlands. p. 563-577.
  104. Fontana, A. and R. Winand, in *Metallurgie XI*. 1971. p. 162-168.
  105. Tozawa, K., T. Nishimura, M. Akahori, and M.A. Malaga, *Comparison between purification processes for zinc leach solutions with arsenic and antimony trioxides.* Hydrometallurgy, 1992. **30**(1-3): p. 445-461.
  106. de Blander, F. and R. Winand, *Influence de l'antimoine et du cuivre sur la cementation du cobalt par le zinc.* Electrochimica Acta, 1975. **20**(11): p. 839-852.
  107. Kroleva, V., Metallurgiya Sofia, 1980.
  108. Boyano, B., V. Konareva, and N. Kolev, *Removal of cobalt and nickel from zinc sulphate using activated cementation.* Journal of Mining and Metallurgy, Section B: Metallurgy, 2004. **40**(1): p. 41-55.
  109. Boyanov, B.S., V.V. Konareva, and N.K. Kolev, *Purification of zinc sulfate solutions from cobalt and nickel through activated cementation.* Hydrometallurgy, 2004. **73**(1-2): p. 163-168.
  110. Younesi, S.R., H. Alimadadi, E.K. Alamdari, and S.P.H. Marashi, *Kinetic mechanisms of cementation of cadmium ions by zinc powder from sulphate solutions.* Hydrometallurgy, 2006. **84**(3-4): p. 155-164.

111. Singh, V., *Technological innovation in the zinc electrolyte purification process of a hydrometallurgical zinc plant through reduction in zinc dust consumption*. Hydrometallurgy, 1996. **40**(1–2): p. 247-262.
112. Zaghloul, A.A., El-Subruiti, G. M., and Ahmed, A.M. , *Kinetic Study of Cementation of Copper on Zinc Metal in Ethanol-Water Mixtures*. J. Mater. Sci. Technol., 1996. **12**: p. 41-45.
113. Jun, D., De-quan, Wang, Lan, Jiang, Man, Jin, *Removal of cobalt from zinc sulphate solution using rude antimony trioxide as additive*. Trans. Nonferrous Met. Soc. , 2002. **12**(6): p. 1172-1175.
114. Lew, R.W., *The removal of cobalt from zinc sulphate electrolytes using the copper-antimony process*. 1994, University of British Columbia.
115. Krause, B. and R.F. Sandenbergh, *Optimization of cobalt removal from an aqueous sulfate zinc leach solution for zinc electrowinning*. Hydrometallurgy, 2015. **155**(0): p. 132-140.
116. Rosenqvist, T., *Volatile Metals in Principles of extractive metallurgy*, B.J. Clark, Editor. 1974, McGraw-Hill: New York. p. 299-321.
117. Truesdale, E.C. and R.K. Waring, *Reduction Equilibria of Zinc Oxide and Carbon Monoxide I*. Journal of the American Chemical Society, 1941. **63**(6): p. 1610-1621.
118. Carlin, J.F., *Antimony Recycling in the United States in 2000*, in *Flow Studies For Recycling Metal Commodities in the United States*. 2000, U.S. Department of the Interior, U.S. Geological Survey.
119. Roine, A., *HSC Chemistry for Windows Version 9.2.2*. 2016, Outokumpu Research, Outotec Technologies: Pori, Finland.
120. Irtyugo, L.A., N.V. Belousova, V.M. Denisov, L.T. Denisova, S.D. Kirik, and L.G. Chumilina, *High-Temperature Heat Capacity of Bismuth Oxide and Bismuth-Zinc Double Oxide with the Sillenite Structure*. Journal of Siberian Federal University, 2012(2): p. 125-130.
121. Gutknecht, T., Y. Colombus, and B.-M. Steenari, *Recycling Zinc from Metal Oxide Varistors Through Leaching and Cementation of Cobalt and Nickel*. Journal of Sustainable Metallurgy, 2016: p. 1-12.
122. JCPDS, *Joint Committee of Powder Diffraction Standards*, in *JCPDS-ICCD 2010*: Philadelphia, USA.
123. Kumari, K.G.V., P.D. Vasu, V. Kumar, and T. Asokan, *Formation of Zinc–Antimony-Based Spinel Phases*. Journal of the American Ceramic Society, 2002. **85**(3): p. 703-705.
124. Gama, L., Paiva-Santos, C., Vila, C., Lisboa-Filho, P., Longo, E. , *Characterization of nickel doped Zn<sub>7</sub>Sb<sub>2</sub>O<sub>12</sub> spinel phase using Rietveld refinement*. Powder Diffraction, 2003. **18**(3): p. 219-223.
125. Gutknecht, T., A.M.K. Gustafsson, C. Forsgren, C. Ekberg, and B.-M. Steenari, *Investigations into Recycling Zinc from Used Metal Oxide Varistors via pH Selective Leaching: Characterization, Leaching, and Residue Analysis*. The Scientific World Journal, 2015: p. 11.
126. Pourbaix, M., *Atlas of electrochemical equilibria in aqueous solutions*. 1974: National Association of Corrosion Engineers.
127. Interactive, P., *Implements PHREEQC 3.1.2*, in *3.1.2.8538*, USGS, Editor. 2014.
128. Daniel Saalfeld, C.B., *MINTEQ database*. 2003, Jon Petter Gustafsson: Stockholm, SE.
129. Bøckman, O. and T. Østvold, *Products formed during cobalt cementation on zinc in zinc sulfate electrolytes*. Hydrometallurgy, 2000. **54**(2–3): p. 65-78.
130. Raghavan, R., P.K. Mohanan, and S.K. Verma, *Modified zinc sulphate solution purification technique to obtain low levels of cobalt for the zinc electrowinning process*. Hydrometallurgy, 1999. **51**(2): p. 187-206.
131. Jakšić, M.M., *Impurity effects on the macromorphology of electrodeposited zinc I: Theoretical considerations and a review of existing knowledge*. Surface technology, 1985. **24**(3): p. 193-217.
132. Peters, E. *The physical chemistry of hydrometallurgy*. in *International Symposium on Hydrometallurgy*. 1973. AIME New York, NY, USA.
133. Van der Pas, V. and D. Dreisinger, *A fundamental study of cobalt cementation by zinc dust in the presence of copper and antimony additives*. Hydrometallurgy, 1996. **43**(1): p. 187-205.

134. Xiong, J. and I. Ritchie. *An electrochemical study of the inhibition of the Co (II)/Zn cementation reaction*. in *Proceedings of the First International Conference on Hydrometallurgy (ICHM'88)*. 1988.
135. Toni Gutknecht, C.F., Britt-Marie Steenari, *Recovery of Antimony: A laboratory study on the thermal decomposition and carbothermal reduction of Sb(III), Bi(III), Zn(II) oxides and antimony compounds from metal oxide varistors*. *Journal of Sustainable Metallurgy*, 2017.
136. Biefeld, R.M. and S.S. White, *Temperature/Composition Phase Diagram of the System Bi<sub>2</sub>O<sub>3</sub>-PbO*. *Journal of the American Ceramic Society*, 1981. **64**(3): p. 182-184.
137. Krüger, J., P. Winkler, E. Lüderitz, M. Lück, and H.U. Wolf, *Bismuth, Bismuth Alloys, and Bismuth Compounds*, in *Ullmann's Encyclopedia of Industrial Chemistry*. 2000, Wiley-VCH Verlag GmbH & Co. KGaA.
138. Chen, H.-K., *Kinetic study on the carbothermic reduction of zinc oxide*. *Scandinavian Journal of Metallurgy*, 2001. **30**(5): p. 292-296.
139. Antao, S., M. Duane, and I. Hassan, *DTA, TG, and XRD Studies of Surmanite and Ettringite*. *The Canadian Mineralogist*, 2002. **40**: p. 1403-1409.
140. Cornelis, G., B. Etschmann, T. Van Gerven, and C. Vandecasteele, *Mechanisms and modelling of antimonate leaching in hydrated cement paste suspensions*. *Cement and Concrete Research*, 2012. **42**(10): p. 1307-1316.
141. Cornelis, G., T. Van Gerven, and C. Vandecasteele, *Antimony leaching from uncarbonated and carbonated MSWI bottom ash*. *Journal of Hazardous Materials*, 2006. **137**(3): p. 1284-1292.
142. Astrup, T., J.J. Dijkstra, R.N.J. Comans, H.A. van der Sloot, and T.H. Christensen, *Geochemical Modeling of Leaching from MSWI Air-Pollution-Control Residues*. *Environmental Science & Technology*, 2006. **40**(11): p. 3551-3557.
143. Steenari, B.-M. and F. Björefors, *Återvinning av metaller från avfallsaska*. 2014, Avfall Sverige.